

TONGJI UNIVERSITY

BACHELOR'S THESIS

Novel On-site LVRT Testing Method for Full Converter Wind Turbines

Authors:

Josep Isidre CASAS TURU and
Santiago MASSÓ MURATEL

Supervisor:

Dr. XIANG Dawei

*A thesis submitted in fulfilment of the requirements
for the B.Eng of Industrial Engineering*

in the

Department of Electrical Engineering



Shanghai, China

July 2014

Declaration of Authorship

We, Josep Isidre CASAS TURU and Santiago MASSÓ MURATEL, declare that this thesis titled, 'Novel On-site LVRT Testing Method for Full Converter Wind Turbines' and the work presented in it are our own. We confirm that:

- This work was done wholly or mainly while in candidature for a research degree at this University.
- Where any part of this thesis has previously been submitted for a degree or any other qualification at this University or any other institution, this has been clearly stated.
- Where we have consulted the published work of others, this is always clearly attributed.
- Where we have quoted from the work of others, the source is always given. With the exception of such quotations, this thesis is entirely my own work.
- We have acknowledged all main sources of help.
- Where the thesis is based on work done by myself jointly with others, we have made clear exactly what was done by others and what we have contributed ourselves.

Signed:

Date:

工欲善其事必先利其器

“He that would perfect his work must first sharpen his tools”

孔子

Confucius

TONGJI UNIVERSITY

Abstract

Department of Electrical Engineering

Industrial Engineering

Novel On-site LVRT Testing Method for Full Converter Wind Turbines

by Josep Isidre CASAS TURU and Santiago MASSÓ MURATEL

Low Voltage Ride-through (LVRT) capability is now required for all large-scale Wind Turbines (WTs) connected to the grid. This thesis presents an on-site LVRT testing method for full-scale converter WTs. The new method makes use of the already installed WT converters to emulate the grid and produce a given fault for the WT under test. To guarantee the safety of the grid, both the WT under test and the grid emulating WTs are disconnected from the grid and operate in stand-alone mode during the test. The system configuration, testing procedure, control strategies are studied in this thesis. A wind farm with typical 2MW full converter Permanent Magnetic Synchronous Generator (PMSG) WTs was modelled and simulated. Practical issues including the minimum converter capability for grid emulation, WT over-speed limitation, grid impedance and fault conditions emulation were studied and discussed. Simulation results have shown that with only proper control algorithm modifications it is feasible to conduct on-site a series of LVRT tests for the full converter WT safely under the given grid capability and fault conditions.

Acknowledgements

Firstly, I would like to express my most sincere gratitude to my tutor Dr. XIANG Dawei (向大为) for the continuous support shown during the research of this Thesis. It is also a pleasure to thank my co-author Santi who has made the research and writting of this thesis possible.

I would like to thank Sino-Spanish Campus, specially by Ms. Jien YU (俞吉恩) and Mr. Sergio Zlotnik, for all the assistance provided during the exchange program. I am very grateful to my home university, Universitat Politècnica de Catalunya, and the Industrial Engineering school, ETSEIB, for making this exchange possible and giving me the opportunity to study abroad.

I want to thank my fellow classmates at Jiading Campus for the stimulating discussions, insightful comments and acute questions we exchanged during our weekly seminars. I am thankful to my friends Jean Pierre and Maj-Britt for all their support and for putting up with my frustration when things did not go as planned. Moreover I am indebted to Maj-Britt for having the patience to proofread and improve the quality of this entire thesis. I am also thankful to all my friends in Tongji University, specially my fellow spanish exchange students, for contributing to such an unforgettable and special experience.

Last but not the least, I want to thank my family: my parents Ricard and Isabel, and my siblings Xavier and Eulàlia, who have always shown their faith in me and have never stopped encouraging and supporting me throughout my life.

Contents

Declaration of Authorship	ii
Abstract	iv
Acknowledgements	v
Contents	vi
List of Figures	xi
List of Tables	xv
Abbreviations	xvii
Nomenclature	xix
1 Introduction	1
1.1 Motivation	3
1.2 Purpose	3
1.3 Focus	4
2 Background	5
2.1 A Brief Introduction to Wind Turbine Technology	5
2.1.1 Wind Turbine Types	6
2.1.1.1 Horizontal Axis Wind Turbines (HAWT)	7
2.1.1.2 Vertical Axis Wind Turbines (VAWT)	8
2.1.2 Wind Turbine Concepts	8
2.1.3 DFIG vs PMSG	12
2.1.3.1 Lifecost and Efficiency Focus	12
2.1.3.2 Reliability	15
2.1.3.3 An Overview of PMG and DFIG Drive Trains	16
2.2 Low Voltage Ride Through (LVRT)	17
2.3 Technical Requirements for Grid Connection of Wind Generation	18
2.3.1 LVRT Capability	18
2.3.2 Voltage Operating Range	21

2.3.3	Frequency Operating Range	21
2.3.4	Reactive Power Control and Voltage Regulation	23
2.3.5	Active Power and Frequency Control	25
2.4	Current LVRT Test Strategies	26
2.4.1	Impedance-based Testing System	27
2.4.2	Converter-based Testing System	29
3	Testing System Configuration and Procedure	31
3.1	Analysis of the Wind Farm	31
3.2	Analysis of the WTs	32
3.2.1	Mechanical Components	33
3.2.2	Electrical Components	34
3.2.3	Rated Mechanical Torque Selection	36
3.3	LVRT Testing Procedure	38
4	Test WT Control Strategies	41
4.1	Normal Control	42
4.1.1	Grid-side Converter for Normal Control	42
4.1.2	Machine-side Converter for Normal Control	43
4.2	LVRT Control	44
4.2.1	Machine-side Converter for LVRT Control	44
4.2.2	Grid-side Converter for LVRT Control	44
5	Grid WT Control Strategies	47
5.1	Machine-side Converter for Grid Emulating Control	48
5.2	Grid-side Converter for Grid Emulating Control	49
5.2.1	3phG Fault ($3\phi - g$)	50
5.2.2	1phG Fault ($\phi - g$)	50
5.2.3	2ph Fault (2ϕ)	51
5.2.4	2phG Fault ($2\phi - g$)	52
5.3	Grid-Side Converter for Network Impedance Emulation Control	53
5.4	Parallel Control for Grid Emulation	54
5.4.1	Voltage Synchronized Autonomous Control	54
5.4.2	Voltage Synchronisation of Grid WTs	55
5.5	Speed Control and Limitations of WTs	57
5.5.1	WT Speed Regulation with Pitch Control	57
5.5.2	Speed Operation Range and Limitation	58
6	Simulation Study	61
6.1	Process of LVRT Testing	61
6.1.1	Grid WT	62
6.1.2	Test WT	63
6.2	LVRT Testing under Different Grid Faults	64
6.2.1	3phG Fault	65
6.2.2	1phG Fault	66
6.2.3	2phG Fault	67
6.2.4	2ph Fault	67
6.3	LVRT Testing under Different Grid Fault Intensities	69

6.4	LVRT Testing with Different Network Impedances	69
6.5	LVRT Testing with Grid WTs In Parallel	71
6.6	Degree of Current Unbalance (Maximum) due to Model Parameter Errors of WT_{Grid2}	73
6.7	WT Speed Regulation and Limitation	76
7	Conclusions	79
8	Future Work	81
A	Wind Turbine PMSG Parameters	83
B	LCL Filter Parameters	85
C	Park Transformation	87
C.1	Instantaneous power theory in the synchronous reference frame	88
D	Commonly used control blocks	91
D.1	Current Loop Control	91
D.2	Phase-Locked Loop (PLL)	93
E	MATLAB Simulink Schematics	95
E.1	Grid emulating WTs: WT_{Grid1} and WT_{Grid2}	96
E.2	Under-test WT: WT_{Test}	104
Bibliography		109

List of Figures

1.1	PMSG Wind turbine connected to the grid through a full-power converter	1
2.1	Evolution of WT sizes	6
2.2	Example of a HAWT-based wind farm	7
2.3	Examples of different VAWT-based WTs.	8
2.4	Common wind turbine concepts: FSWT	10
2.5	Common wind turbine concepts: PVSWT	10
2.6	Common wind turbine concepts: DFIGWT	11
2.7	Common wind turbine concepts: VSCWT	11
2.8	DFIG and PMG efficiency curves for two different suppliers.	13
2.9	Magnet price development 2011-2014	15
2.10	LVRT requirements in various grid codes	20
2.11	World electrical voltage and frequency map (edited from Pawanexh Kohli's image)	22
2.12	Typical voltage and frequency dimensioning for wind generators	23
2.13	Typical reactive power-limiting curve for wind generators	25
2.14	Typical grid code-limiting curve for frequency-controlled regulation of the active power	26
2.15	LVRT impedance-based testing system scheme	27
2.16	Overview of the impedance-based method truck	27
2.17	Reactance room placed inside the truck	28
2.18	Placing and connecting the testing system unit	28
2.19	LVRT converter-based testing system scheme	29
3.1	Wind Farm scheme	32
3.2	Wind Farm schematics in MATLAB Simulink	32
3.3	PMSG Wind Turbine blocks: mechanical and electrical components	33
3.4	Power characteristics of the WT for $\beta = 0$	34
3.5	Electrical components of WT	35
3.6	Circuit configuration of two-level back-to-back converters	35
3.7	LVRT testing procedure flow chart	39
4.1	Voltage regulator control scheme	42
4.2	MPPT characteristics curve	43
4.3	MPPT control scheme	44
4.4	VCCF control ccheme	45
4.5	VCCF Control implemented in MATLAB Simulink	46
5.1	Differrent VSC control strategies used in the Wind Farm	48

5.2	Outer control loop for machine-side converter for grid emulation control	48
5.3	Inner control loop for machine-side converter for grid emulation control	49
5.4	Typical diagram of the power system integrated with wind farm	49
5.5	3phG fault MATLAB Simulink schematics	50
5.6	1phG fault MATLAB Simulink schematics	51
5.7	2phG fault MATLAB Simulink schematics	52
5.8	2ph fault MATLAB Simulink schematics	52
5.9	Principle of grid impedance emulation	53
5.10	Configuration of grid WTs in parallel	55
5.11	Principle of grid WT voltage synchronization	56
5.12	Equivalent circuit of LCL filter	57
5.13	PLL tracker control scheme	57
5.14	Block diagram of pitch-controller for WT speed regulation	58
5.15	Time sequences of LVRT test	59
6.1	Timeline of events in the LVRT testing procedure	61
6.2	The process of a LVRT testing for grid emulating WTs (conditions: 1phG fault, $\alpha=0$, $\lambda=0$, $Z_{eq}=0.2$)	63
6.3	The process of a LVRT testing for under-test WT (conditions: 1phG fault, $\alpha=0$, $\lambda=0$, $Z_{eq}=0.2$)	64
6.4	V_{PCC} and $I_{C,Grid1}$ for WT_{Grid1} for a 3phG fault	65
6.5	Fault start and recovery details of V_{PCC} and $I_{C,Grid1}$ in WT_{Grid1} for a 3phG fault	65
6.6	V_{PCC} and $I_{C,Grid1}$ for WT_{Grid1} for a 1phG fault	66
6.7	Fault start and recovery details of V_{PCC} and $I_{C,Grid1}$ in WT_{Grid1} for a 1phG fault	66
6.8	V_{PCC} and $I_{C,Grid1}$ for WT_{Grid1} for a 2phG fault	67
6.9	Fault start and recovery details of V_{PCC} and $I_{C,Grid1}$ in WT_{Grid1} for a 2phG fault	67
6.10	V_{PCC} and $I_{C,Grid1}$ for WT_{Grid1} for a 2ph fault	68
6.11	Fault start and recovery details of V_{PCC} and $I_{C,Grid1}$ in WT_{Grid1} for a 1ph fault	68
6.12	3phG fault LVRT testing under different λ (conditions: $\alpha=0$, $Z_{eq}=0.2$).	69
6.13	LVRT testing with different network impedances (conditions: 1phG fault, $\alpha=0$, $\lambda=0$)	70
6.14	LVRT testing with different network impedances (conditions: 3phG fault, $\alpha=0$, $\lambda=0$)	71
6.15	LVRT testing with two grid WTs in parallel (conditions: 3phG fault, $\alpha=0$, $\lambda=0$, $Z_{eq}=0.1$, $\theta_{g20}=8^\circ$).	72
6.16	DC-link voltage for each of the WTs (WT_{Grid1} , WT_{Grid2} , WT_{Test}); (conditions: 3phG fault, $\alpha=0$, $\lambda=0$, $Z_{eq}=0.1$, $\theta_{g20}=8^\circ$).	73
6.17	LVRT testing with different Model Parameter Errors of WT_{Grid2} (conditions: 1phG fault, $\lambda=0$, $\alpha=0$, $Z_{eq0}=0.1$)	75
6.18	Detailed overview of Phase A of I_G for WT_{Grid2}	75
6.19	Current unbalance in the parallel grid WTs (same conditions as Fig. 17 but $L_{F1} = 60\%L_{F10}$ in the controller of WT_{Grid2})	76
6.20	WT speed regulation during start-up by pitch control (wind speed $v_w = 10$ m/s)	77

6.21 Grid WT speed rise during LVRT for WT_{Grid1} , WT_{Grid2} and WT_{Test} (conditions: 1phG fault, $\alpha=0$, $\lambda=0$, $Z_{eq} = 0.2$)	77
C.1 qd plane representation	88
C.2 Example of three-phase voltages in the abc and $qd0$ frames	89
D.1 Current loop controller implementation	92
D.2 Phase-locked loop control scheme	93
D.3 An example of phase-locked loop initial transient	94
E.1 MATLAB Simulink Schematics of WT_{Grid1}	96
E.2 MATLAB Simulink Schematics of WT_{Grid2}	97
E.3 MATLAB Simulink Schematics of WT_{Grid1} and WT_{Grid2} Grid-Side Controller for Normal Operation	98
E.4 MATLAB Simulink Schematics of WT_{Grid1} and WT_{Grid2} Machine-Side Controller for Normal Operation	99
E.5 MATLAB Simulink Schematics of WT_{Grid1} Grid-Side Controller for Grid-Emulating Operation	100
E.6 MATLAB Simulink Schematics of WT_{Grid1} Machine-Side Controller for Grid-Emulating Operation	101
E.7 MATLAB Simulink Schematics of WT_{Grid2} Grid-Side Controller for Grid-Emulating Operation	102
E.8 MATLAB Simulink Schematics of WT_{Grid2} Machine-Side Controller for Grid-Emulating Operation	103
E.9 MATLAB Simulink Schematics of WT_{Test}	104
E.10 MATLAB Simulink Schematics of WT_{Test} Grid-Side Controller for Normal Operation	105
E.11 MATLAB Simulink Schematics of WT_{Test} Machine-Side Controller for Normal Operation	106
E.12 MATLAB Simulink Schematics of WT_{Test} Grid-Side Controller for LVRT Operation	107
E.13 MATLAB Simulink Schematics of WT_{Test} Machine-Side Controller for LVRT Operation	108

List of Tables

2.1	Review of advantages and disadvantages of DFIG and PMSG	17
2.2	Voltage level classification	21
3.1	Switching state of two-level converter	36
3.2	Calculated inertias based on different WT manufacturers	38
5.1	Different VSC control strategies used in the Wind Farm	48
6.1	Events in the LVRT testing procedure	62
6.2	Relative error due to model parameters error of WT_{Grid2}	76
A.1	Wind Turbine PMSG (nonsalient poles) parameters [1]	83
B.1	LCL Filter Parameters for grid-emulating WTs [2]	85

Abbreviations

AC	Alternating Current
AEP	Annual Energy Production
BPF	Band-Pass Filter
DC	Direct Current
DFIG	Double-fed Induction Generator
DFIGWT	Double-fed Induction Generator Wind Turbine
FPC	Full-Power Converter
FRT	Fault Ride-Through
F SWT	Fixed Speed Wind Turbine
GCP	Grid Connection Point
HAWT	Horizontal Axis Wind Turbine
HVDC	High-Voltage Direct Current
LVRT	Low Voltage Ride-Through
MPPT	Maximum Power Point Tracking
O&M	Operating and Maintenance
PCC	Point of Common Coupling
PLL	Phase-Locked Loop
PMG	Permanent Magnet Generator
PMSG	Permanent Magnet Synchronous Generator
PMSM	Permanent Magnet Synchronous Machine
PVSWT	Partial Variable Speed Wind Turbine
PWM	Pulse-Width Modulation
ph	phase
phG	phase Ground
pu	per unit

RMS	Root Mean Square
SCIG	Squirrel Cage Induction Generator
SPWM	Sinusoidal Pulse Width Modulation
TSO	Transmission System Operator
UPC	Universitat Politècnica de Catalunya
VAWT	Vertical Axis Wind Turbine
VCCF	Vector Current Controller with Feedforward
VR	Voltage Regulator
VSC	Voltage Source Converter
VSCWT	Voltage Source Converter-based Wind Turbine
VSG	Voltage Sag Generator
WRIG	Wound Rotor Induction Generator
WT	Wind Turbine

Nomenclature

λ_{WT}	tip-speed-ratio	<i>adimensional</i>
β	pitch angle	$^\circ$
C_p	power coefficient of WT	<i>adimensional</i>
ω_r	angular speed rotor	rad/s
v_ω	wind speed	m/s
P_m	wind power captured by WT	W
ρ	air density	kg/m^3
r	radius of surface covered by WT blades	m
T_m	mechanical torque	Nm
J_{WT}	inertia WT	kgm^2
m	mass of WT blades	kg
L_{blade}	length of WT blade	m
n_{blade}	number of WT blades	<i>adimensional</i>
E_{WT}	energy stored in rotor	J
H_{WT}	inertia constant	s
S_{WT}	rated apparent power	MVA
V_{DC}	DC-link voltage	V
V_{DC}^*	DC-link voltage command	V
I_q	q -reference of grid current	A
I_d	d -reference of grid current	A
I_q^*	q -reference of grid current command	A
I_d^*	d -reference of grid current command	A
T_{em}	electro-mechanical torque	Nm
T_{em}^*	electro-mechanical torque command	Nm
λ	relative distance between fault and WT	m

α	impedance angle	$^{\circ}$
V_{GCP}	voltage at GCP	V
V_G	voltage grid	V
V_g	voltage grid-side converter	V
V_+	positive-sequence component of voltage	V
V_-	negative-sequence component of voltage	V
Z_F	fault impedance	Ω
Z_S	grid impedance	Ω
Z_{WF}	Wind Farm impedance	Ω
Z_V	virtual impedance	Ω
Z_{eq}	equivalent network impedance	Ω
Z_T	transformer impedance	Ω
V_{gc}	grid-side VSC voltage	V
V_{gc}^*	grid-side VSC voltage command	V
V_g^*	virtual VSC voltage	V
I_g	PCC current for a WT	A
I_{gc}	grid-side VSC current for a WT	A
I_c	circular current	A
Θ_{err}	phase error	$^{\circ}$
β_{off}	pitch angle to turn off pitch control	$^{\circ}$
$\beta_{optimal}$	pitch angle for maximum power output	$^{\circ}$
$\omega_{r,Grid}^*$	grid angular speed command	rad/s
$\omega_{r,Grid}$	grid angular speed	rad/s
$\omega_{r,Test}^*$	converter angular speed command	rad/s
$\omega_{r,Test}$	converter angular speed	rad/s
$N_{WT,grid}$	number of WT in the wind farm	adimensional
P_{Test}	power output during the LVRT test	W
$T_{PowerOn}$	time to power on for LVRT test	s
T_{Fault}	grid fault duration	s
$T_{Recovery}$	time necessary for the recovery of the WT	s
T_{Test}	total time for a test	s

Dedicated to our parents, for everything they have done.

Chapter 1

Introduction

After rapid development in the recent decade, wind power has already become one of the most used renewable energy in the world. It is widely accepted that wind power generation is an important technology will help to solve the energy and environmental crisis. With more and more WTs being integrated into grid, the LVRT problem started to draw attention in the industry since the beginning of the 2000s. According to the grid code, which may differ slightly from country to country, all the large-scale (i.e. in the order of MW) WTs are required to remain grid connection and provide reactive power to support the electric system during a grid fault. Due to advances made in both the industry as well as academics in the past few years, different protection and control methods have been studied and the LVRT performance of WT has been improved significantly [3].

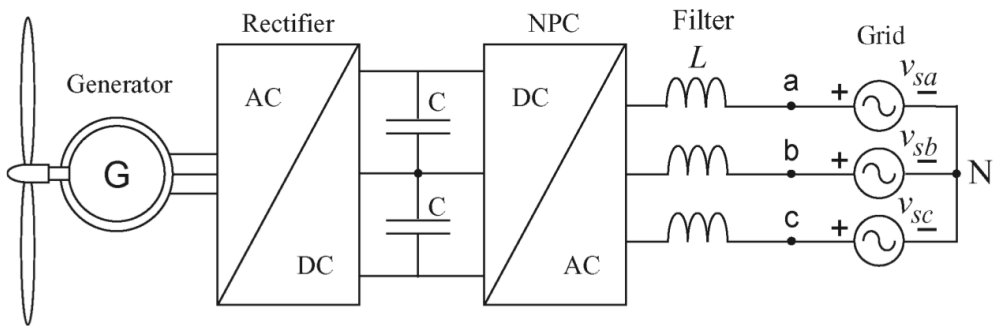


FIGURE 1.1: PMSG Wind turbine connected to the grid through a full-power converter

As a widely used WT technology in the industry, the full converter WT shown in Figure 1.1 can fulfill the LVRT requirements of grid code with LVRT control. The full-rated converter between WT and grid works as a interface to avoid the magnetic coupling effect which causes troubles for the Doubly-Fed Induction Generator (DFIG) WT, an also

widely used WT, during a grid fault LVRT. In this thesis we focus on the full converter WT. The LVRT of DFIG is out of its scope.

To verify the effectiveness and evaluate the performance of LVRT functionality, a WT LVRT test is needed [4]. The corresponding technology has already been studied in [5] [6]. Generally, there are mainly three different Voltage Sag Generator (VSG) topologies available to emulate a grid fault: transformer based, impedance based and Voltage Source Converter (VSC) based sag generator. By quickly switching the tap points, a transformer based VSG is described in [7]. As the most applied equipment for LVRT testing, the impedance based VSG is composed of a number of bulky reactances. With complicated configurations and switching, different grid fault conditions including the depth and duration of voltage dip and the fault types (symmetrical or asymmetrical faults) can be emulated at a limited grid short-circuit current for safety [8]. The VSC based VSG is a newly developed LVRT testing technology, which use a power converter to emulate a grid and apply fault. Due to the control flexibility of power electronics, the VSC based VSG can emulate different grid faults and grid short-circuit capability conveniently. However it is more expensive than the impedance based one.

The LVRT test must be done for any large-scale grid connected WT by the manufacturer in a laboratory and it has to be certified before it can be sold in the market. Carrying out a LVRT test on-site is still necessary sometime for the following reasons. Firstly, there is a requirement for the wind farm operator and/or grid company to be confident that all the installed WTs have the LVRT capability [9]. Secondly, the testing condition in laboratory may be different from the real system. Moreover, a LVRT test is also need, if possible, after any major system software and or hardware maintenance. Currently, the mobile LVRT testing system with VSG equipped in a heavy truck is available to provide the WT LVRT on-site testing service [10]. However, it is expensive due to the cost of equipment, transportation and testing. Since the testing system needs to be connected between the wind farm and the grid, the installation and safety issue must also be carefully considered. This is always troublesome because different parties (i.e. the manufacturer, operator and grid companies) might be involved.

It is therefore agreed that the conventional mobile LVRT testing system cannot fully meet the safety, cost-effectiveness and frequency requirements for field LVRT testing. To overcome these limitations, this thesis presents a novel on-site LVRT testing method for wind farms with full converter WTs. The basic idea is to make use of the existing WT converters in the wind farm to emulate a grid and generate a given fault condition

for the WT under going a test. There's no hardware modification needed for the new method, which means a cheaper and safer solution. During the test, both the WT under going testing and the grid emulating WTs are disconnected from the grid and operate in stand-alone mode. Thus, the LVRT test has no negative effect on the grid.

To clarify and prove the initial idea, the testing system configuration, testing procedures and control strategies are discussed in this thesis. A wind farm with 2MW full converter Permanent Magnetic Synchronous Generator (PMSG) WTs was modeled and simulated. Practical issues including the WT over-speed limitation, grid impedance and fault conditions emulation are studied and discussed. Simulation results show that with proper control algorithm modifications it is feasible to conduct a series of LVRT tests in a wind farm safely under any preset grid capability and fault conditions.

1.1 Motivation

We have spent our last semester of our degree as exchange students at Tongji University in Shanghai, China. Both of us are interested in Electrical Engineering. Santi is specializing in it and Josep has interned with a research group in Electrical Engineering at Universitat Politècnica de Catalunya (UPC). Dr. Dawei Xiang (向大为) from the Electrical Engineering department at Tongji University was assigned as our thesis advisor.

At the time of our meeting Dr. Dawei Xiang was peer reviewing a paper that proposed a new converter-based system for LVRT testing of WTs. WT technology has experienced an incredible amount of progress in the last few decades but there is still a lot of research to be done. LVRT testing is one of those WT technologies that still remain considerably undeveloped. Current methods are costly, inflexible and cannot be performed on site.

Dr. Dawei Xiang proposed we work on the development of a new procedure that would solve many of the problems current LVRT testing methods had.

1.2 Purpose

The purpose of this thesis is to propose a new method for WT LVRT testing. The goal is to create a method that is cheap, flexible and can be tested on site. A MATLAB Simulink simulation will be used to validate the results.

1.3 Focus

This thesis has two main foci, firstly, to study and prove the validity of the new LVRT testing procedure. Secondly, to review the three main control strategies for WT (Normal Control, LVRT control and the proposed LVRT grid simulation control). Even though the design of the WT simulation is needed, it is not central to the thesis and therefore no research has been done in this area. To prove the results a computational simulation has been used. The use of a testing rig would have been desirable but it is out of the scope of this thesis.

Chapter 2

Background

2.1 A Brief Introduction to Wind Turbine Technology

The need for renewable energy sources such as wind energy, solar energy, wave energy and others has increased during the 20th century because of limited fossil fuel reserves and environmental concerns. The oil crises in the 1970s prompted the search for alternative energy sources. Among the different renewable energy sources, wind turbine technology has achieved the fastest growth due to its high potential and its cost-effective way of producing electricity [11] .

Throughout human history, wind power has been used for irrigation, pumping water and milling grain. In the 20th century small windmills started to be used for electricity production, especially in remote rural areas. The modern wind power industry took off in the late 1970's when companies, mainly in Denmark, started serial production of wind turbines. These early wind turbines were small by today's standards, but their size and power output increased rapidly, as shown in Figure 2.2 [1] [12].

Wind turbines harvest this kinetic energy of the air current flowing across the earth surface and convert it into usable power which can provide electricity to homes, farms, schools and businesses on small (residential), medium (community), or large (utility) scales. As said before, wind energy is one of the fastest growing sources of new electricity generation in the world today. These growth trends can be linked to the multi-dimensional benefits associated with wind energy.

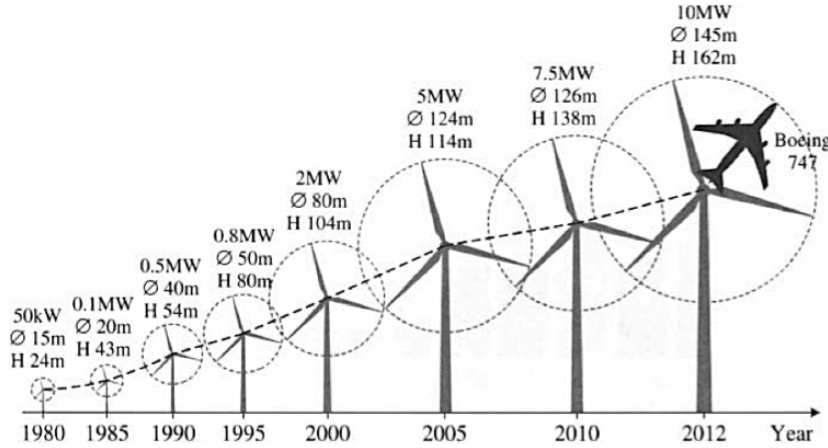


FIGURE 2.1: Evolution of WT sizes

- Green Power: The electricity produced from wind power is said to be "clean" because its generation produces no pollution or greenhouse gases. As both health and environmental concerns are on the rise, The demand for clean energy resources continues to grow.
- Sustainable: Wind is a renewable energy resource; it is inexhaustible and requires no "fuel" besides the wind that blows across the earth. This infinite energy supply is a security that many users view as a stable investment in our energy economy as well as in our children's' future.
- Affordable: Wind power is a cost-competitive source of electricity, largely due to technological advancements, as well as economies of scale as more of these machines are manufactured and put online around the world.
- Economic Development: As well as being affordable, wind power is a locally-produced source of electricity that enables communities to keep energy expenditure in their economy. Job creation (manufacturing, service, construction, and operation) and tax base increase are other development benefits for communities utilizing wind energy.

2.1.1 Wind Turbine Types

Electricity-producing WTs can be distinguished according to which way their rotor spins:

- Horizontal Axis Wind Turbines (HAWT), if they rotate around a horizontal axis (e.g. windmill).

- Vertical Axis Wind Turbines (VAWT), if they rotate around a vertical axis. They are less frequently used.

2.1.1.1 Horizontal Axis Wind Turbines (HAWT)

Horizontal axis wind turbines (HAWTs) are the most frequently used WTs. Their blades spin around a horizontal axis, looking like a windmill. An example of a HAWT is shown in Figure 2.2.



FIGURE 2.2: Example of a HAWT-based wind farm

HAWT have the rotor shafts and electrical generators at the top of the tower, and they must be pointed into the wind. This is done in a different way depending on the size of the WT. Large WTs typically use a wind sensor connected to a servomotor (a rotary actuator that allows for precise control of angular position, velocity and acceleration) to turn the WT into the wind, while small WT are pointed by a simple wind vane located behind the rotor blades.

Since a tower produces turbulence behind it, the turbine is usually pointed upwind of the tower. The stiffness of WT blades is essential in order to prevent them from being pushed into the tower when high winds develop, as well as a significant distance has to be left between the tower and the blades.

Nowadays, almost all commercial wind turbines connected to the grid have horizontal-axis three blades rotors [13].

2.1.1.2 Vertical Axis Wind Turbines (VAWT)

Vertical axis wind turbines (VAWTs) have the rotor shaft positioned vertically, so its blades spin around a vertical axis. Consequently, the WT does not have to be pointed into the wind, thus becoming its main advantage, especially in areas where the wind direction is extremely variable. Different examples of VAWT are shown below, in Fig. 2.3.



(A) *Savonius-based VAWT*



(B) *Darrieus-based VAWT*

FIGURE 2.3: Examples of different VAWT-based WTs.

These kinds of WTs with vertical axes, the generator and other components can be located near the ground because the tower does not have to support it. This is an advantage in terms of maintenance. On the other side, its main drawback is that they generally create drag when rotating.

2.1.2 Wind Turbine Concepts

Wind turbines can be separated into four basic concepts, determined by its speed control capability and its power control capability [14] [15].

Considering the speed control capability, they are classified in:

- fixed-speed WTs, operating in a limited range of rotor speed slightly above the synchronous speed.
- variable-speed WTs, operating in a wide range of rotor speeds both above and below the synchronous speed, and being allowed to optimize the rotational speed in order to maximize the incoming power.

Considering the power control capability, they are classified in:

- fixed-pitch WTs, where the pitch angle does not change dynamically (fixed blades).
- variable-pitch WTs, usually with blade-angle control, that allows the WT to optimize the output power by adjusting the global pitch angle according to incoming wind, so the power output is maximized in normal operation.

Considering the equipment they are built, they are classified in:

- WT equipped with no-load compensated induction generators, with shorted rotor circuits.
- WT equipped with doubly-fed induction generators, controlled by partial-load frequency converters.
- WT equipped with multi-pole synchronous generators, and also with full-load frequency converters.

Considering different concepts, perhaps other categorization criteria can be found in the literature.

The most commonly WT designs can be distinguished into four different concepts [14] [15], also shown in the following Fig. 2.4, 2.5, 2.6 and 2.7:

- fixed speed WTs (FSWTs), Fig. 2.4
- partial variable speed WTs with variable rotor resistance (PVSWTs), Fig. 2.5
- variable speed WTs with partial-rating frequency converter, known as doubly-fed induction generator-based concept (DFIGWTs), Fig. 2.6

- variable speed WTs with full-rating power converter, also known as Voltage Source Converter (VSC)-based WTs (VSCWTs), Fig. 2.7

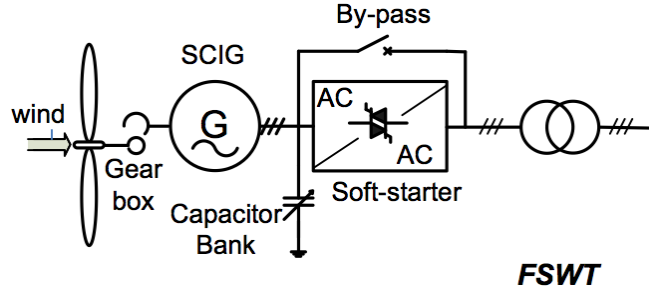


FIGURE 2.4: Common wind turbine concepts: FSWT

In fixed speed WTs, Fig. 2.4, a squirrel cage induction generator (SCIG) is directly connected to the grid using a transformer. The rotor speed is blocked to the grid frequency as very low slip is faced in normal operation (typically underneath 2%). A capacitor bank is needed in order to compensate the absorption of the reactive power by the generator, as well as a soft-starter to perform a grid connection without trouble. This configuration is very reliable because of the robust construction of the standard SCIG and the simplicity of the applied power electronics [14].

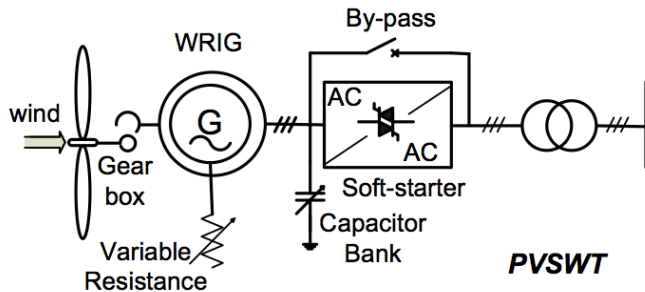


FIGURE 2.5: Common wind turbine concepts: PVSWT

In partial variable speed WTs, Fig. 2.5, a wound rotor induction generator (WRIG) is directly connected to the grid using a transformer. A variable rotor resistance typically accompanies the generator. The generator rotor windings are connected in series with a converter working as an external resistance. The function of the converters is to change the torque characteristic and the operating speed in a narrow range (typically 0-10% underneath the synchronous speed). A capacitor bank is also needed to perform

the reactive power compensation, as well as a soft-starter to perform a grid connection without trouble [14].

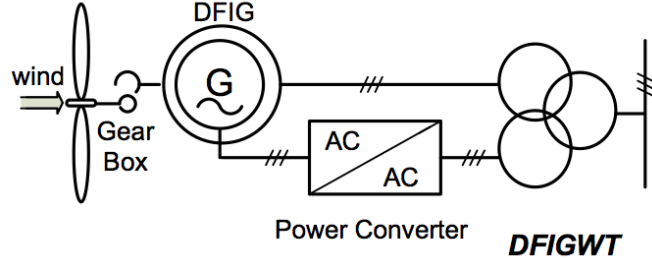


FIGURE 2.6: Common wind turbine concepts: DFIGWT

In DFIGWTs, Fig. 2.6, the stator is connected directly to the grid. The rotor is connected to a partial-rating power converter that controls the rotor frequency and the rotor speed. Then, the converter is connected to the grid. The partial-rating power converter is rated at 20%-30% of the DFIG rating so that the speed can be varied within $\pm 30\%$ or more of the synchronous speed. However, slip rings reduce the power efficiency and reliability, as well as increase the operating and maintenance (O&M) costs [14].

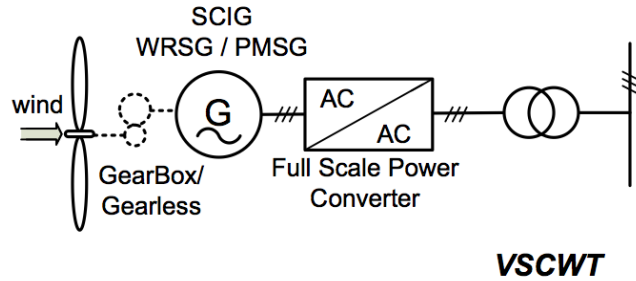


FIGURE 2.7: Common wind turbine concepts: VSCWT

In variable speed VSCWTs, Fig. 2.7, the generator is connected to the grid by using a full-rated frequency converter. The generator can be either a SCIG, WRSG or PMSG. The converter performs the reactive power compensation as well as a soft and safe connection to the grid [14].

2.1.3 DFIG vs PMSG

This section aims to explain why the thesis is focused on using a PMG with a full-power converter (FPC) as generator, which is currently the best technology, regardless of which key decision-making criteria is used. DFIG and PMSG generators represent the most common developed generators, so the first objective was deciding which type of generator was going to be used.

A lot of literature has been written and the debate on which generator and converter option gives the best modern wind turbine drive trains is still raging in the wind power industry. Many experts and industry professionals support the use of the double-fed induction generator technology, while expressing doubts about the advantages of PMG technology [16].

2.1.3.1 Lifecost and Efficiency Focus

It is sometimes claimed that permanent magnet generators (PMG) with full-power converter (FPC) drive trains are more expensive than double-fed induction generator (DFIG) drive trains. Nevertheless, research has confirmed that when every investment and operational cost is taken into account, PMG-FPC drive trains prove to be a cheaper and more cost-effective option over the total life cycle of a wind turbine.

- **Grid connection costs:**

The lower grid connection costs of wind turbines equipped with PMG-FPC technology represent a significant advantage over DFIG models. Efficiency and grid code compliance are the top demands when a generator selection is required. These factors, as well as reliability and a high annual energy production (AEP), are very important from an investment point of view.

Although partial converters may have improved slightly in grid code compliance, full-power converters remain the better and preferable option. As said in the report *Power System Architecture: Finding the Best Solution for a 5MW Turbine* [17], PMG is also a good choice for grid code compliance. Due to the full converter, all requirements for harmonics, power factor control and grid fault ride-through can be met easily.

DFIG technology now complies with the grid codes by adding hardware and software at the expense of extra costs. This is a simplistic answer to the problem, and is more of a quick fix than a concrete solution. With regards to DFIG, the report mentioned before [17] explains the following: “there is extra cost related to meeting new grid codes with the DFIG. With fault ride-through and power factor capability, the DFIG converter becomes similar in size and cost to the full converter.”

One of the most important benefits of PMG-FPC drive train technology is the fact that it already includes features such as reactive power generation and low voltage ride-through (LVRT). If these benefits are considered when making comparisons with the cheaper costs of double-fed induction generator drive trains, which also need more investment to make a connection to the grid, it’s easy to conclude that both options are perfectly valid.

- **Power efficiency and energy production:**

The higher power curve efficiencies of PMG technology, which produces remarkable extra energy, becomes its best long-term advantage. PMG technology is based in maximizing energy production and this is what gives notably higher productivity and profitability. In fact, PMG-FPC drive trains improve efficiency over the full operational range of the wind turbines. Although some researchers claim that DFIGs are more efficient than PMGs at full load generation [16], the efficiency of the PMG-FPC and the DFIG (partial converter based) are similar when operating at 100% power. Figure 2.8 [17] shows this similitude, as well as the better performance of the PMG efficiency curve. Nevertheless, it is well known that this operation point rarely happens and in general working conditions PMG drive trains have proven to be the most efficient ones (Fig. 2.8). Actually, the lower the power, the lower the efficiency of the DFIG.

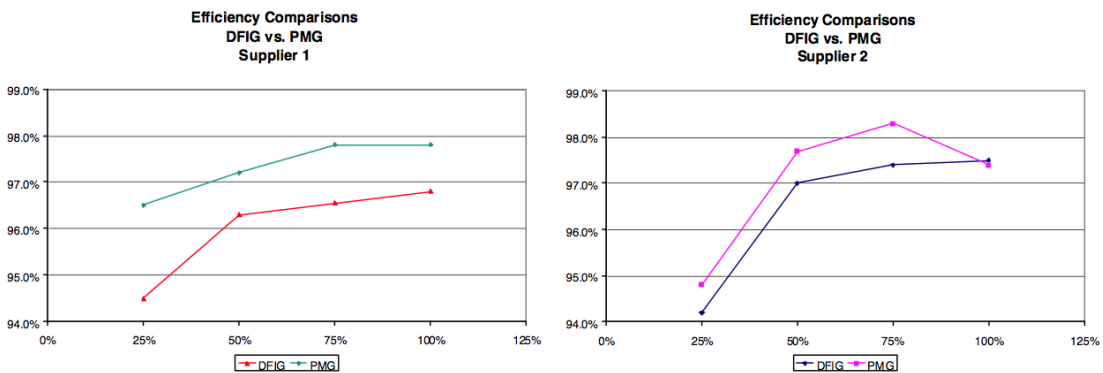


FIGURE 2.8: DFIG and PMG efficiency curves for two different suppliers.

In terms of operational performance, DFIGs are not used in direct-drive or medium-speed turbines because the lower the nominal speed of the DFIG is, the poorer are its operating characteristics, essentially regarding efficiency and power factor. Therefore, the only choice for those turbines is a synchronous machine; DFIG cannot be used on direct-drive machines due to poor electrical performance.

In addition, generator losses are always lower with PMG than with DFIG since there are no excitation losses which is why a PMG drive train results in higher annual energy production (AEP).

- **Operating and maintenance costs:**

PMG technology also improves reliability and serviceability, leading to lower operating and maintenance (O&M) costs. A wind energy report by Sciemus declares that PMG designs have an average of 0.59 electrical faults and failures per year, which is lower than the 0.69 for other technologies [16]. As they say, the latest PMG machines are most reliable in terms of downtime per unit at 1.98 days per year, where all other technologies are over 2.36 failures per year; this means an 18% improvement and indicates that wind industry is learning and progressing adequately.

In the report mentioned several times before [17], it is estimated that annual service costs for DFIGs would be between 20-30% higher than for PMGs. The report continues to say that a PMG will achieve a lower cost of energy compared to a wind turbine equipped with a DFIG.

PMG are built with rare-earth magnets. These required magnets can seem an obvious risk in terms of cost, availability and price instability. But magnets needed for PMG turbines are not as expensive as they once were. The price level has stabilized significantly, as it can be seen in the above figure 2.9 [16].

The amount of rare-earth magnets needed varies depending on the generator type: direct drive, medium speed or high speed. Finally, this price difference is balanced by the lack of winding needed in the rotor, as needed with DFIG; manufacturing and assembling the rotor winding is time-consuming and expensive.

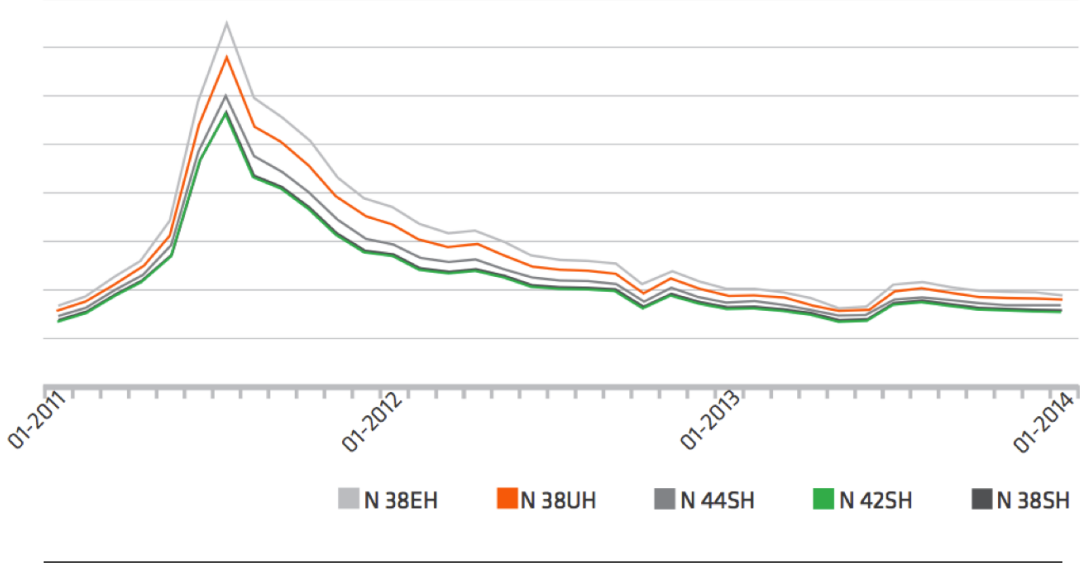


FIGURE 2.9: Magnet price development 2011-2014

In summary, PMGs are the optimal solution as they achieve good results in all factors affecting the lifecycle cost and efficiency of a wind turbine.

2.1.3.2 Reliability

- **PMG-FPC simplicity:**

It is commonly admitted that PMG-FPC solutions require lots of potentially unreliable electronics. This is just a myth because they rely on well studied power electronics, which might be more exposed to faults than gearboxes. Indeed, the amount of electronics used in PMG-FPC drive trains is nearly comparable to DFIG systems [16].

Moreover, it is important to notice that there are no electronics used in the PMG generator itself, only in the converters. If a multi-megawatt system is considered, a DFIG solution usually consists of only one converter for the rotor connection, while a full-power converter system can consist of several parallel power threads. As semiconductors do fail, it is better to have healthy power threads in operation despite a failure in one of them (turbine running at limited power), than having the whole wind turbine stopped due to a single failure in power electronics.

- **Heat performance:**

The NextWind report [17] concludes that PMGs have lower costs and higher reliability maintenance than DFIGs due to better heat performance, as well as being able to work without slip rings or encoders. According to this, in recent studies it has been proved that the reliability of PMGs is higher than other generator technologies.

Some industry researchers point out that PMGs need the use of neodymium ($\text{Nd}_2\text{Fe}_{14}\text{B}$) magnets, which are vulnerable to corrosion and heat [16]. If excessive heat happens, electrical losses could appear quickly as well as loosing magnetic field strength. This is why the industry decided to coat all the manufactured magnets, which helps to protect them from corrosion effectively and efficiently. Hermetic sealing is also applied when assembling the rotor, which also helps in this regard, so the high heat performance of PMG is ensured.

- **Maintenance conditions:**

As it has been explained before, PMG designs do not require slip rings or brushes to work and they comply easier with grid codes than DFIG. As long as DFIGs use brushes, they are exposed to face problems such as sparks and regular maintenance. To fix this, there exist brushless DFIG machines, but this is not a solution because brushless DFIG machines have lower efficiencies, complex construction and large sizes. These drawbacks are the reason of why they are not used in wind applications.

In summary, PMG-FPC solutions offer much better maintenance conditions than DFIG.

2.1.3.3 An Overview of PMG and DFIG Drive Trains

Table 2.1 shows a summary of all the characteristics of both DFIG and PMSG discussed previously [16].

TABLE 2.1: Review of advantages and disadvantages of DFIG and PMSG

Performance	DFIG	PMSG
Stator	Same	Same
Rotor	Rotor coil	Permanent magnet
Bearing	Same	Same
Slip ring and carbon brush	Available	Not needed
Manufacturing	Complicated process to manufacture rotor	Simple process to manufacture rotor
Maintenance	Heavy maintenance work and costly for rotor slip rings	No need for rotor maintenance
Converter	25-30% output power	Full power
Ability of LVRT	Available	Available
Reactive and adjustment ability	Varies according to the generator speed	100% across the entire speed range
Ability to connect and support power grid	Poor	Very good
Advantages	The initial investment is lower	<ol style="list-style-type: none"> 1. No coils, coil connection or slip ring needed 2. No need for rotor maintenance 3. Applicable to all-speed generator 4. High efficiency 5. Generator is lighter and size is smaller 6. Smaller cogging force 7. Higher annual power output
Disadvantages	<ol style="list-style-type: none"> 1. Difficult to service rotor 2. Not applicable to medium/low-speed generator 3. Low efficiency 4. Larger and unstable cogging force 5. Larger bearing current 	<ol style="list-style-type: none"> 1. The investment cost is higher 2. Professional software required for calculation 3. Requires more sophisticated process

2.2 Low Voltage Ride Through (LVRT)

A low voltage ride through (LVRT) or fault ride through (FRT) is the ability to react to a major decrease in energy input for alternative energy sources, such as wind turbines. In other words, it is the ability of a power-generating device to maintain its output voltage in short-term power dips. LVRT capability allows the power grid time to self-adjust during temporary faults by maintaining uninterrupted grid connection, thus increasing power grid stability. During the LVRT, the wind turbine remains connected to the electric system and returns to its normal operation quickly after the disturbance ends. Modern large-scale wind turbines are normally required to include systems that allow them to operate through such an event, and thereby "ride through" the low voltage [18].

In a grid containing many distributed wind turbines subject to voltage dips, it is possible to create a chain reaction that causes one of the generators to disconnect from the grid. As voltage dips are often caused by little generation for the load, removing generation can cause the voltage to drop further. This may bring the voltage low enough to cause another generator to trip out, and causing a cascading failure such as the one happened

in Jiuquan, China [19].

In order to prevent these failures a variety of standards exist and vary across jurisdictions. Examples of such grid codes are the German BDEW [20] and the UK National Grid code [21]. For wind turbines, LVRT testing is described in the standard IEC 61400-21 (2nd edition August 2008). [22]

2.3 Technical Requirements for Grid Connection of Wind Generation

Anybody connected to a public electric network, whether generator or consumer, has to comply with the agreed technical requirements and demands, in order to operate efficiently and safely. Electric power systems are based on generators, where the technical exigencies are complex. These technical requirements are frequently known as “grid codes”. As there are different voltage levels of connection and different system sizes, the “grid code” term should be used with care.

The impact and penetration of wind generation represents a significant power contribution to the electric grid, and therefore plays a very important role in power system operation and control. Consequently, high technical requirements are expected, in order to define the technical obligations and characteristics of both the wind generators and the system operator.

Included in this chapter are the main technical requirements found in the majority of grid codes concerning wind generation, such as fault ride-through capability, system voltage and frequency operating range, reactive power and voltage regulation, active power regulation and frequency control as well as voltage flicker emission and harmonics emission.

2.3.1 LVRT Capability

An important point when integrating large-scale wind generation is the impact on the system stability and the transient performance. System stability is largely associated with power system faults in the network, such as tripping of transmission lines, loss of production capacity and short circuit. These failures alter the balance of active and

reactive power, and change the power flow. Although the capability of the operating generators must be appropriate, large voltage drops can occur suddenly, being propagated widely and affecting a great number of wind generators. The unbalance and re-distribution of active and reactive power in the network may force the voltage to vary beyond its limit of stability, which means that a *brownout* (a period of low voltage) may occur, and perhaps be followed by a *blackout* (a complete loss of power).

Many faults in the power system are cleared by relay protections either by disconnection or by disconnection and fast reclosing. In all these situations the result is a short period of very low voltage followed by a period of voltage recovery. Previously when the wind generation was not a significant power source, a fault in the grid caused a short voltage drop at the wind turbine, also known as voltage dip or voltage sag. The wind turbine was basically disconnected from the grid and had to be reconnected again when the fault was cleared and the voltage returned to the normal values.

Due to the insignificant levels of wind power generation during those years, the stability of the power system was not affected significantly when a sudden disconnection of a wind turbine or even a wind farm from the grid occurred. Nowadays, where wind generation has increased its importance and penetration in the power system, the contribution of power generated by WTs is becoming a big problem. If a wind farm is suddenly disconnected when operating at high speeds, the power system may lose a large percentage of production capacity, and consequently a power disturbance can happen, possibly followed by a complete loss of power. Therefore, preventing extra generation losses due to power system faults is essential. Wind generators should be able to remain connected to the system during faults, where the 3-phases voltage could fall considerably.

For this reason, grid codes published during the last years strongly recommend that wind generation (especially for high voltage grids) withstand voltage dips to a stipulated percentage of the nominal voltage (from 0% to 15%) and for a specified duration (according to country regulations). Such requirements are known as Low Voltage Ride-Through (LVRT) or Fault Ride-Through (FRT) capabilities, and its characteristic curve (time-nominal voltage) for different grid codes is shown in Figure 2.10 [23].

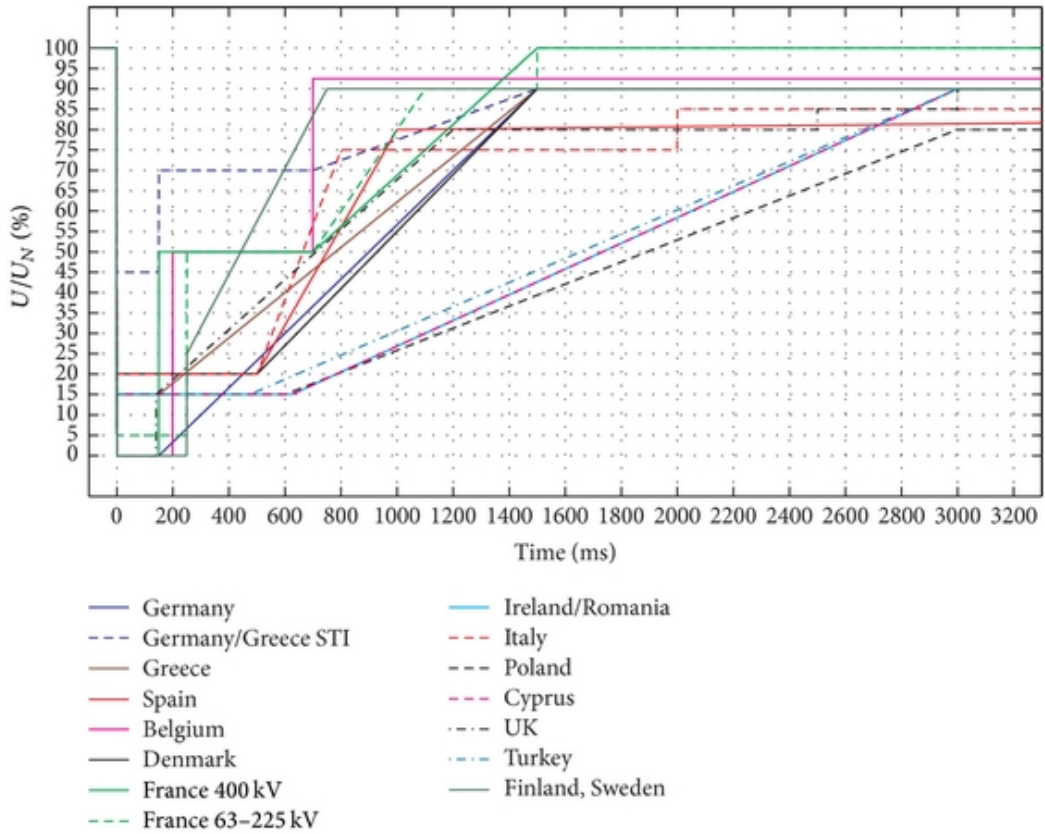


FIGURE 2.10: LVRT requirements in various grid codes

It is denoted that the minimum required immunity of the wind power generator is the 15% of nominal voltage, which is a standard required value. After this, and as time goes by, the generator voltage should be recovering up to 90% of the nominal voltage in a 3-second period of time.

Grid codes are mainly focused on the LVRT requirements under voltage dip and, after the system returns to its normal operation voltage, they also include fast active and reactive power restoration to previous values (before failure). The requirements depend on the specific characteristics of each power system and the protection used, and vary from region to region. The latest grid codes require that wind farms must remain in operation during severe grid faults, guarantee fast restoration of active power to the pre-fault levels (as soon as the fault is cleared) and, if needed, produce reactive current in order to support grid voltage during faults. Depending on their type and technology, wind turbines can fulfill these requirements to different degrees.

2.3.2 Voltage Operating Range

Wind farms must be capable of operating uninterrupted within the voltage and frequency variation limits faced in normal operation. Moreover, they should remain in operation in case of voltage and frequency fluctuations outside the normal operation limits, for a limited time and sometimes at reduced output power capability.

Tolerance to voltage fluctuations depends on the voltage level at the point of common coupling (PCC) of the wind generator connected to the network. It is worth remembering that the operating voltages at each voltage level, as seen in 2.2, are highly dependent on the local conditions and can be different in each country.

TABLE 2.2: Voltage level classification

Voltage level	From	To
Extra high voltages	230 kV	>230 kV
Transmission voltages	115 kV	230 kV
Sub-transmission voltages	33 kV	115 kV
Distribution voltages	0	33 kV

The lowest values are reached during operational instabilities and are usually not lower than 90% of the nominal voltage in the transmission level. These values can be down in some countries to 70% of the initial voltage for duration of up to 10 seconds, which must not lead to instability of the wind farm.

Voltages above the upper limit for full-load voltage range rarely occur, happening only while establishing the supply after major operational disturbances. These top values are usually not higher than 113% in the transmission level, as the system voltage operating range is generally narrower for higher voltage levels.

2.3.3 Frequency Operating Range

The frequency is one of the most important parameters in all power networks. The frequency of the electrical system varies by country; most electric power is generated at either 50 or 60 Hz, as shown in the figure below, Fig. 2.11:

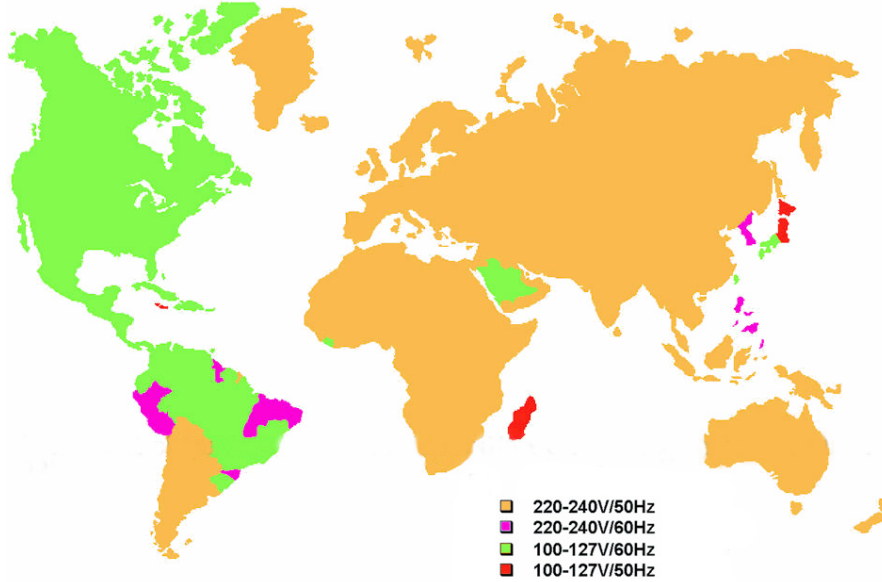


FIGURE 2.11: World electrical voltage and frequency map (edited from Pawanexh Kohli's image)

All the electrical generating equipment is designed to operate within very strict frequency margins. Grid codes specify that all generating plants should be able to operate continuously between a frequency interval around the nominal frequency of the grid (between 49.5 and 50.5 Hz, for 50 Hz systems such as in Africa and Europe), and to operate for different periods of time when lower/higher frequencies down/up to a minimum/maximum limit, typically 47.5 and 52.5 Hz. Operating outside these limits would damage the wind generators; even if it is for a short duration, relays would be activated and generation capacity would be lost. This loss of generation leads to additional frequency deviation and a *blackout* can happen.

In Figure 2.12 it is shown more accurately how wind farms have to be dimensioned to generate power at voltages and frequencies deviated from rated values, showing the power restriction in different operating areas [23]:

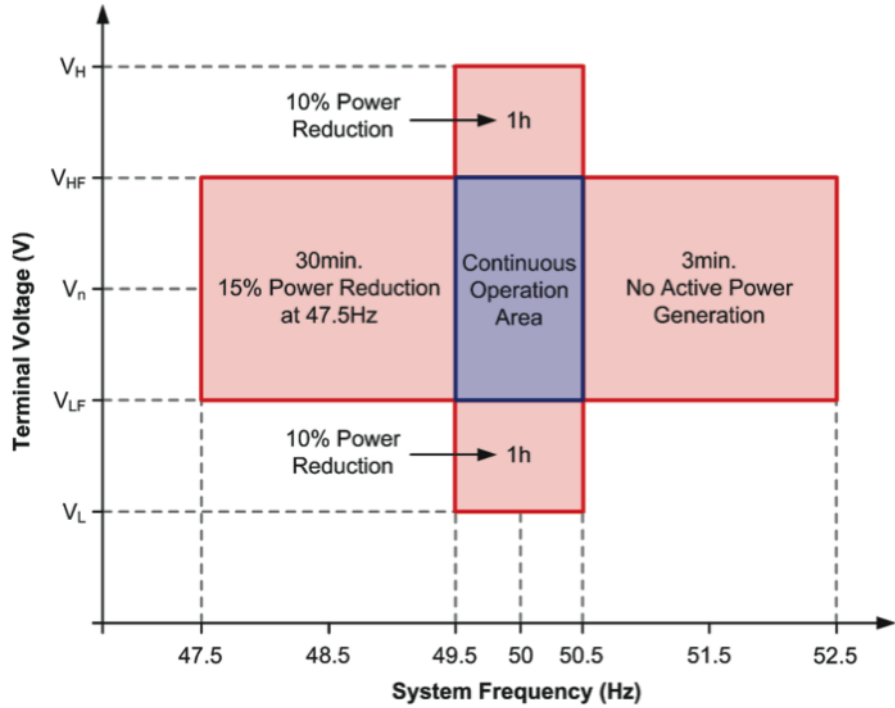


FIGURE 2.12: Typical voltage and frequency dimensioning for wind generators

Briefly, V_L is the lower voltage limit while V_{LF} is the lower voltage limit for full-load range for a nominal voltage V_N . Similarly, V_H is the upper voltage limit while V_{HF} is the upper voltage limit for full-load range. The full-load range (between V_{LF} and V_{HF}) indicates the voltage range within which the wind farm can supply its nominal power without any restriction (continuous operation area).

2.3.4 Reactive Power Control and Voltage Regulation

Reactive power control is important for wind farms because not all wind generation technologies have the same capabilities. Wind farms are frequently installed in remote areas, thus reactive power has to be transported over long distances producing inevitably power losses. Wind farms are required to have enough reactive power compensation to be neutral in reactive power at any working point. Recent grid codes request from wind farms to provide reactive output regulation, often in response to power system voltage variations.

The reactive power control requirements are related to the characteristics of each network and the determined voltage level for each situation, since the influence of the

reactive power injection on voltage is directly determined by the short-circuit capacity and impedance at the PCC of the wind farm. The short-circuit capacity in the electrical network represents the system strength or robustness. Clearly, generated power is entirely related to voltage variations at PCC. This means if the impedance is small, the grid is strong, so the voltage variations are also small. On the other hand, if the impedance is large, the grid is weak, so the voltage variations are also large.

Wind turbines with the ability of controlling reactive power are able to regulate the PCC voltage, as voltage is closely related to reactive power. Current wind farms are required to have the ability to control both active and reactive power. In the case of power electronic converter-based variable speed wind turbines, such as DFIG systems or with full-scale power converters, reactive power control can be performed by the converter itself.

A Voltage Regulator (VR) is included in wind generators in order to control its terminal voltage value to supply, or absorb the required amount of reactive power to the transmission system. There are rigorous requirements regarding the deviation in between the system voltage and its nominal values ($\pm 10\%$ for low voltage networks and $\pm 5\%$ for medium or high voltage networks).

Voltage or reactive power requirements in the grid codes are frequently detailed with a limiting curve such as shown in Fig. 2.13 [23].

The mean value of the reactive power should stay inside the power-limiting curve for over several seconds. When the wind generator is operating under nominal conditions, the power factor must be kept close to 1.0, so that it avoids excessive currents.

As the reactive power is locally generated and locally consumed, the current through all devices and the power losses in the network are reduced. Consequently, the wind farm should have the capability to control the voltage and the reactive power at the PCC. This is essential in order to guarantee safe operation of the system.

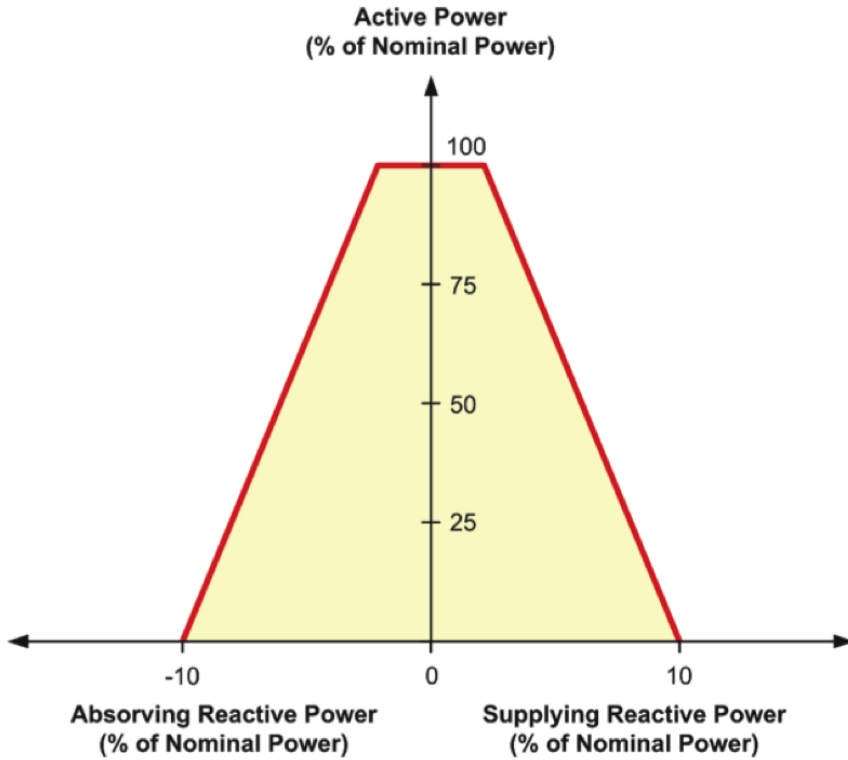


FIGURE 2.13: Typical reactive power-limiting curve for wind generators

2.3.5 Active Power and Frequency Control

A very significant factor in wind power integration into the grid is the spinning reserve constantly needed. This is a really limiting factor because of the unpredictability of wind, which may cause a sudden loss of wind generation. In order to avoid a failure in the power system, acceptable spinning reserve or very strong connections with neighbour countries are required.

Active power control requirements for stabilizing and supporting the system frequency are concerned with the ability of wind farms to regulate (habitually reducing) their power output to a rated point (active power restriction), either by pitch control (speed wind turbines) or by disconnecting turbines. Additionally, wind farms are required to regulate their active power output according to frequency deviations.

In some countries, generation based on intermittent sources of energy (wind and solar generation, for example) are not required to supply primary reserves. As a general remark, it is clear that most grid codes demand wind farms (especially high capacity ones)

to provide frequency response in order to regulate the system frequency accurately. It should be emphasized that the active power ramp rates must comply with the respective rates applicable to conventional power units 2.14 [23].

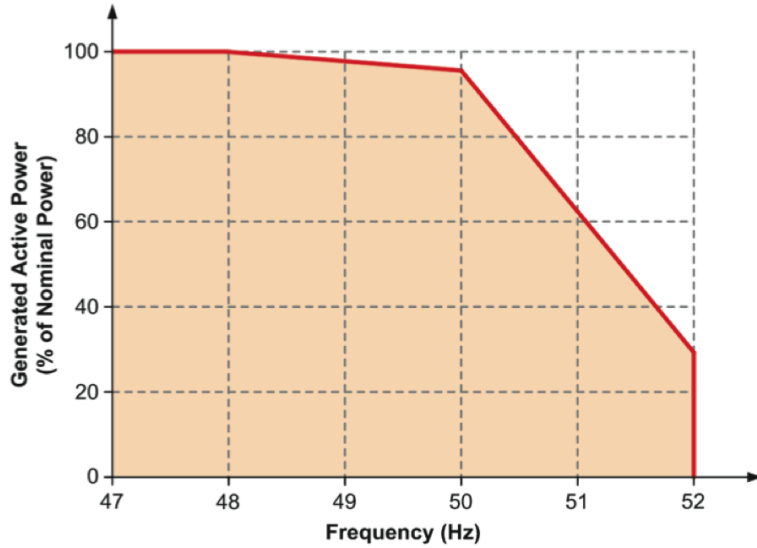


FIGURE 2.14: Typical grid code-limiting curve for frequency-controlled regulation of the active power

In the previous typical curve, it is shown that high-frequency response can be provided from full output to a reduced output when the frequency exceeds 50 Hz. It is also required that generating wind farms should decrease their output at a certain rate when the frequency increases over the rated value. Otherwise, the wind farms would be required to limit their power output under the maximum reachable power level, at nominal frequency.

2.4 Current LVRT Test Strategies

The IEC 61400-21 standard [24] defines the procedure to test part of the requirements detailed in grid codes for interconnection of wind turbines with the electrical grid. In the following sections, two different existing LVRT testing systems are described. Both systems consist in different methodologies to emulate a grid fault using extra hardware. Therefore a new approach for LVRT testing for wind turbines without using extra hardware is presented in this thesis.

2.4.1 Impedance-based Testing System

The standard grid code testing system for LVRT is formed by a set of impedances arranged to form a voltage divider, by which it is possible to control the amplitude and phase of the applied voltage at the test point [10]. In Fig. 2.15 is shown an overview of the standard LVRT impedance-based test equipment connected to a generic wind turbine system.

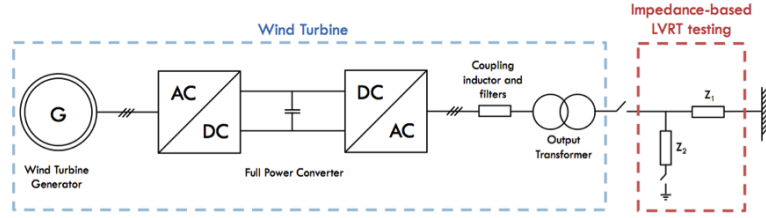


FIGURE 2.15: LVRT impedance-based testing system scheme

The advantages of using the standard equipment can be essentially summarized in its simple and robust design and its capability of managing high short-circuit currents fed from the tested generator. In addition, it fulfills the testing procedure required by the IEC standard for grid code testing [24].

Impedance-base test systems can be built in a modular container, helping its transportation [25]. The container is placed in a truck (Fig. 2.16), which is detailed in the next images (Fig. 2.17 and Fig. 2.18).



FIGURE 2.16: Overview of the impedance-based method truck



FIGURE 2.17: Reactance room placed inside the truck



FIGURE 2.18: Placing and connecting the testing system unit

The main disadvantage of this testing equipment is that it is limited only to voltage step variations. This means it is not capable of reproducing the voltage recovery ramp determined in the LVRT profile for the majority of the grid codes. Furthermore, in order to reproduce the desired voltage dip, the device is dependent on the short-circuit power of the grid at the connection point, which will impact the applied voltage profile during the test[10]. All tests that cannot be carried out with the standard LVRT testing system need to be performed using simulation models.

2.4.2 Converter-based Testing System

The following solution represents a methodology for grid code testing of wind turbines based on Voltage Source Converter (VSC) technology. In particular it focuses on LVRT tests of full converter-based wind turbines. The investigated testing setup consists of a 4 MW wind turbine and an 8 MW back-to-back VSC system, operating as test equipment [10]. It is demonstrated that this test is more flexible than the impedance-based one, having the ability to emulate the short-circuit impedance of the grid at the connection point and to control the voltage at the wind turbine terminals.

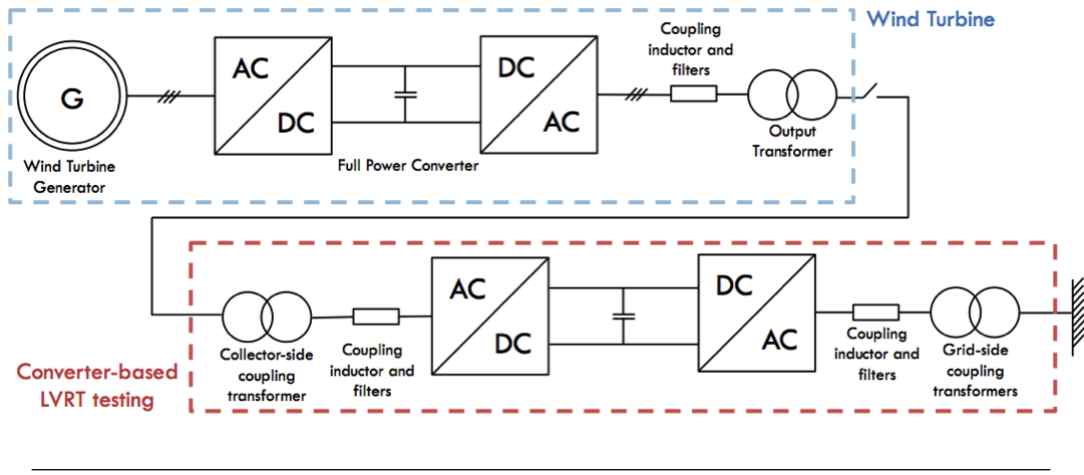


FIGURE 2.19: LVRT converter-based testing system scheme

Figure 2.19 shows an overview of a full power converter-based wind turbine connected to an HVDC system back-to-back. The converter controls the voltage at the wind turbine terminals and can emulate either an infinitely strong grid, as well as a grid with a pre-defined short-circuit power. As a difference compared with the impedance-based test system, the converter-based testing method allows the emulation of any kind of voltage profile at the connection point.

The applied voltage imposed by the converter is completely controllable in terms of magnitude, phase angle and frequency. Moreover, the ability of emulating the short-circuit impedance of the grid allows testing of the voltage controller of the turbine during the voltage dip, when reactive power injection is allowed by the transmission system operator (TSO).

Although this solution is more expensive than the impedance-based one, it is a huge advance that allows for a wider possibility of tests that can be performed. However,

the advantages of using VSC-system in wind turbine testing applications have not been fully investigated.

Chapter 3

Testing System Configuration and Procedure

This chapter includes the description of the model system used to evaluate the validity of the proposed on-site LVRT testing system. Section one, Analysis of the wind farm, will explain the connections between the WTs and the grid. In section two, Analysis of the model WT, the mechanical and electrical components of the modelled WT are discussed. Section three details the equations used to calculate the mechanical torque of the WT. Finally, the last section, proposes the general LVRT testing procedure. Some of the technical details are explained in Chapters three, four and five because further knowledge on the control scheme is needed.

3.1 Analysis of the Wind Farm

The model system is a wind farm that contains three identical wind turbines. Two of these wind turbines are the grid emulating wind turbines, WT_{Grid1} and WT_{Grid2} . The other WT, known as the WT_{Test} , is the one under test. All three WTs are connected together by means of the PCC. Each WT has a switch in between the filter and the PCC to be able to connect or disconnect them from the wind farm. Moreover, there is also a switch, K_{PCC} that allows the disconnection of the wind farm from the grid. The schematics of the wind farm can be seen in Figure 3.1. The implementation of the wind farm can be seen in Figure 3.2. It is important to note that the reason why there is no grid simulation in Figure 3.2 is because at no point during the LVRT test procedure the switch K_{PCC} is on (i.e. the wind farm is isolated from the grid).

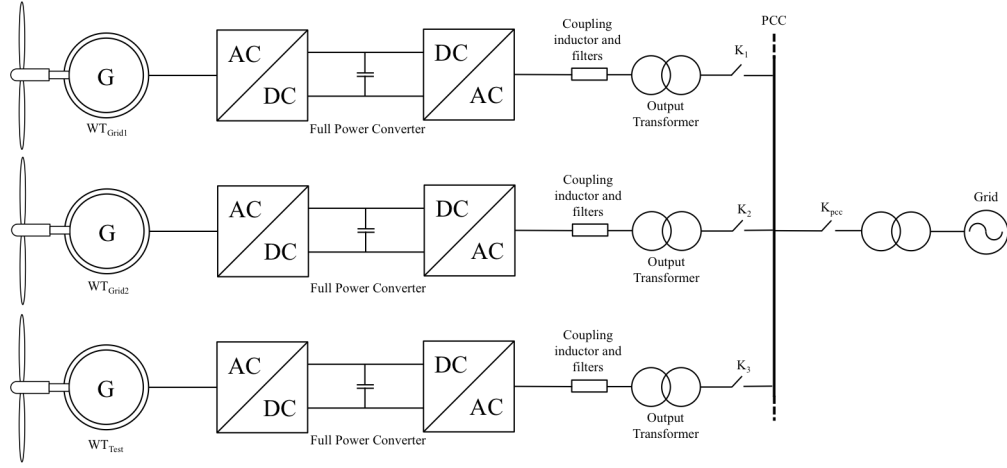


FIGURE 3.1: Wind Farm scheme

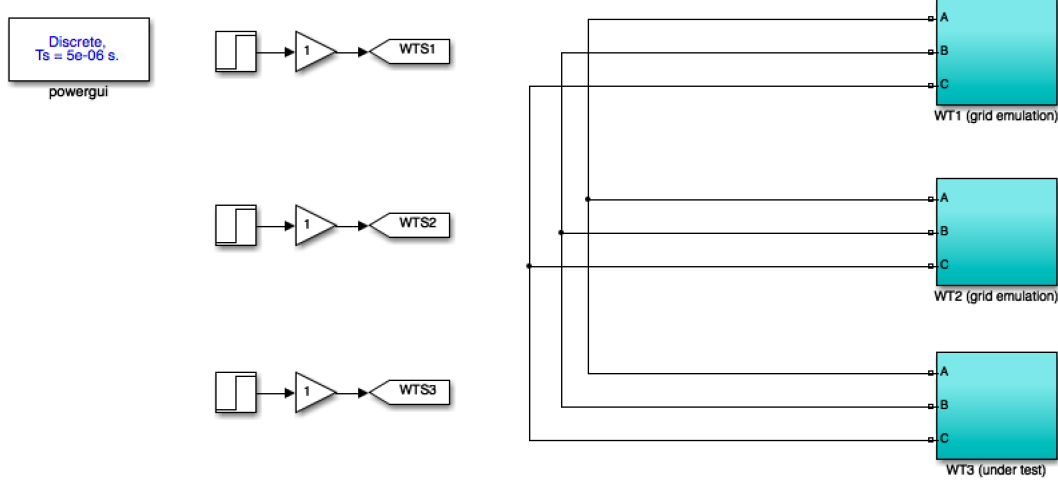


FIGURE 3.2: Wind Farm schematics in MATLAB Simulink

3.2 Analysis of the WTs

We can divide the blocks in each WT in two different categories:

Mechanical components They are in charge of transforming the energy in the form of wind speed to torque, which will rotate the electrical machine.

Electrical components They convert the mechanical torque into electrical current that is later injected into the grid.

Figure 3.3 shows the distinction between these two types of blocks. Inside the blue box are included all the blocks that simulate the mechanical part of the turbine. Inside the green one there are the electrical blocks.

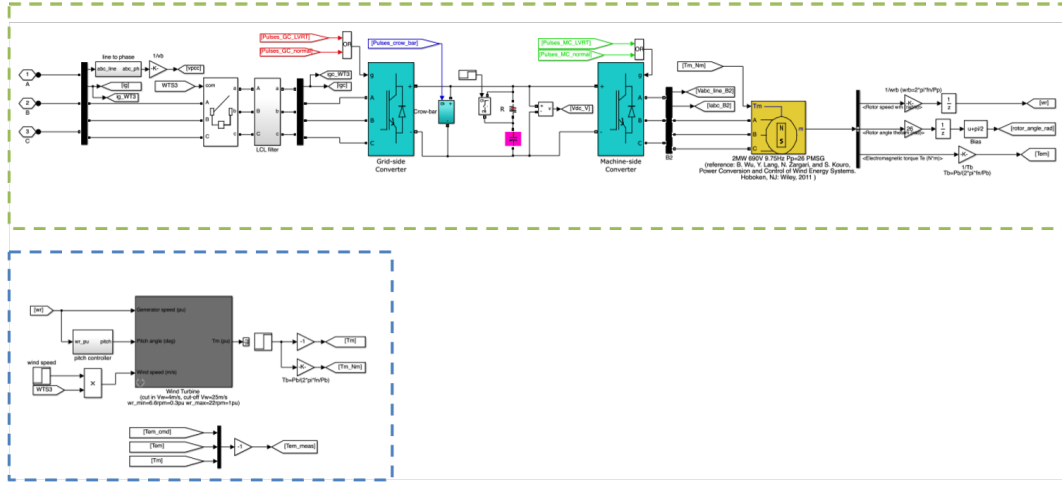


FIGURE 3.3: PMSG Wind Turbine blocks: mechanical and electrical components

3.2.1 Mechanical Components

To implement the mechanical part of the WT, Wind Turbine Simulink® block has been used [26]. This block uses the well known $C_p - \lambda_{WT} - \beta$ curves to define the aerodynamic model of the WT. C_p is the power coefficient, which is a function of both the tip-speed-ratio, λ_{WT} , and the blade pitch angle, β . The tip-speed-ratio is defined as the ratio between the tangential speed of the tip of the blade and the actual velocity of the wind [27] [28] [29]:

$$\lambda = \frac{\omega_r \cdot R}{v_w} \quad (3.1)$$

where R is the blade length in m , ω_r is the wind turbine rotational speed in rad/s , and v_w is the wind speed in m/s . The power coefficient C_p is given by equation 3.2 [29] [30]:

$$C_p(\lambda_{WT}, \beta) = c_1 \cdot \left(\frac{c_2}{\lambda_{WT,i}} - c_3 \cdot \beta - c_4 \right) \cdot e^{-\frac{c_5}{\lambda_i}} + c_6 \cdot \lambda \quad (3.2)$$

and $\lambda_{WT,i}$ is given by equation 3.3 [28] [29] [30]:

$$\frac{1}{\lambda_{WT,i}} = \frac{1}{\lambda_{WT} + c_7 \cdot \beta} - \frac{c_8}{\beta^3 + 1} \quad (3.3)$$

The coefficients from c_1 to c_8 are defined according to Ref. [29] [30].

The $C_p - \lambda_{WT} - \beta$ curves depend on the blade and are given by the manufacturer of the WT. Thus, the performance coefficient C_p of the WT is the mechanical output power of the turbine divided by wind power and a function of wind speed, rotational speed, and pitch angle (β). C_p reaches its maximum value when β equals to zero. Figure 3.4 shows the WT power characteristics for $\beta = 0$. The cut in wind speed for the WT is $V_W = 4m/s$ and the rotor speed is $W_r = 0.3pu$. The cut off wind speed is $V_W = 25m/s$ and cut off rotor speed is $W_r = 1.2pu$.

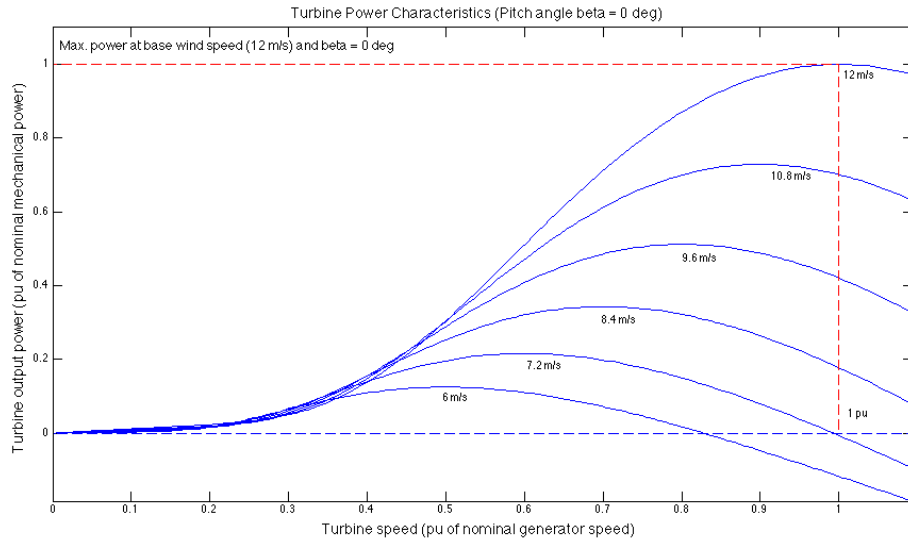


FIGURE 3.4: Power characteristics of the WT for $\beta = 0$

The power transferred from the wind to the turbine can be calculated using equation 3.4 [27] [28] [29]:

$$P_m = \frac{1}{2} \cdot \rho \cdot C_p \cdot r^2 \cdot c_v^3 \quad (3.4)$$

where ρ is the air density in kg/m^3 , C_p is the power coefficient of the WT, r is the radius of the surface covered by WT blades, and c_v is the wind speed in m/s . Therefore, we can obtain the mechanical torque, T_m , using equation 3.5, which is then input into the generator.

$$T_m = \frac{P}{\omega_r} \quad (3.5)$$

3.2.2 Electrical Components

The function of the electrical components is to transform the mechanical energy of the turbine into electrical energy and transport it through the grid so it can be distributed.

All the electrical components are showed in Figure 3.5.

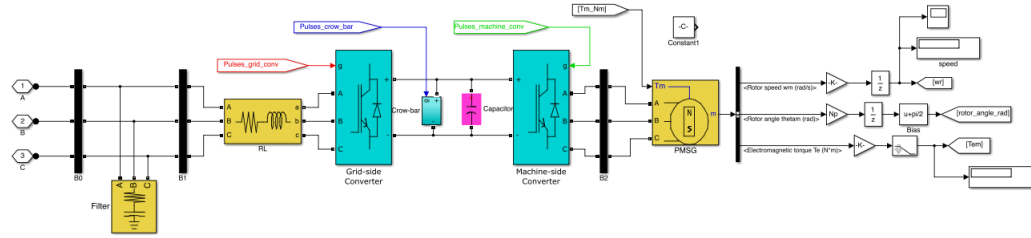


FIGURE 3.5: Electrical components of WT

The electrical motor used is a round rotor 2MW PMSG. The parameters of this motor can be found in Appendix A. The generator is connected to the PCC by means of a two-level back-to-back converter architecture.

A back-to-back converter provides an indirect AC-DC-AC connection in variable speed wind turbines, resulting independence between the rotational speed of the blades and the frequency of the grid connected. This connection gives some advantages: voltage and frequency control of the local grid, improvement of the power quality, and better integration of wind energy to the electrical grid under both steady-state and transient operations [31].

Figure 3.6 [32] shows a two-level back-to-back converter. The back-to-back converter shown consists of two three-phase PWM converters with a common DC-link circuit.

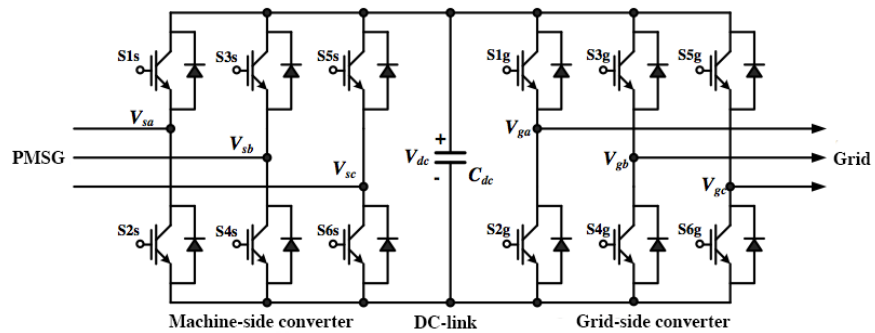


FIGURE 3.6: Circuit configuration of two-level back-to-back converters

In two-level converters a power circuit of three-phase voltage-source back-to-back converters is composed of twelve power semiconductor switches as shown in Figure 3.6,

where the two converters are linked through a DC capacitor. The machine-side converter has three-phase input voltages (V_{sa} , V_{sb} , V_{sc}) and converts them to DC voltage (V_{dc}), which is the input voltage of the grid-side converter, whereas the three-phase voltages (V_{ga} , V_{gb} , V_{gc}) are the output voltages of the grid-side converter [32].

The SPWM technique for modulation is considered [32]. A triangular carrier waveform is compared with the reference sinusoidal waveform at the fundamental frequency of the output voltage. Then, the switching pulses ($S_1; S_2$) for phase A, ($S_3; S_4$) for phase B, and ($S_5; S_6$) for phase C, are generated [31] [33]. The switching states of the switches and the input voltage for three phase converters are listed in Table 3.1.

TABLE 3.1: Switching state of two-level converter

Input voltage	Switching states					
	S_1	S_2	S_3	S_4	S_5	S_6
$+V_{dc}/2$	1	0	0	1	0	0
$+V_{dc}/2$	1	0	0	0	0	1
0	0	0	1	0	0	1
$-V_{dc}/2$	0	1	1	0	0	0
$-V_{dc}/2$	0	1	0	0	1	0
0	0	0	0	1	1	0

Both voltage source converters, grid-side converter and machine-side converter, are connected by a DC-link, which operates at a nominal voltage of 1150 V [29]. A crowbar protection is included in the DC-link to prevent overvoltages that may harm the electrical components [34] [35] [36]. In between the grid-side converter and the PCC there is a LCL filter whose parameters can be found in Appendix B.

3.2.3 Rated Mechanical Torque Selection

Rated mechanical torque of a wind turbine is commonly known as its inertia. Inertia is the resistance of any physical object to any change in its state of motion, including changes to its speed and direction. In other words, it is the tendency of objects to keep moving in a straight line at constant linear velocity.

The main objective of an accurate inertia selection is to have more time to maintain the rotor speed in a rated interval. As long as the WT have a high inertia, it will have more time to keep the rotor speed at an appropriate working value.

The inertia of horizontal-axis wind turbine (HAWT) is defined by equation 3.6 [37]:

$$J_{WT} = m \cdot \left(\frac{L_{blade}}{n_{blades}} \right)^2 \quad (3.6)$$

Supported by the energy stored in the rotor mass (E_{WT}) and the inertia constant (H_{WT}) equations (3.7 and 3.8 respectively), which are used to verify if the inertia is adjusted accurately [37].

$$E_{WT} = \frac{1}{2} \cdot J_{WT} \cdot (\omega_r)^2 \quad (3.7)$$

$$H_{WT} = \frac{E_{WT}}{S_{WT}} \in [5, 8] \quad (3.8)$$

where S_{WT} is the rated apparent power in MVA .

Applying equations 3.6, 3.7 and 3.8 to the parameters of a standard 2.0MW wind turbine given in Appendix A it is possible to calculate J_{WT} , E_{WT} and H_{WT} , obtaining the following results:

$$J_{WT} = m \cdot r^2 = m \cdot \left(\frac{L_{blade}}{n_{blades}} \right)^2 = 40000 \cdot \left(\frac{37.5}{3} \right)^2 = 6.25 \cdot 10^6 \text{ kg} \cdot \text{m}^2$$

$$E_{WT} = \frac{1}{2} \cdot J \cdot (\omega_r)^2 = \frac{1}{2} \cdot (6.25 \cdot 10^6) \cdot \left(\frac{2 \cdot \pi \cdot 9.75}{26} \right)^2 = 1.73 \cdot 10^7 \text{ J}$$

$$H_{WT} = \frac{E_{WT}}{S_{WT}} = \frac{1.73 \cdot 10^7 \text{ J}}{2.2419 \text{ MW}} = 7.73 \in [5, 8]$$

To make sure these results are accurate we have compared them with other 2.0MW WT used in the industry. Table 3.2 shows the comparison between the 2.0MW WT used, two 2.0MW WT manufactured by Vestas and two 2.0 MW WT manufactured by Gamesa. It is possible to observe that the results obtained are in the same order of magnitude than the ones from industry, therefore we can assume they do not have any significant error.

TABLE 3.2: Calculated inertias based on different WT manufacturers

Wind turbine	Manufacturer	$m[\text{kg}]$	$L_{\text{blade}}[\text{m}]$	$J_{\text{WT}}[\text{kg} \cdot \text{m}^2]$
Typical 2.0 MW	Reference [37]	40	37.5	$6.25 \cdot 10^6$
V80-2.0 MW	Vestas Wind Systems	37.5	39	$6.34 \cdot 10^6$
V90-2.0 MW	Vestas Wind Systems	38.1	44	$8.19 \cdot 10^6$
G80-2.0 MW	Gamesa	37	39	$6.25 \cdot 10^6$
G90-2.0 MW	Gamesa	38.4	44	$8.26 \cdot 10^6$

3.3 LVRT Testing Procedure

The LVRT testing procedure section include the steps necessary to carry out the LVRT test. This procedure supposes that in its initial state the wind farm is disconnected from the grid (i.e. PCC is isolated from the grid). This means that the operator of the grid farm has already informed the grid operator company. The procedure can be divided into these distinc parts:

Planning The first part of the LVRT testing procedure is to plan the LVRT test. The parameters of the grid fault should be defined. These parameters are explained in Chapter 5, where the control of all converters is detailed. Multiple LVRT can be scheduled consecutively. Once the parameters are defined, they must be loaded into the control of the Grid WT converters.

Mechanical Startup The goal of this part is to reach the rotor speed at which the LVRT test will be performed (the technical details of the mechanical start-up can be found on Chapter 5). This step is relative slow and takes about 2 or 3 minutes depending on the desired speed.

Electrical Startup Firstly, the grid turbine is prepared. This preparation includes a two-step synchronisation problem that is further discussed in Chapter 5. Secondly, connect the test WT to the PCC and begin the control of its power.

LVRT test Firstly, the grid turbine is prepared. This preparation includes a two-step synchronisation problem that is further discussed in Chapter 5. Secondly, connect the test WT to the PCC and begin the control of its power. Finally, the LVRT test can be performed. The LVRT is formed by the grid fault simulated by the Grid WT and the subsequent recovery. At this point a decision must be made. If more test are needed, start again the electrical startup with the new parameters loaded in the WTs. Otherwise, proceed to the electrical and mechanical shutdown.

A flow chart of the full procedure has been done in order to understand clearly how the testing process is (Figure 3.7).

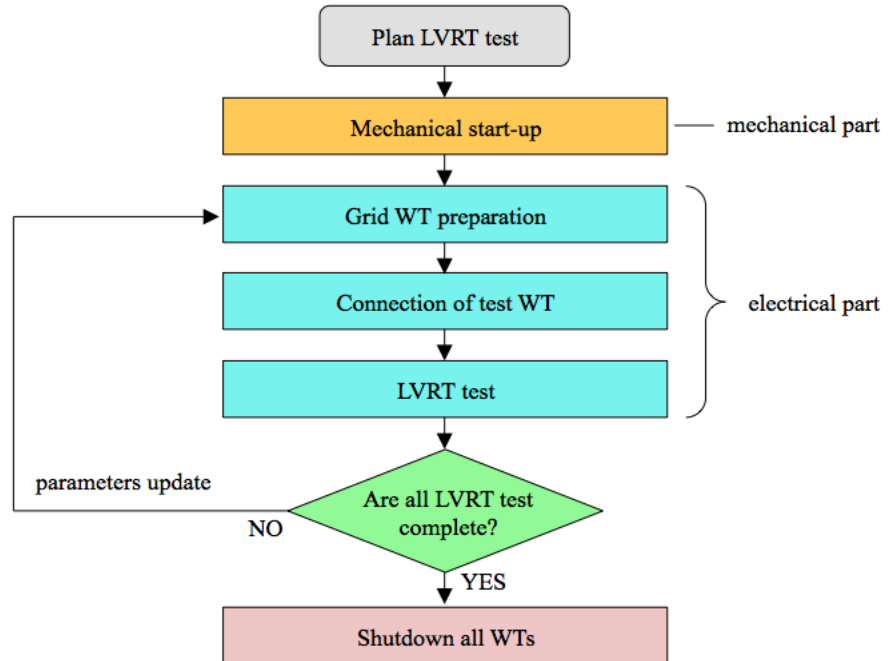


FIGURE 3.7: LVRT testing procedure flow chart

Chapter 4

Test WT Control Strategies

This chapter introduces the control strategies found in the Test WT. In section one, the control for normal mode of operation is explained, for both the grid-side and the machine-side converter. In section two the LVRT control strategy is discussed, also for the grid-side and the machine-side converter.

Normal control and LVRT control are well studied and both have multiple architectures. The aim of this chapter is not to be a discussion of the different ways to control the converters but to present the control architectures used in the simulation.

For each control, we have explained the overall structure and operation. Generally speaking, both Normal Control and LVRT control have a similar structure but oriented towards different goals. This structure is based on two loops, an outer one to control the desired variable and an inner one which is the classical current loop found in most VSCs.

There are also some control elements that are common to all controls and are further discussed in the Appendix D. A filter is used to eliminate noise in all the variables. To obtain the electrical speed and the phase angle we used a PLL control (Appendix D). This information is later used to apply the Park Transformation (Appendix C) to the voltages and currents measured. The current loop, which is used in all converters (grid-side normal, machine-side normal, grid-side LVRT and machine-side LVRT) is also discussed in Appendix D to avoid repetition. Finally, SPWM is used to send the information from the control to the converter.

4.1 Normal Control

The normal control is the control scheme that WTs operate the most time. Its goal is to maximize the power output from the WT injected into the grid. The grid-side converter is responsible for holding the DC-link voltage and ensuring the power balance. The machine-side converter function is to transform the electricity from the three-phase AC generated by the WT to the single phase AC used in the DC-link. To maximize the power output, a speed control scheme is used.

4.1.1 Grid-side Converter for Normal Control

The use of VSC allows controlling two electrical variables in the $qd0$ frame. In the control used, these variables are the active and reactive power, which in the $qd0$ frame can be represented by the currents I_q and I_d respectively (see Appendix C - Park Transformation). The reactive power is usually defined by a higher-level control system (i.e. grid operator). In this case, the active power is set to zero. On the other hand, the active power is used to regulate the DC-link voltage and to ensure power balance.

The control scheme is based in a two-level cascade control system. The higher-level controller, DC-link regulator, deals with the regulation of the DC bus voltage. This voltage regulator is required to ensure the power balance between the power generated by the WT and the power injected into the PCC. Figure 4.1 shows the feed-forward control scheme used. The two inputs are the measured voltage at the DC-link, V_{DC} , and the command voltage, V_{DC}^* , which is 1150 V [29]. The output is the q -reference current command, I_q^* .

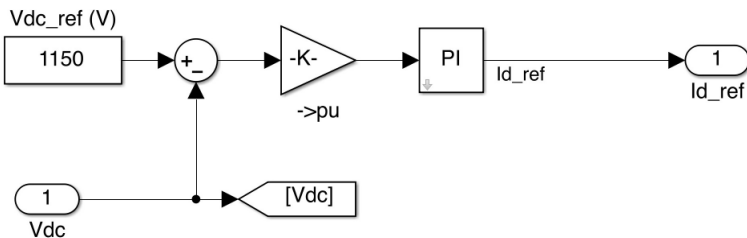


FIGURE 4.1: Voltage regulator control scheme

The lower level of the grid-side VSC control implements that current loop that it is at the center of most VSC control schemes. The details of the current loop can be found in Appendix D [38].

4.1.2 Machine-side Converter for Normal Control

The machine-side converter for normal control is formed by two loops. The outer loop is the speed regulator while the inner loop is the classical current loop found in most converter controls.

The speed control is in charge of regulating the rotor speed for maximum power output. The control is based on Maximum Power Point Tracking (MPPT). The MPPT characteristics of the WT can be obtained from the Wind Turbine block. By calculating the maximum power point for each wind speed, we can find the function that returns the optimal torque for each rotor speed. The MPPT characteristics for the WT used can be seen in Figure 4.2. The control scheme is shown in Figure 4.3.

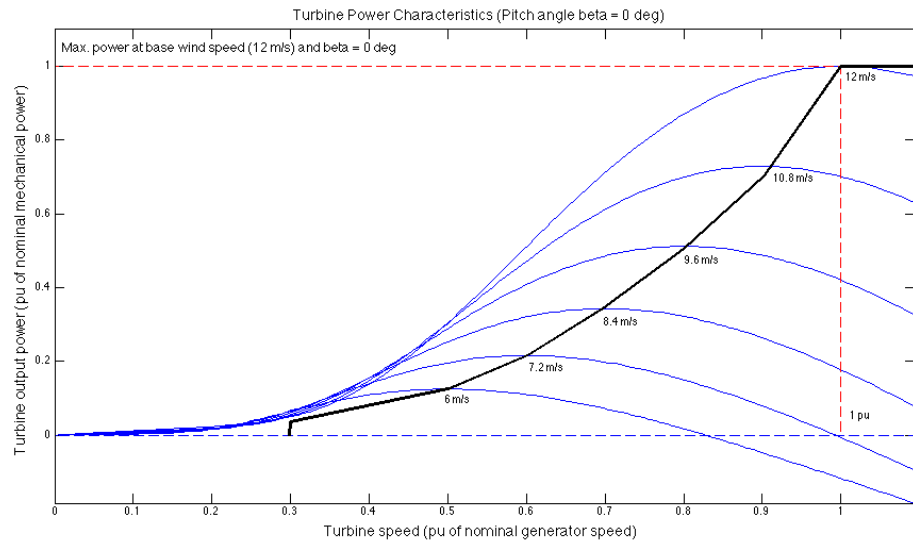


FIGURE 4.2: MPPT characteristics curve

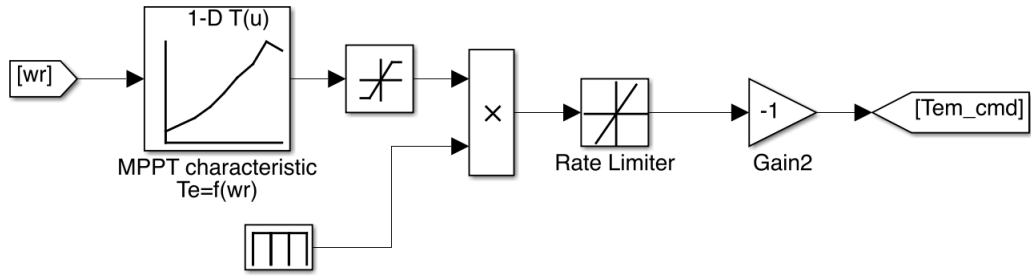


FIGURE 4.3: MPPT control scheme

The inner current loop control is the classical current loop found in most converter controls and it is further explained in Appendix D.

4.2 LVRT Control

The LVRT control is only activated in case of a grid fault. Its aim is to keep the electrical machine operating during the grid fault while inputting reactive power to the grid to help rise the voltage to nominal values. The machine-side converter's goal is to maintain the DC-link voltage constant at nominal value of 1150 V. The grid-side converter is responsible for inputting the reactive power into the grid [39].

4.2.1 Machine-side Converter for LVRT Control

The machine-side converter for LVRT test is a fairly simple control. The goal of this control is to maintain the voltage and the DC-link at the nominal value of 1150 V. The control strategy follows the typical two-loop scheme, where the outer loop calculates the reactive current reference and the inner loop is the current loop.

4.2.2 Grid-side Converter for LVRT Control

The machine-side converter control makes the DC-link voltage constant. This allows to decouple the machine- and grid-side converter controls in steady state. The state-space model in the positive and negative synchronous reference frames for the system is seen in equations 4.1 and 4.2 [28] [39] [40] [41].

$$\begin{cases} \frac{d}{dt} i_{dp} = \omega \cdot i_{qp} - \frac{R_L}{L} \cdot i_{dp} + \frac{1}{L} \cdot v_{VSI dp} - \frac{1}{L} \cdot v_{sdp} \\ \frac{d}{dt} i_{qp} = \omega \cdot i_{dp} - \frac{R_L}{L} \cdot i_{qp} + \frac{1}{L} \cdot v_{VSI qp} - \frac{1}{L} \cdot v_{sqp} \end{cases} \quad (4.1)$$

$$\begin{cases} \frac{d}{dt} i_{dn} = \omega \cdot i_{qn} - \frac{R_L}{L} \cdot i_{dn} + \frac{1}{L} \cdot v_{VSI dpn} - \frac{1}{L} \cdot v_{sdn} \\ \frac{d}{dt} i_{qn} = \omega \cdot i_{dn} - \frac{R_L}{L} \cdot i_{qn} + \frac{1}{L} \cdot v_{VSI qn} - \frac{1}{L} \cdot v_{sqn} \end{cases} \quad (4.2)$$

where

- i_{dp}, i_{qp} positive-sequence dq grid currents;
- i_{dn}, i_{qn} negative-sequence dq grid currents;
- $v_{VSI dp}, v_{VSI qp}$ positive-sequence dq voltage generated at inverter terminals;
- $v_{VSI dn}, v_{VSI qn}$ negative-sequence dq voltage generated at inverter terminals;
- v_{sdp}, v_{sqp} positive-sequence dq grid voltage;
- v_{sdn}, v_{sqn} negative-sequence dq grid voltage;

The grid-side converter for LVRT is based on the vector current controller with feed-forward of negative-sequence grid voltage (VCCF). The current controller is implemented in the positive reference frame, while the negative-sequence grid voltage is fed-forward and added to the reference voltage given by the controller. Therefore, the voltage generated by the converter has exactly the same negative-sequence voltage as the grid voltage, and only positive-sequence currents (hence, balanced) flow to the grid through the filter. Current references can be easily calculated from active and reactive power references in the positive reference frame. The control scheme of this control is shown in Figure 4.4 [39] and the Matlab implementation in Figure 4.5.

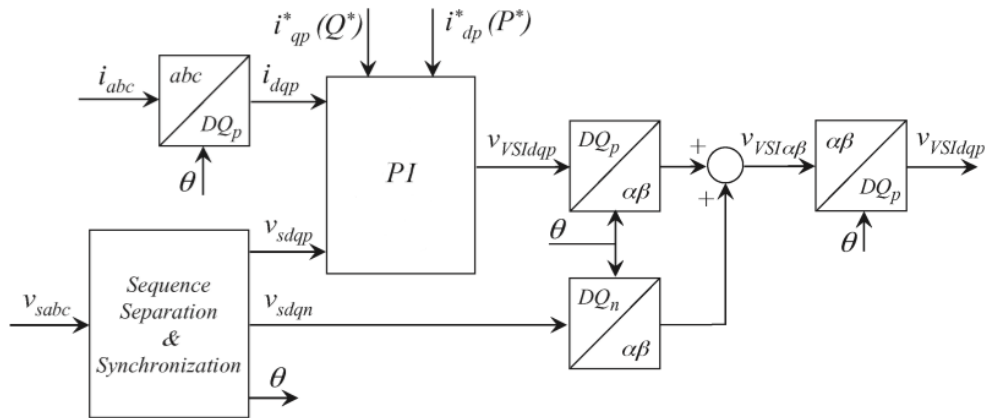


FIGURE 4.4: VCCF control scheme

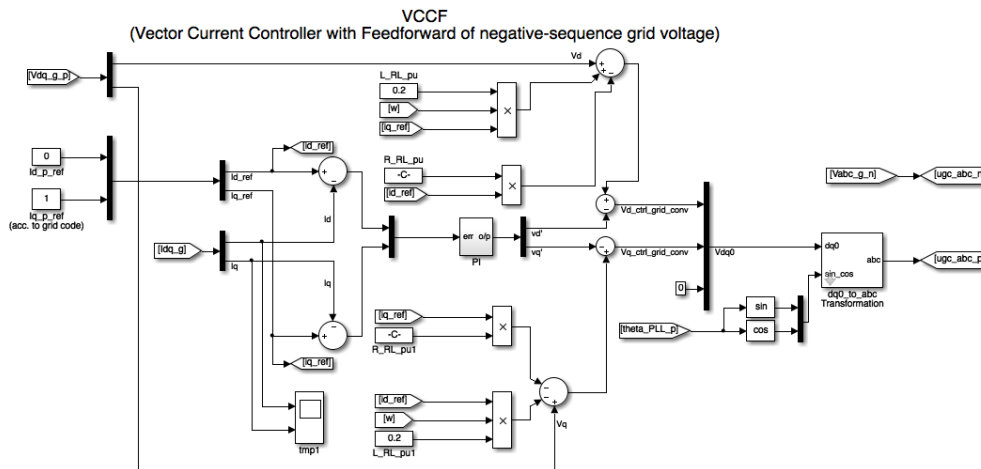


FIGURE 4.5: VCCF Control implemented in MATLAB Simulink

Chapter 5

Grid WT Control Strategies

In this chapter the characteristics of the new LVRT test control are explained. The aim of this control is to simulate a grid fault taking into consideration the type of grid fault, its severity and the network impedance.

Section one and two present the machine-side control and grid-side control respectively. In section three the details to create a network impedance emulation are detailed. In section four we introduce the parallel control which will allow the use of several WTs to simulate the grid. Finally, in the last section we deal with the control and limitation of over-speeding the rotor.

Altogether we have used 5 different VSC control strategies on top of normal control which is used by all VSC. Figure 5.1 and Table 5.1 shows the arrangement of these controls in the Wind Farm during the LVRT test. In yellow is the grid-side LVRT control which is used in the Test WT and its goal is to inject the necessary reactive power during the grid fault. The orange control represents the machine-side LVRT control. Green, blue and red are the new control schemes developed. In green is the machine-side grid emulating in parallel which is very similar to the machine-side LVRT control. In blue is the grid-side grid emulating in parallel which is used to set the grid fault voltage. Finally, in green is the grid-side grid emulating in parallel with synchronisation which is responsible for the synchronisation process of the Grid WT.

TABLE 5.1: Different VSC control strategies used in the Wind Farm

Color	Control	VSC	Goal	Chapter
Yellow	Grid-side LVRT	Grid-side WT_{Test}	Output reactive power	4.2.2
Orange	Machine-side LVRT	Machine-side WT_{Test}	Hold DC-link voltage	4.2.1
Green	Machine-side grid emulating in parallel	Machine-side WT_{Grid1} and WT_{Grid2}	Hold DC-link voltage	5.1
Blue	Grid-side grid emulating in parallel	Grid-side WT_{Grid1}	Create grid fault	5.2
Red	Grid-side grid emulating in parallel with synchronisation	Grid-side WT_{Grid2}	Synchronize Grid WTs and create grid fault	5.4

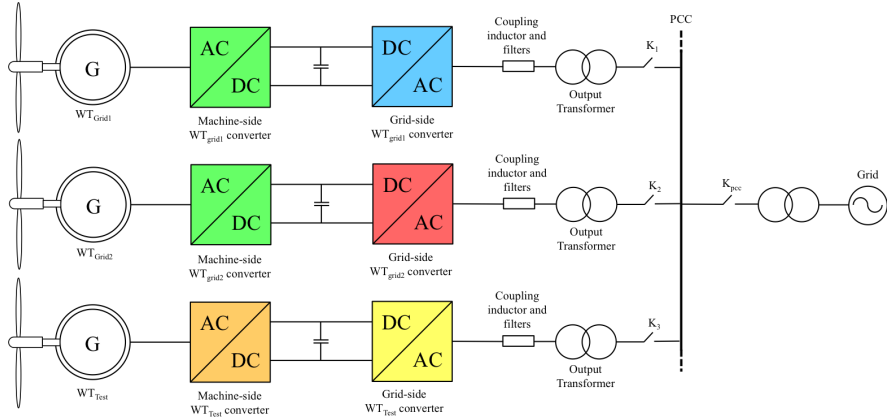


FIGURE 5.1: Differenrent VSC control strategies used in the Wind Farm

5.1 Machine-side Converter for Grid Emulating Control

The machine-side converter is very similar to the LVRT machine-side converter. The control goal of machine-side converter is to maintain the voltage in the DC-link. The control scheme is similar to the one used in normal operation and contains two control loops. As shown in Figure 5.3 , the inner loop is the standard current loop found on most converter controls. However, the outer loop (show in Figure 5.2) controls the DC-link voltage instead of the electromagnetic torque, as is the case in Normal Control [38]. Thus, a constant DC-link voltage can be achieved by keeping power balance between the grid-side and machine-side converters.

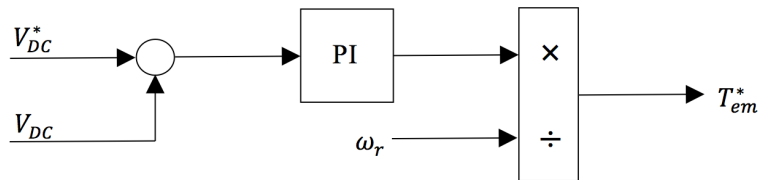


FIGURE 5.2: Outer control loop for machine-side converter for grid emulation control

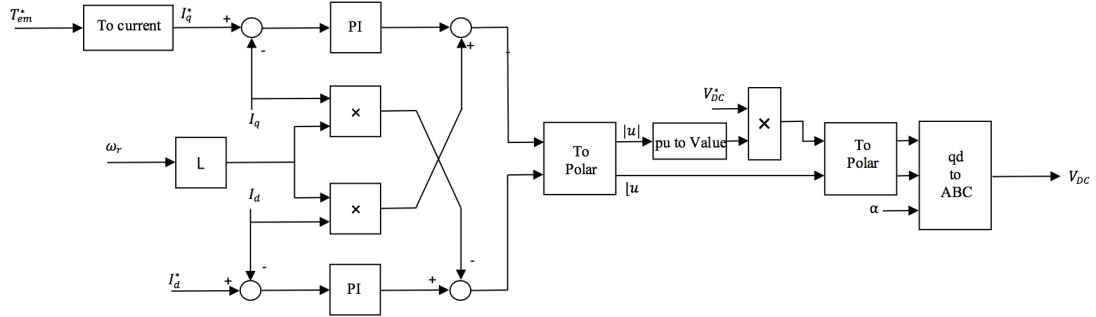


FIGURE 5.3: Inner control loop for machine-side converter for grid emulation control

5.2 Grid-side Converter for Grid Emulating Control

The grid-side converter of WT_{Grid1} is responsible for the control of the grid-side voltage. It has to be able to simulate all four types of grid faults. Figure 5.4 shows the distribution of a grid fault and the wind farm in the grid. The line connecting all the WTs inside the wind farm is known as Point of Common Coupling (PCC). The wind farm connects to the grid at the Grid Connection Point (GCP). Z_F is the line impedance between the fault and GCP. Z_{WF} is the line impedance between GCP and PCC. Z_S is the grid impedance. V_G is the grid voltage.

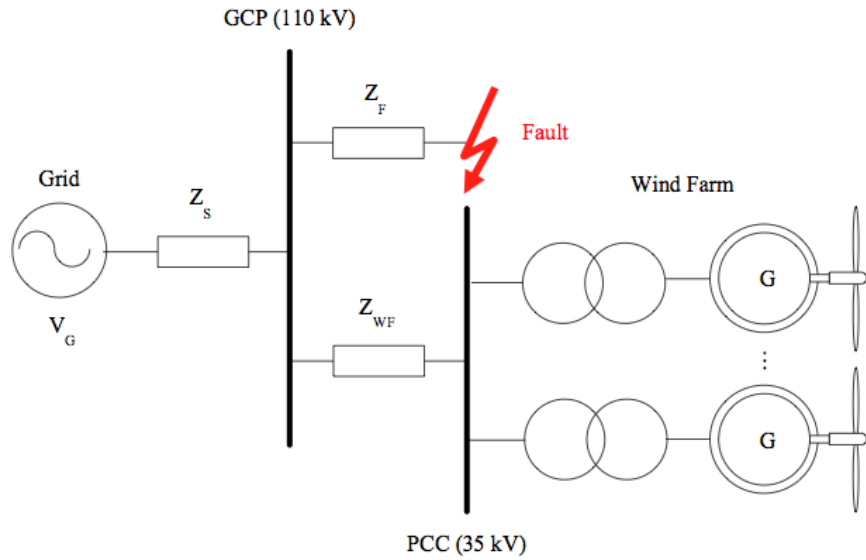


FIGURE 5.4: Typical diagram of the power system integrated with wind farm

From [8] it is known that the equations to calculate the voltage during a grid fault at the Grid Connection Point (GCP) are a function of two parameters: the impedance angle

α and the fault distance λ . The impedance angle α is fixed for any given source-fault impedance combination and its values are usually between -60° and 0° [8]. The fault distance λ is the relative distance between the fault and the wind farm. The equations and control schemes for each of the grid fault types are detailed in the following subsections. Using these equation it is possible to simulate any type of fault by changing its parameters. Thus, with a 3-phase PWM generator, these signals can be sent to the converter and no further control is required.

5.2.1 3phG Fault ($3\phi - g$)

It is the only symmetrical fault where all three phases connect to the ground resulting in a sudden drop in voltage. The voltage at the GCP only has the positive-sequence component, which is

$$V_{gcp} = V_g \cdot \frac{Z_f}{Z_s + Z_f} = V_g \cdot \frac{\lambda e^{j\alpha}}{1 + \lambda e^{j\alpha}} \quad (5.1)$$

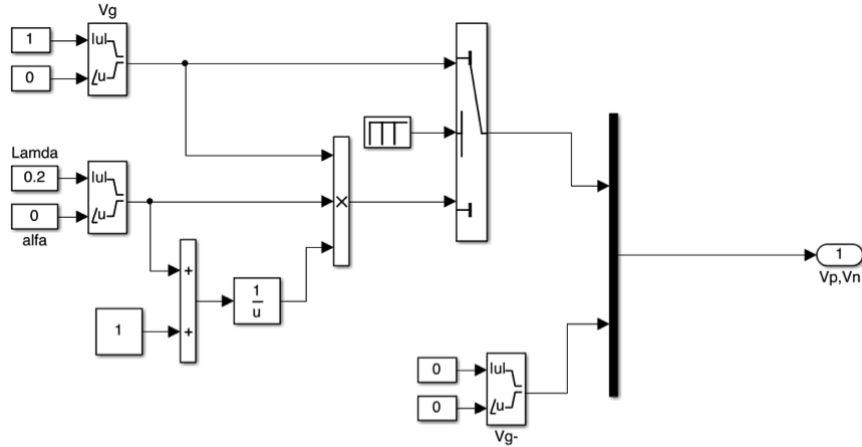


FIGURE 5.5: 3phG fault MATLAB Simulink schematics

5.2.2 1phG Fault ($\phi - g$)

It is an asymmetrical fault where one phase connects to ground, and thus has different positive- and negative-sequence components. The voltage at GCP is defined as,

$$\begin{cases} \vec{V}_{gcp} = \vec{V}_+ + \vec{V}_- \\ \vec{V}_+ = \frac{1}{3} \cdot \vec{V}_g \cdot \left(3 - \frac{1}{1+\lambda \cdot e^{j\alpha}} \right) \\ \vec{V}_- = -\frac{1}{3} \cdot \vec{V}_g \cdot \left(\frac{1}{1+\lambda \cdot e^{j\alpha}} \right) \end{cases} \quad (5.2)$$

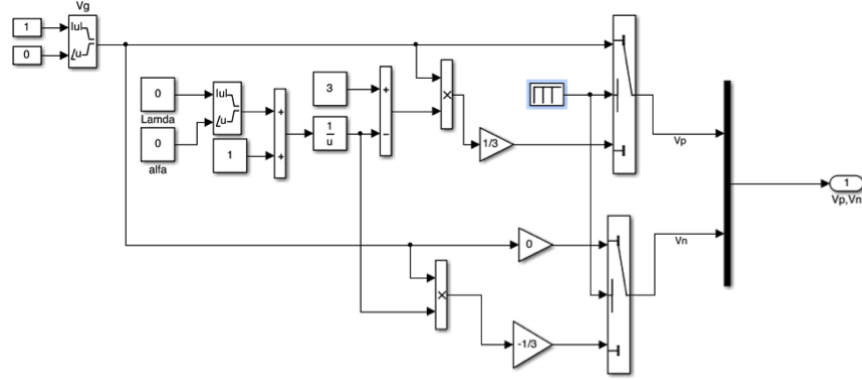


FIGURE 5.6: 1phG fault MATLAB Simulink schematics

5.2.3 2ph Fault (2ϕ)

This asymmetrical fault is characterised by the short-circuit of two of the three phases. The voltage at GCP is defined by,

$$\begin{cases} \vec{V}_{gcp} = \vec{V}_+ + \vec{V}_- \\ \vec{V}_+ = \vec{V}_g \cdot \left(1 - \frac{1}{2} \cdot \frac{1}{1+\lambda \cdot e^{j\alpha}} \right) \\ \vec{V}_- = \frac{1}{2} \cdot \vec{V}_g \cdot \left(\frac{1}{1+\lambda \cdot e^{j\alpha}} \right) \end{cases} \quad (5.3)$$

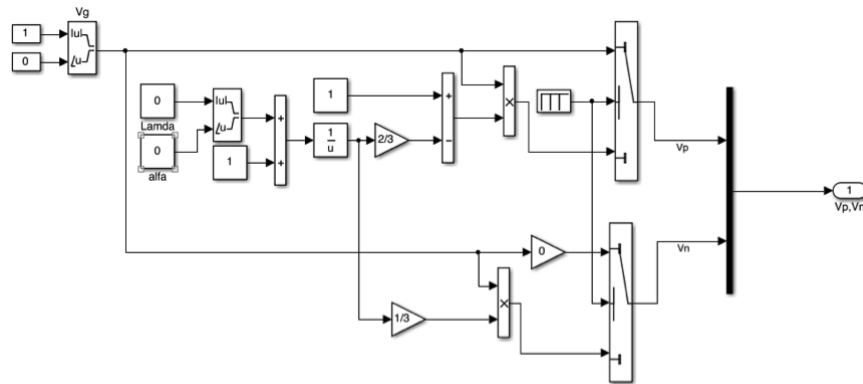


FIGURE 5.7: 2phG fault MATLAB Simulink schematics

5.2.4 2phG Fault ($2\phi - g$)

This asymmetrical fault occurs when two of the phases connect to the ground.

$$\begin{cases} \vec{V}_{gcp} = \vec{V}_+ + \vec{V}_- \\ \vec{V}_+ = \vec{V}_g \cdot \left(1 - \frac{2}{3} \cdot \frac{1}{1+\lambda \cdot e^{j\alpha}}\right) \\ \vec{V}_- = \frac{1}{3} \cdot \vec{V}_g \cdot \left(\frac{1}{1+\lambda \cdot e^{j\alpha}}\right) \end{cases} \quad (5.4)$$

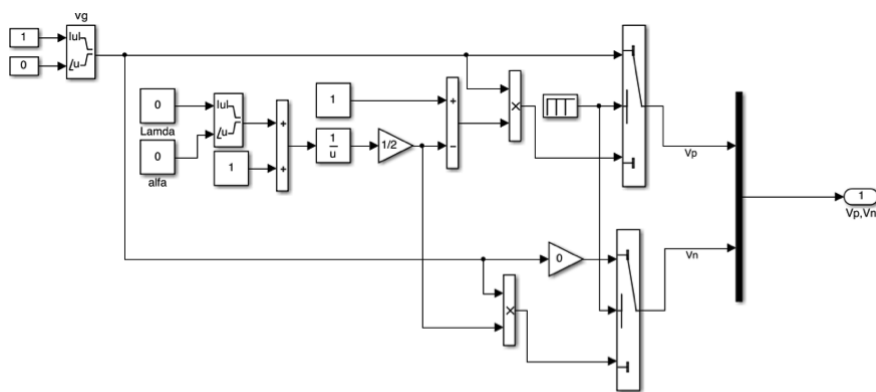


FIGURE 5.8: 2ph fault MATLAB Simulink schematics

5.3 Grid-Side Converter for Network Impedance Emulation Control

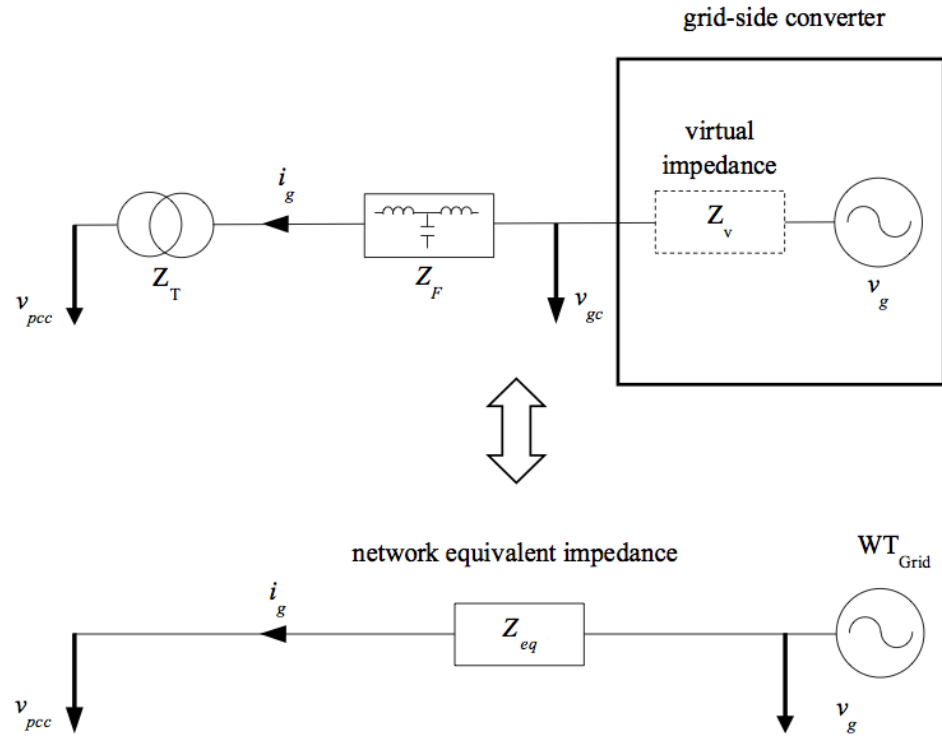


FIGURE 5.9: Principle of grid impedance emulation

The proposed LVRT testing method is also capable of simulating different network impedances (i.e. the total impedance between the location of the fault and the PCC). This impedance is simulated using the filter and the grid-side converter as seen in Figure 5.9. Thus, the converter is emulating an ideal voltage source and a virtual impedance, which can have negative values if needed.

The filter used is a LCL whose values can be found in Appendix B. To calculate the virtual impedance simulated by the converter, the LCL filter has been approximated as a filter with no C (i.e. only two inductances), since the value of C is much larger than of the inductances. The voltage of the virtual ideal voltage source can be calculated using equation 5.5 while the virtual impedances is derived from equation 5.6.

$$\vec{V}_{gc} = \vec{V}_g - \vec{I}_{gc} \cdot Z_V \quad (5.5)$$

$$Z_V = Z_T + Z_F - Z_{eq} \quad (5.6)$$

5.4 Parallel Control for Grid Emulation

Previous literature on converter based LVRT simulating systems has shown that the grid WT converters have to be considerably larger than the converters in the test WT. Since typically all WTs in a wind farm are equal, the sizes of the converters are the same [10]. There are two reasons why multiple converters are needed. Firstly, the capacity of the emulated grid is constrained by 5.7 to ensure the electrical safety during a LVRT test. Secondly, if the test is too long, the energy output through the rotor of the grid simulating WT might accelerate it to dangerous speeds, which may cause permanent damage to the hardware [42]. By using two WTs, the power is distributed equally. Therefore a parallel control of multiple WTs is needed to simulate the grid and to distribute the power equally between these WTs.

$$S_{WTgrid} \geq S_{WTtest} \quad (5.7)$$

There exist two main control strategies for converters operating in parallel but none of them is suitable for the proposed method. The master-slave control requires a high-speed transfer of information between the converters. Current wind farms do not have high-speed connection installed and using this control strategy would require hardware modifications. Since the goal of the method proposed is to not require any additional hardware, this method cannot be used.

On the other hand, there is the autonomous parallel control, where the converters operate independently. This method is mainly used in micro-grids where the characteristics of the load are well known. Moreover, this control strategy can only be applied during steady-state operation. In the proposed method, there is not a defined load and, due to the nature of LVRT, the wind farm operates in transient-state mode. Thus, the autonomous parallel control cannot be applied either.

A hybrid solution by the name of *Voltage Synchronized Autonomous Control* is proposed.

5.4.1 Voltage Synchronized Autonomous Control

In the voltage synchronized autonomous control the grid-side converters of each of WT work independently, as shown in Figure 6.15. Since the value of the ideal voltage source

and virtual impedance are known for every WT, the only piece of information missing is the angle between them. Therefore a synchronisation process is needed to avoid the existence of circular currents.

The goal of this control is to distribute, as needed, the amount of current that flows through each of the grid WTs. As shown in Figure 6.15, once the phase error is eliminated, the current shared between WTs is only decided by the equivalent impedance of each converter. According to the circuit theory, higher impedance leads to smaller current. If the values of the ideal voltage source and the virtual impedance are the same for each of the WTs, the current flowing through each of them will be equal. However, this has not to be the only case. By modifying the impedance values, it is possible to control the amount of current through each WT.

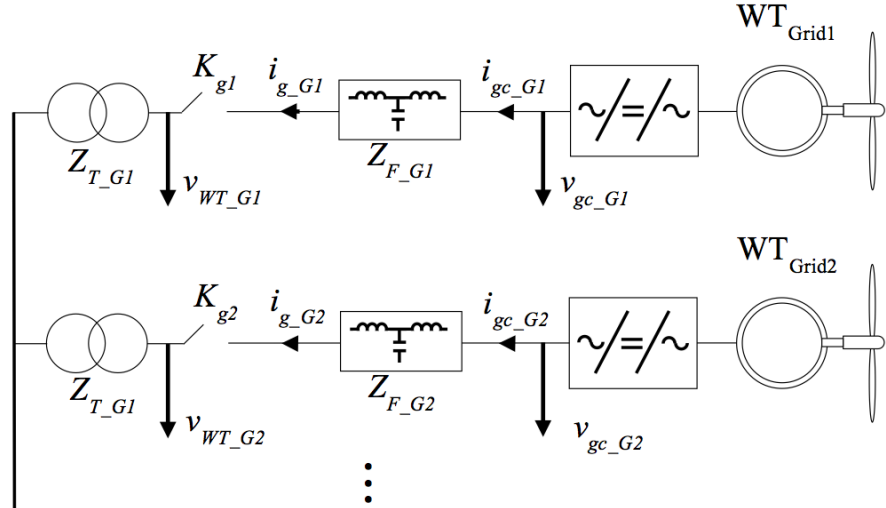


FIGURE 5.10: Configuration of grid WTs in parallel

5.4.2 Voltage Synchronisation of Grid WTs

To avoid the existence of circular currents, the phase difference between the grid WTs should be zero. A special process called voltage synchronisation must be carried out before the LVRT test. The synchronisation has two steps.

In the first step, or initial synchronisation, WT_{Grid1} is started up and connected to the PCC. Then, before turning K_{g2} on, WT_{Grid2} measures the voltage at PCC v_{PCC} . Since there's no current flowing in WT_{Grid1} , the measured voltage at PCC is the same as

v_{gcp1} (the grid voltage of WT_{Grid1}). Of course, some phase difference may still remain in practice due to the measure error. Figure 5.11 shows the circular current that might appear and its representation in the vector space.

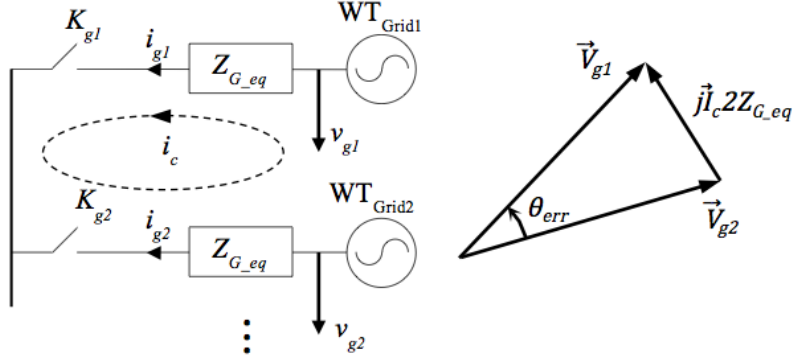


FIGURE 5.11: Principle of grid WT voltage synchronization

In the first step, or initial synchronisation, WT_{Grid1} starts up and is connected to the PCC. Then, before turning K_{g2} on, WT_{Grid2} measures the voltage at PCC. Since there is no current flowing through PCC, the voltage at PCC is the same as the voltage in the grid-side converter.

The second step of the voltage synchronisation is the PLL track process. The goal of this control loop is to cancel the error of v_{g2} (WT_{Grid2}) by eliminating the circular current between WT_{Grid1} and WT_{Grid2} when WT_{Test} is off. The basic idea is to cancel the circular current i_g between WT_{Grid1} and WT_{Grid2} by adjusting the phase angle of WT_{Grid2} using a PI feedback control. Since i_g is not measured directly in the LCL filter (Figure 5.12), the grid-side converter current i_{gc} is controlled correspondingly to its no-load value i_{gc0} according to 5.8. A Band-Pass Filter (BPF) is used to filter out the current harmonics. Starting from θ_{g20} (which is the result of step 1), the phase angle will gradually approach the command value. Once the current error is smaller than a threshold (i.e. 0.02pu), the synchronization is complete and the phase angle of WT_{Grid2} will be fixed at the final value during the subsequent LVRT test. It is noted that, the $d(\Delta I)/dt$ must be kept under zero during the PLL tracking process. Otherwise, it means the voltage of WT_{Grid2} leads the voltage of WT_{Grid1} and the sign of PI must be reversed. The schematics of this control can be seen in Figure 5.13.

$$Z_{F0} = R_{FY} + j\omega - \frac{1}{j\omega C_{FY}} \quad (5.8)$$

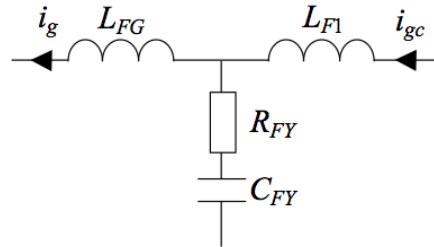


FIGURE 5.12: Equivalent circuit of LCL filter

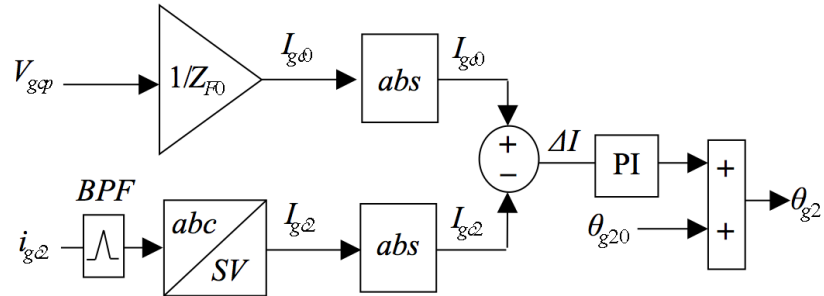


FIGURE 5.13: PLL tracker control scheme

5.5 Speed Control and Limitations of WTs

During a LVRT test, both grid and test WTs are required to run at a set speed (i.e. 0.4pu-1pu), so that the kinetic energy stored in turbines can be used to perform the LVRT test. For the test WT, it is required to run at any given speed according to the testing conditions. On the other hand, the grid WT(s) should have the capability to absorb the electrical power generated by the test WT during a LVRT test at a safe speed.

5.5.1 WT Speed Regulation with Pitch Control

Since the aforementioned machine-side converter is used to control the DC-link voltage, the speed of the WT can only be regulated by the pitch control during the test. Unlike

the conventional normal operation, in which the pitch control will not be activated until the wind speed or turbine speed exceed the rated value, in the LVRT test the pitch control is enabled at the beginning of WT start-up. Although the existing close-loop pitch control can be applied directly with some modifications, an open-loop control strategy is presented here for safety and simplification considerations.

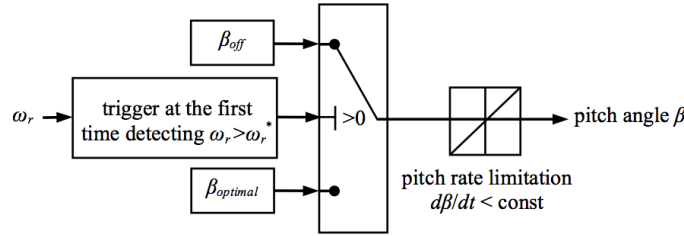


FIGURE 5.14: Block diagram of pitch-controller for WT speed regulation

As shown in the control block diagram in Figure 5.14, it is devised that the pitch is initialized as the optimal angle of attack (typically 0°) to start-up the turbine as soon as possible. Once the rotational speed reaches the reference value, the blade will be pitched completely out of the direction of the wind rapidly at a limited rate (e.g. $7^\circ/\text{s}$) and then no wind power is captured. When all the WTs operate at the required speeds, the LVRT test is ready to go and will be finished shortly (typically 2-3s). After that, the WTs enter the shut-down mode and stop in the end. It is noted that the open-loop control may cause some speed overshoot due to the limited rate at which the blade pitches out. However, this might not be a problem in a real system, because the requirement for speed accuracy is not high and also the controller can wait for the WT to slow down gradually with the effect of system damping. When the speed decreases to the reference value, the LVRT test is ready to be activated.

5.5.2 Speed Operation Range and Limitation

As discussed previously, the speed of the test WT, $\omega_{r,test}$, is decided according to the test condition (typically, 0.4pu-1pu). At the same time, the speed of the grid WT needs to be controlled coordinately as expressed in 5.9, which is decided for safety reasons with two main considerations.

$$\omega_{r,grid}^* \geq \omega_{r,test}^*/N_{WT,grid} \leq 1 \text{ pu} \quad (5.9)$$

where $N_{WT_{grid}}$ is the number of grid WTs in parallel.

Firstly, the speed is constrained by the current rating of the machine-side converter. Assuming the current sharing evenly in the parallel grid WTs and the control performance of machine-side converter is perfect, the power being handled by the machine-side converter can be expressed as equation 5.10, where $T_e = 1$ pu in the worst scenario. Since the voltage of PMSG is proportional to the rotational speed, then the speed with $\omega_{r_test}/N_{WT_{grid}}$ is the minimum requirement to ensure the converter and generator are not being overloaded. In practice, some margin might be needed for safe operation.

$$P_{MC_grid} = P_{test}/N_{WT_{grid}} = T_e \cdot \omega_{r_test}^* \quad (5.10)$$

Secondly, over-speeding is prohibited any time to prevent the turbine from mechanical damage. During a LVRT test, the grid WT(s) will be accelerated by the energy absorbing from the test WT. In the worst scenario, a rated power of test WT ($P_{test} = 1$ pu) can be imported to the grid WT(s). The only way to limit the speed rise is to reduce the test time, which is approximately proportional to the energy. Thanks to the fast response of converter electrical control (typically less than 100ms), the test time T_{test} can be set to less than several seconds.

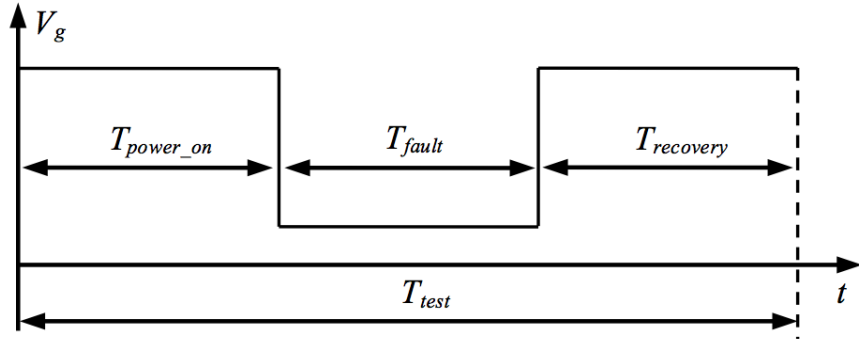


FIGURE 5.15: Time sequences of LVRT test

$$\omega_{r_grid} = \frac{1}{J} \cdot \int T_{e_grid} dt \approx \frac{1}{J} \cdot \int \frac{P_{test}}{N_{WT_{grid}} \cdot \omega_{r_grid}} dt \quad (5.11)$$

As shown in Figure 5.15, the test time consists of three parts including the power-on, fault ride-through and fault recovery. Once the test finishes, the power of all WTs will be switched-off as soon as possible and then the WTs will slow down gradually. According to the mechanical dynamic equation 5.11, a theoretic calculation for a typical 2MW WT

with the inertia time constant $H=8.5\text{s}$ and $T_{test}=3\text{s}$ can be made. The calculated speed rise is less than $0.2 \text{ pu} / N_{WT_{grid}}$ in the worst scenario ($P_{test}=1 \text{ pu}$, $N_{WT_{grid}} = 1$ and $\omega_{test} = 1 \text{ pu}$). This means that the grid WT can operate in safe range with a speed not exceeding 1.2 pu . Moreover, since the fault voltage drops significantly, by ignoring the small active power during the fault (part 2) the maximum speed could even lower.

Chapter 6

Simulation Study

To prove the validity of the proposed method we have developed a MATLAB Simulink® simulation. The simulation has been tested in different scenarios and under different conditions to test all the features of the system. The wind farm modelled is a three WT farm, where WT_{Grid1} and WT_{Grid2} operate as the grid simulating wind turbines. WT_{Test} is the WT under the LVRT test.

6.1 Process of LVRT Testing

In this section we have simulated the electrical part of the procedure. Table 6.1 shows the list and description of each of the events in the LVRT testing procedure. These events have been plotted in the timeline in figure 6.1. The results of the simulation can be checked in Figures 6.2a, 6.2b and 6.3a.

In Figures 6.2 and 6.3 a 1phG grid fault with $\alpha = 0$, $\lambda = 0$ and $Z_{eq} = 0.2$ has been simulated. We have chosen to simulate a 1phG since it is the most common type of fault.

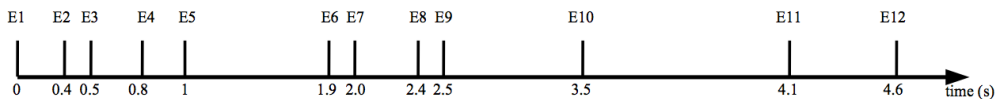


FIGURE 6.1: Timeline of events in the LVRT testing procedure

TABLE 6.1: Events in the LVRT testing procedure

Event	Time(s)	Description
E1	0.0	WT_{Grid1} switch on and connected to PCC
E2	0.4	Switch off the DC capacitor charge current protection resistors of WT_{Grid1} and WT_{Grid1}
E3	0.5	Activation of the machine-side converters of WT_{Grid1} and WT_{Grid2} for DC voltage control
E4	0.8	Activation of the grid-side converter of WT_{Grid1} to provide grid voltage
E5	1.0	WT_{Grid2} switch on and synchronization
E6	1.9	WT_{Grid1} synchronization finish
E7	2.0	Switch on WT_{Test}
E8	2.4	Activation of the grid-side converter of WT_{Test} to control DC voltage
E9	2.5	Activation of the machine-side converter of WT_{Test} to control power
E10	3.5	Start of LVRT
E11	4.1	Recovery of LVRT
E12	4.6	LVRT test finish

6.1.1 Grid WT

We have simulated two WTs operating as Grid WTs to be able to test all the features of the new method. By using two WTs, we can evaluate the performance of the parallel control and the synchronisation process and make sure everything works correctly. Figure 6.2 shows the results for both Grid WTs, where the left column shows the parameters of the grid-side converter and the right column the parameters of the machine-side. It can be clearly seen that all parameters behave as expected. In V_{PCC} the grid fault occurs during the 3.5 s to 4.1 s as specified by the LVRT test conditions. The current flowing through the WT does not exceed 1 pu, and the voltage and the DC-link perform at acceptable levels. There is a drop in active power and a decrease in the reactive power during the grid fault that complies with the LVRT grid code requirements. It is also important to note the presence of second order harmonics due to the unbalanced nature of a 1phG grid fault.

On the machine side, the rotor speed accelerates due to the new input of power but stays at acceptable levels. There is a negative torque before the grid fault which is also caused by the power generated by WT_{Test} .

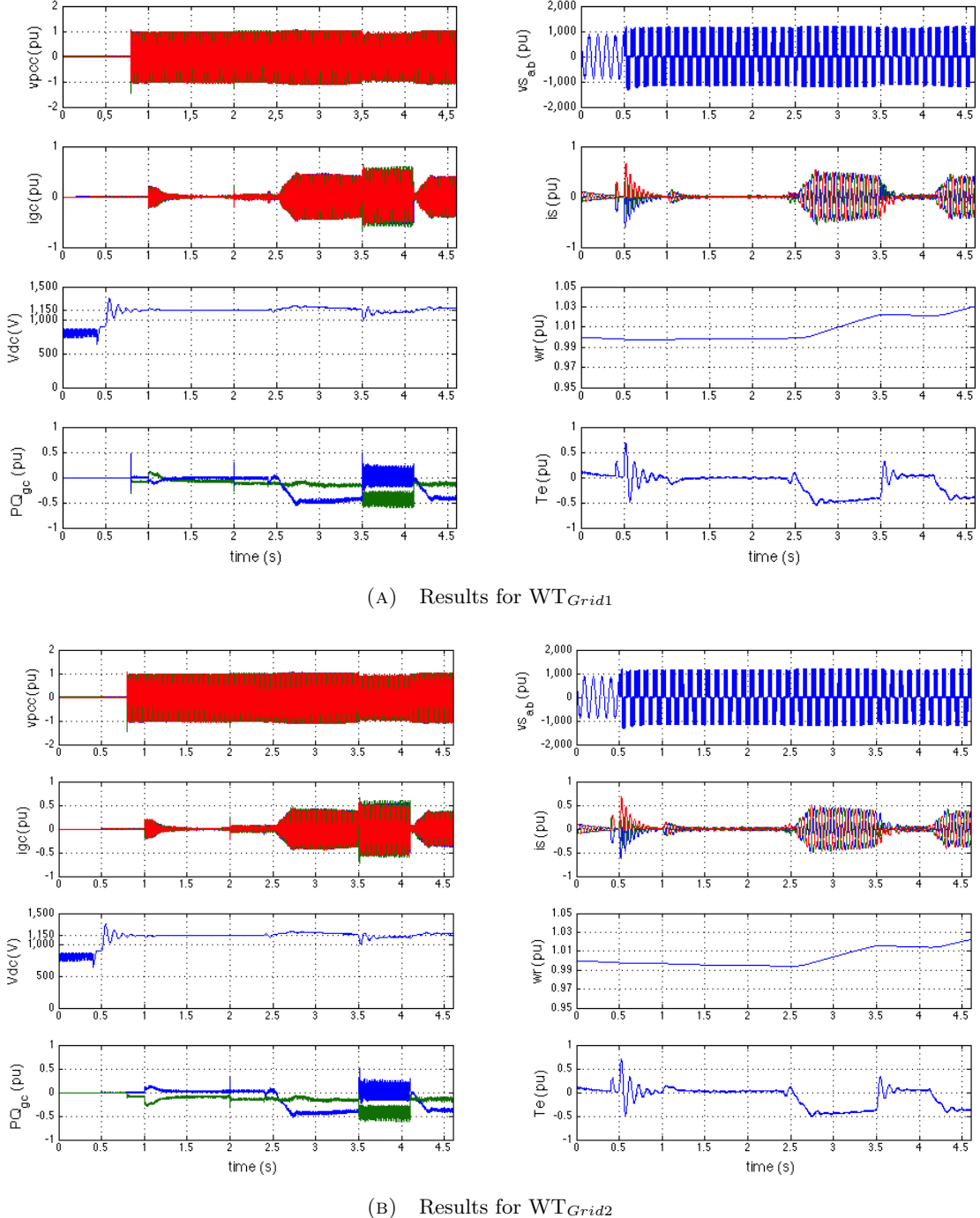


FIGURE 6.2: The process of a LVRT testing for grid emulating WTs (conditions: 1phG fault, $\alpha=0$, $\lambda=0$, $Z_{eq}=0.2$)

6.1.2 Test WT

Figure 6.3 shows the results for Test WT. V_{PCC} is common to all three WTs. The current flowing through the grid-side converter is the sum of the two currents from the Grid WT. The DC-link voltage remains stable during the whole test, except for a small

peak at the beginning. From the graph showing the active and reactive power we can conclude that the converter can successfully swap the power output from active to reactive when the grid fault starts.

Regarding the machine-side converter, there is a decrease in the rotor speed and rotor during the grid fault. All in all, the parameters behave according to what is expected.

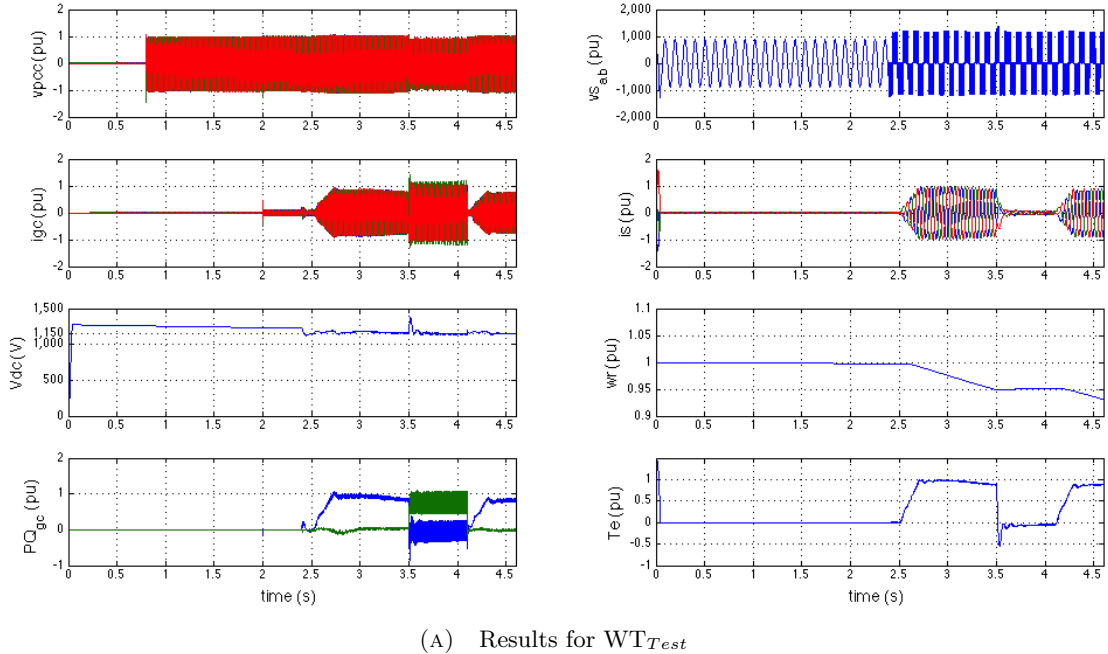


FIGURE 6.3: The process of a LVRT testing for under-test WT (conditions: 1phG fault, $\alpha=0$, $\lambda=0$, $Z_{eq}=0.2$)

6.2 LVRT Testing under Different Grid Faults

The aim of this section is to show the capability of the method by simulating all four types of grid fault. In the first step, we simulate each of the the grid faults (3phG, 2phG, 2ph and 1phG). Each subsection includes a close up graph of V_{PCC} to check the type of grid fault and a close up graph of the current of $WT_{Grid1} I_{C,Grid1}$ to see the response of the Grid WT under the LVRT test.

We have simulated each of the grid faults under the following condition: $\alpha = 0$, $\lambda = 0$ and no Z_{eq} compensation. The results are showed below. It is important to note how fast the grid converters can simulate a grid fault.

6.2.1 3phG Fault

3phG faults are the only symmetrical type of grid faults. Therefore all three phases have the same nominal value. The simulated case in Figure 6.4 has no impedance compensation and a $\lambda = 0$ which means the grid fault happens right at the PCC. Therefore the voltage drops to zero.

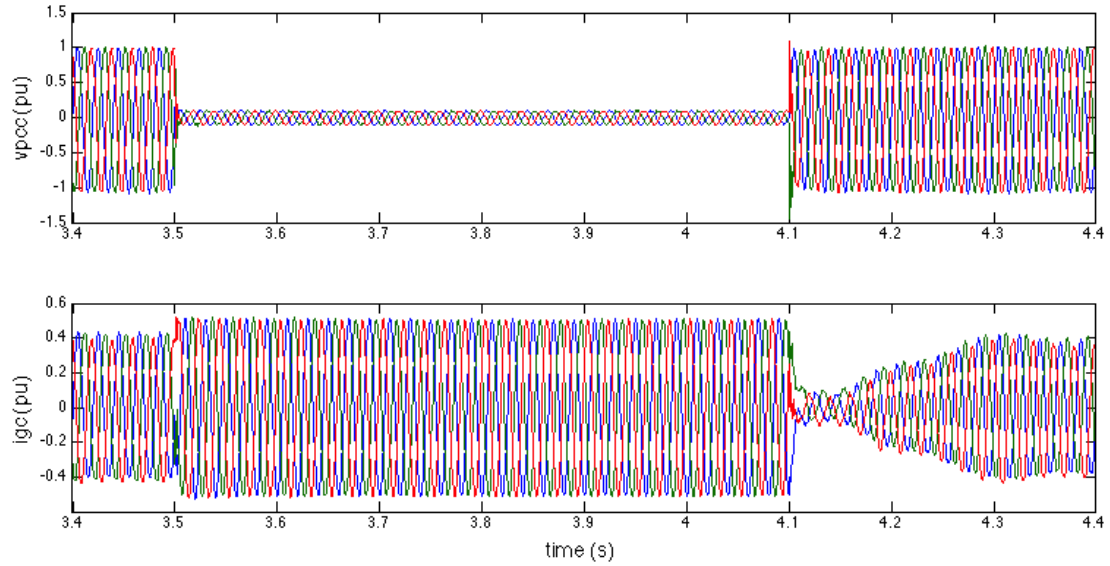


FIGURE 6.4: V_{PCC} and $I_{C,Grid1}$ in WT_{Grid1} for a 3phG fault

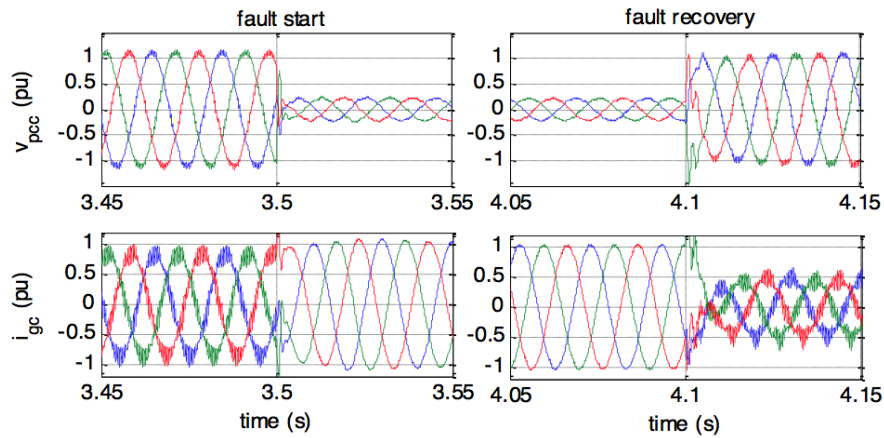


FIGURE 6.5: Fault start and recovery details of V_{PCC} and $I_{C,Grid1}$ in WT_{Grid1} for a 3phG fault

6.2.2 1phG Fault

In 1phG faults only one of the voltage phases is affected by the fault. In Figure 6.6 V_{PCC} phase A is reduced to 0.4 pu approximately while phases B and C remain at 1 pu. On the other hand, we can see a minor increase in the current $I_{C,Grid1}$. Moreover, there is distortion in this current due to the voltage limitation of the converters. The only way to prevent the appearance of this distortion is to reduce the current command. Another suggestion would be to use SVPWM instead of SPWM.

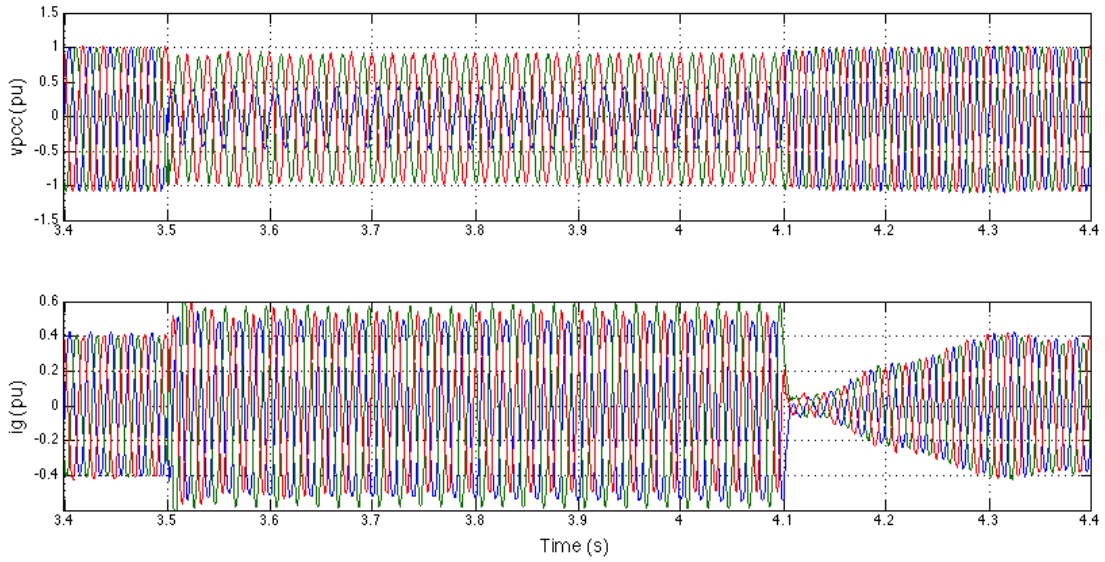


FIGURE 6.6: V_{PCC} and $I_{C,Grid1}$ in WT_{Grid1} for a 1phG fault

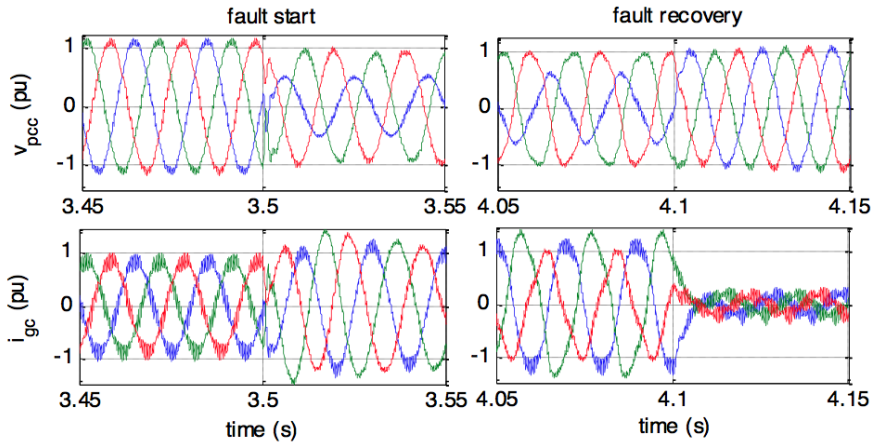


FIGURE 6.7: Fault start and recovery details of V_{PCC} and $I_{C,Grid1}$ in WT_{Grid1} for a 1phG fault

6.2.3 2phG Fault

Figure 6.8 shows the results for the 2phG fault. All three phases of the voltage V_{PCC} are reduced, although the two fault phases have a lower voltage. The current also presents some distortion but not as big as in 1phG.

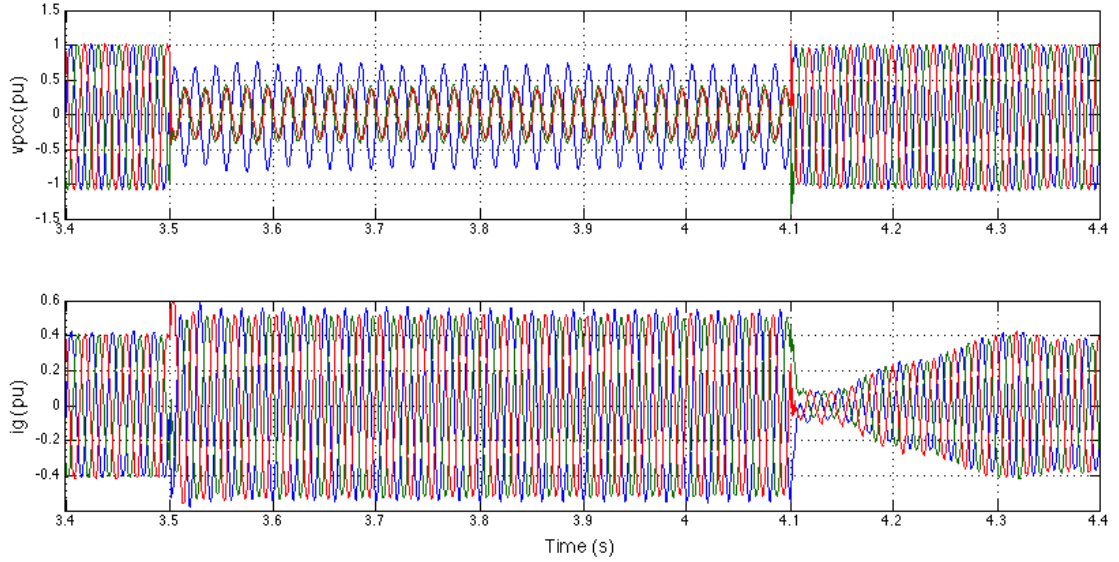


FIGURE 6.8: V_{PCC} and $I_{C,Grid1}$ in WT_{Grid1} for a 2phG fault

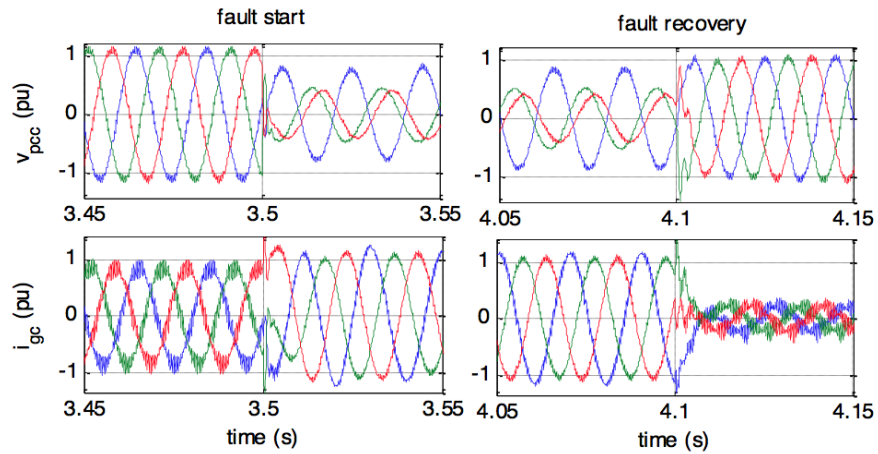
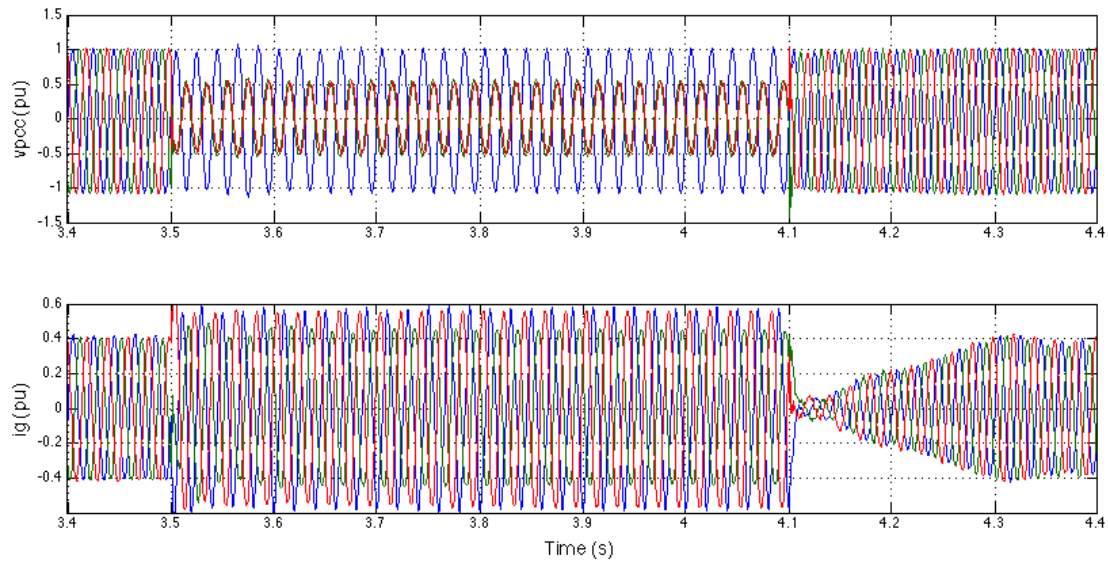
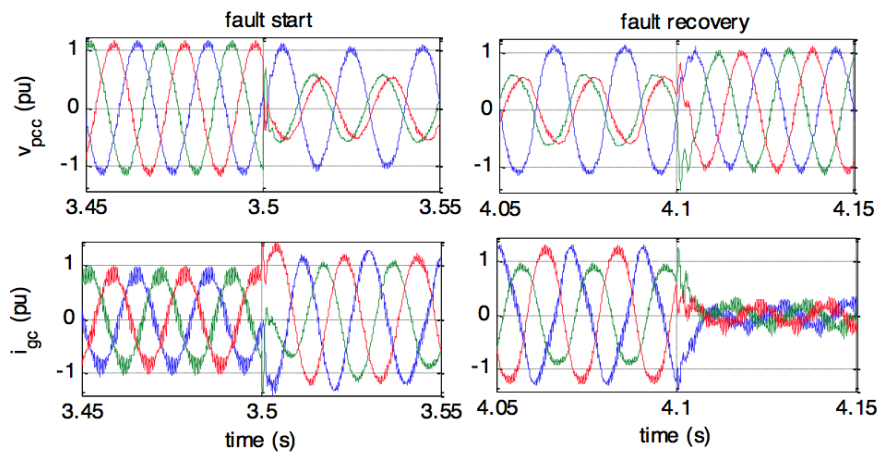


FIGURE 6.9: Fault start and recovery details of V_{PCC} and $I_{C,Grid1}$ in WT_{Grid1} for a 2phG fault

6.2.4 2ph Fault

The final grid fault is the 2ph fault. Figure 6.10 shows V_{PCC} and $I_{C,Grid1}$.

FIGURE 6.10: V_{PCC} and $I_{C,Grid1}$ in WT_{Grid1} for a 2ph faultFIGURE 6.11: Fault start and recovery details of V_{PCC} and $I_{C,Grid1}$ in WT_{Grid1} for a 1ph fault

6.3 LVRT Testing under Different Grid Fault Intensities

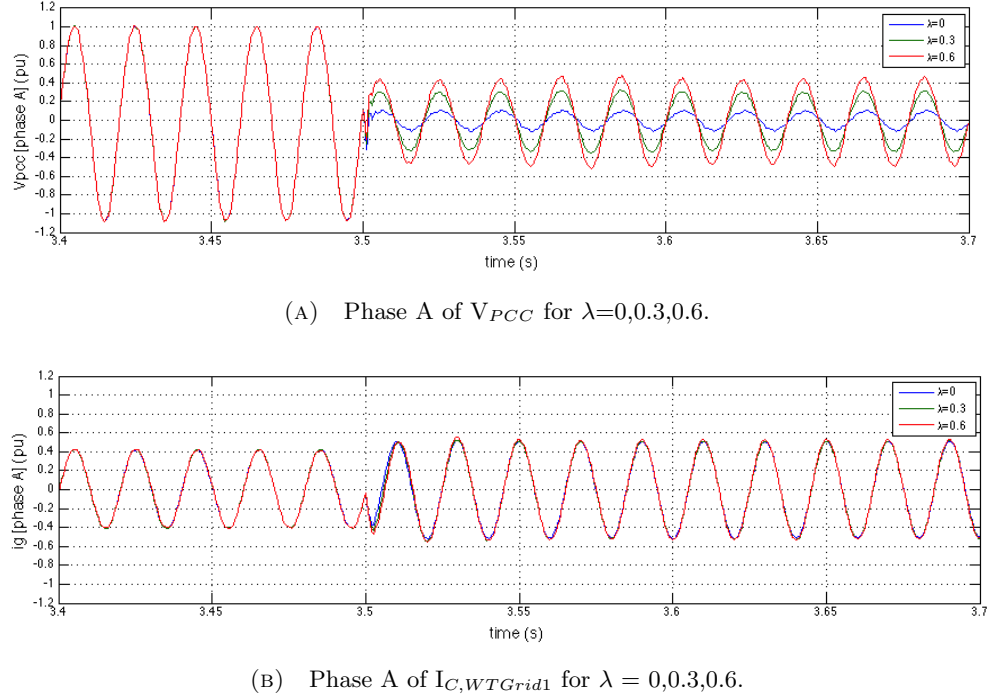


FIGURE 6.12: 3phG fault LVRT testing under different λ (conditions: $\alpha=0$, $Z_{eq}=0.2$).

In the second section we simulate different grid fault intensities of a 3phG fault by modifying its parameter λ , which indicates the network distance between the grid fault and the Wind Park.

Figure 6.12a shows V_{PCC} . It is possible to see how λ affects the severity of the fault. The further the fault happens (i.e. the bigger λ is) the less severe it will be. However, from 6.12b it is possible to see that the severity of the fault has hardly any effect on $I_{C,Grid1}$.

6.4 LVRT Testing with Different Network Impedances

The LVRT system is also capable of simulating grid faults with different network impedances. Figures 6.13 and 6.14 show V_{PCC} and $I_{C,Grid1}$ with grid impedances 0.1 and 0.4, for different grid faults (1phG and 3phG) in order to compare a symmetrical fault (3phG) and an asymmetrical one (1phG).

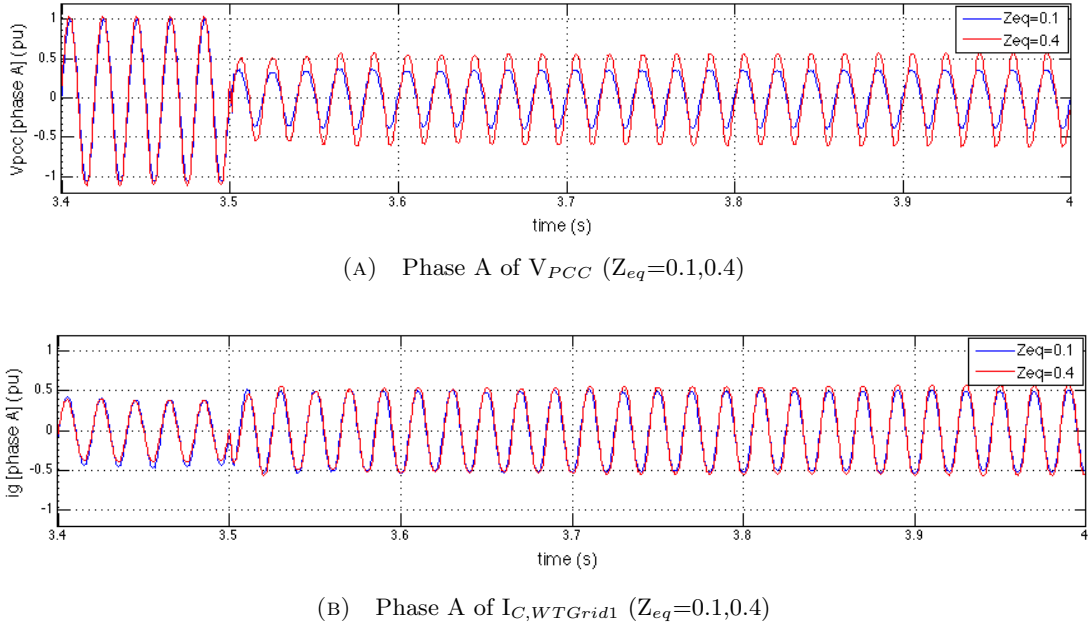


FIGURE 6.13: LVRT testing with different network impedances (conditions: 1phG fault, $\alpha=0$, $\lambda=0$)

Figure 6.13a shows that when the Z_{eq} increases, the V_{pcc} does the same. This can be explained easily with the following equation

$$(V_{pcc} - V_g) = Z_{eq} \cdot I \quad (6.1)$$

by referring to Figure 5.9. It is simple to understand that as the current is constant and Z_{eq} increases (Fig. 6.13b), V_{pcc} increase proportionally.

Although the behavior of V_{PCC} and $I_{C,Grid1}$ is quite good in 1phG fault, there is some distortion, specially in Figure 6.13b, due to the asymmetry of 1phG fault. In order to obtain a better quality output without distortion, the same LVRT test has been done simulating a symmetrical 3phG fault. Figure 6.14 shows the results of this simulation, where the distortion is reduced quite a lot (Fig. 6.14b).

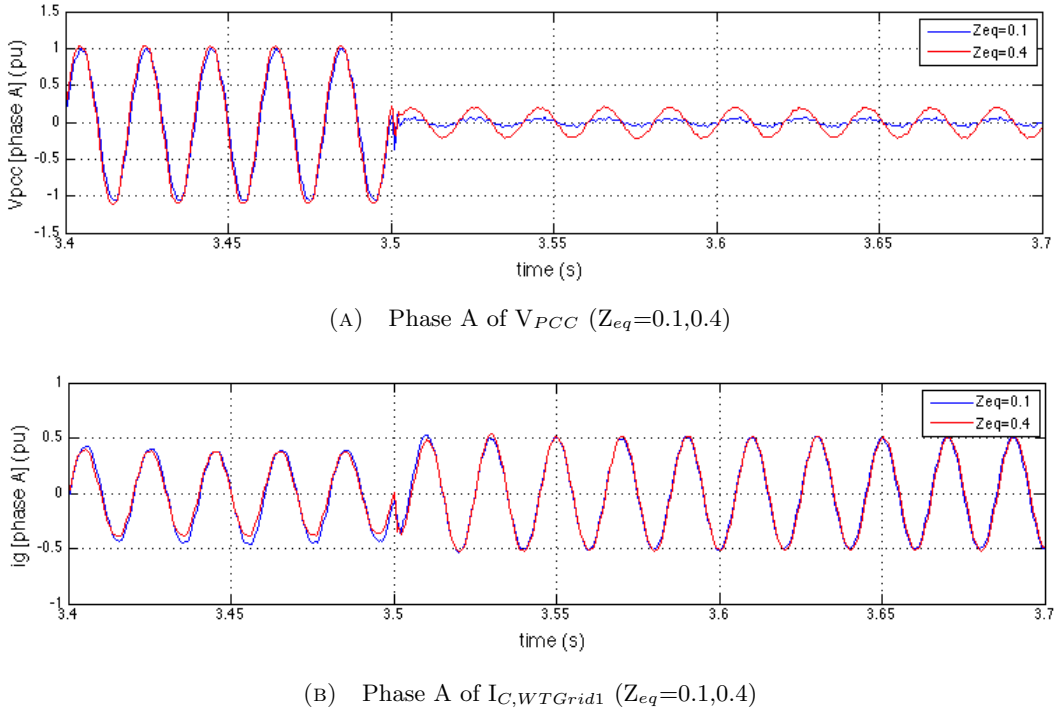


FIGURE 6.14: LVRT testing with different network impedances (conditions: 3phG fault, $\alpha=0$, $\lambda=0$)

6.5 LVRT Testing with Grid WTs In Parallel

This section aims to show the importance of parallel control. Parallel controlled is introduced so that the grid emulating converter can handle the high currents produced by WT_{Test} during the LVRT. However, the use of parallel control requires a synchronisation process between the grid WT. Figure 6.15 displays the results of this synchronisation process. Figure 6.15a shows phase A of I_G for WT_{Grid1}, WT_{Grid2} and WT_{Test} before the synchronisation test. The presence of a circular current can be observed from the 180° phase difference between WT_{Grid1} and WT_{Grid2}. On the other hand, Figure 6.15b displays the same phase for the three WTs once the synchronisation process has been completed and circular current has been eliminated. In Figure 6.15c it is possible to observe the evolution of the phase θ_{Grid2} .

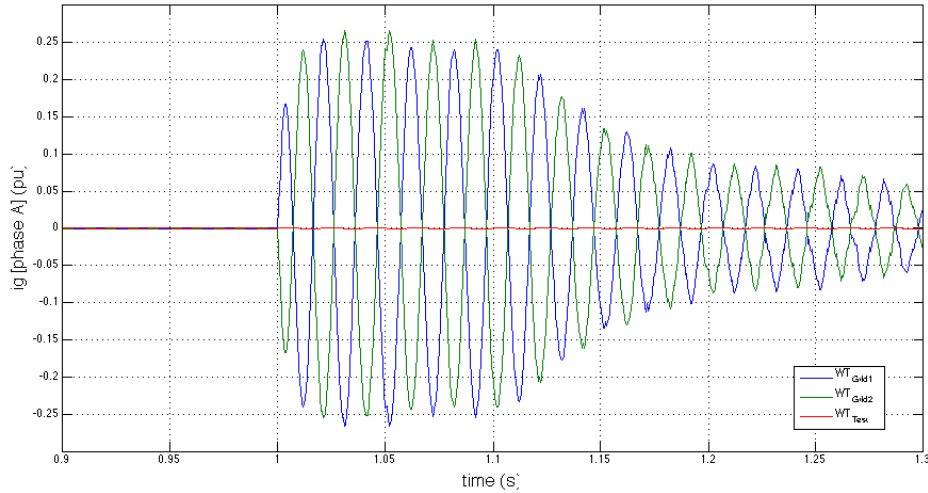
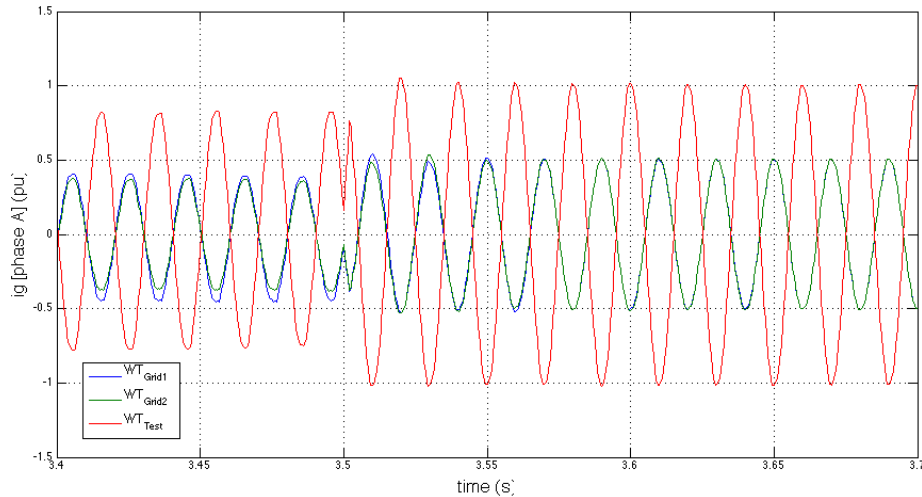
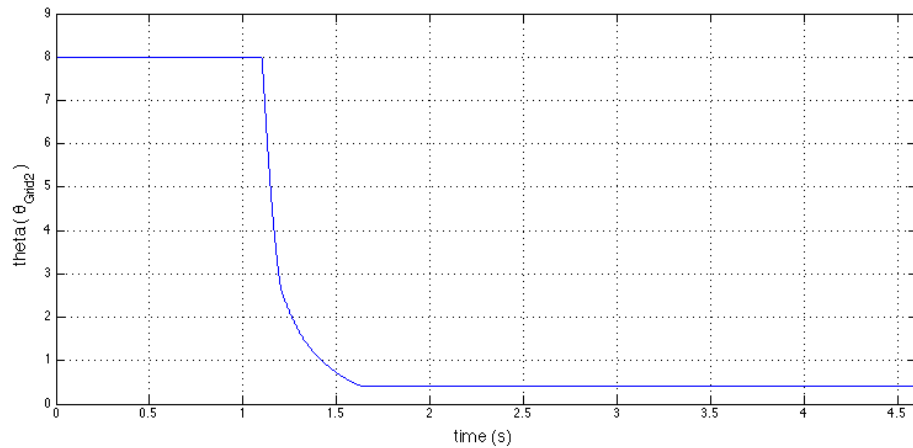
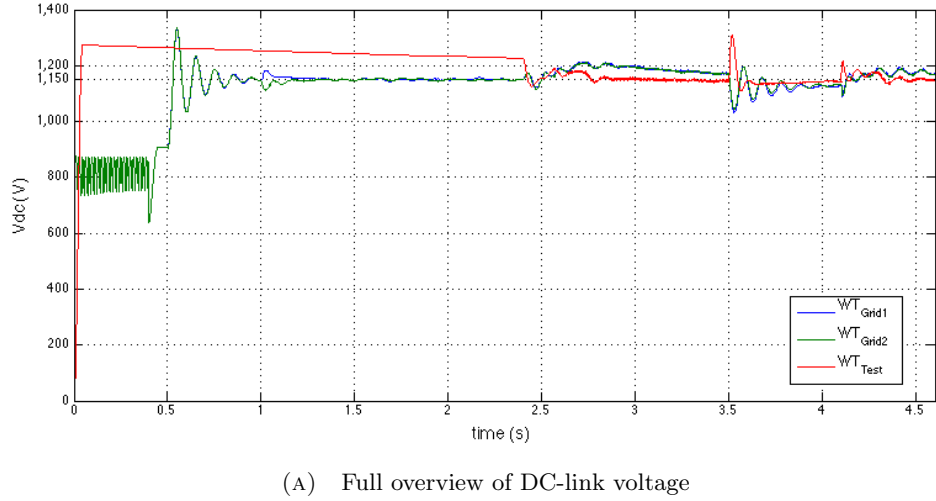
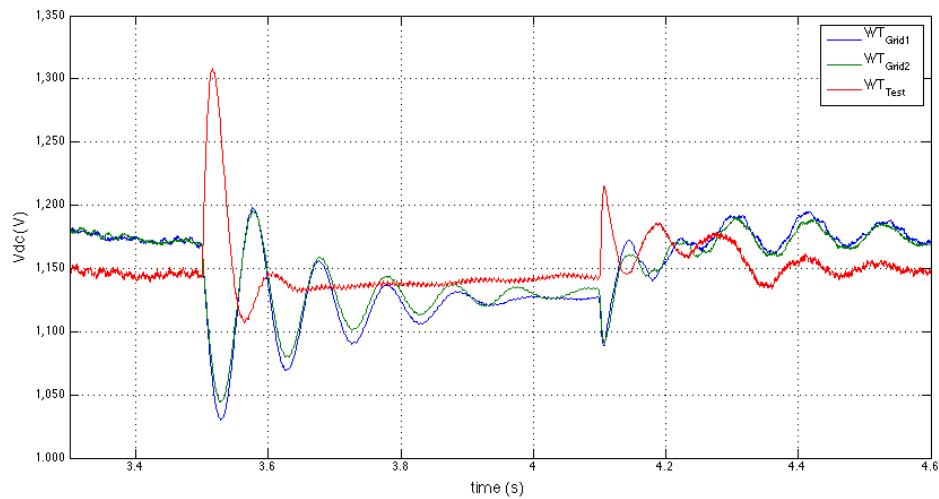
(A) Phase A of I_g for WT_{Grid1} , WT_{Grid2} and WT_{Test} (time: 0.9–1.3 s)(B) Phase A of I_g for WT_{Grid1} , WT_{Grid2} and WT_{Test} (time: 3.4–3.7 s)(C) Angle θ between $I_{G,WT_{Grid1}}$ and $I_{G,WT_{Grid2}}$ FIGURE 6.15: LVRT testing with two grid WTs in parallel (conditions: 3phG fault, $\alpha=0$, $\lambda=0$, $Z_{eq}=0.1$, $\theta_{g20}=8^\circ$).

Figure 6.16 shows the DC-link voltage for each WT. An overview of the complete process has been plotted in Figure 6.16a. Once the DC-link control has been activated, the performance of the voltage is more than acceptable, even during the LVRT test (Fig. 6.16b).



(A) Full overview of DC-link voltage



(B) Detail of DC-link voltage while fault (time: 3.3-4.6 s)

FIGURE 6.16: DC-link voltage for each of the WTs (WT_{Grid1} , WT_{Grid2} , WT_{Test}); (conditions: 3phG fault, $\alpha=0$, $\lambda=0$, $Z_{eq}=0.1$, $\theta_{g20}=8^\circ$).

6.6 Degree of Current Unbalance (Maximum) due to Model Parameter Errors of WT_{Grid2}

The grid-side converter of WT_{Grid2} uses the value of the parameters in the LCL filter in its control. The values of the LCL filter might change with time and thus it might be

hard to estimate them with precision. In this section, we have tested the robustness of the system by introducing a 0.6 pu error in the parameters used for the control. This error affects two different parts of the control: the synchronisation test and the impedance emulation. In the synchronisation test the values of the LCL filter are used to calculate the current command. In the impedance emulation they are needed to calculate equation 5.6.

To quantify the error we have calculated the Degree of Current Unbalance (DCU=ΔI%). The definition of DCU is given in (11) and simulation results are summarised in Figure 6.19 and Table 6.2.

$$\Delta I\% = \frac{I_{error}}{I_{nominal}} \cdot 100\% = \frac{|I_{gc,G2} - I_{gc,G1}|}{I_{nominal}} \cdot 100\% \quad (6.2)$$

Figure 6.17 and 6.18 display the current flowing through WT_{Grid1} when different errors are introduced.

Simulation results prove the robustness of the VSA control. the current error between the two WTs in parallel is less than 10% in the presences of 40% parameter error. Comparing to Fig. 17(b), current unbalance can be found in Figure 6.19 due to the error of machine-side inductance of the LCL filter. Theoretically, this error affects two parts of the control: the PLL synchronisation and the impedance emulation. In the PLL synchronisation (shown in Figure 5.13) the values of LCL filter are used to calculate the current reference. On the other hand, they are needed in 5.6 to calculate virtual impedance for network impedance emulation.

Some current DC offset can also be observed, which is related to the nonlinear control characteristics of the test WT as discussed before.

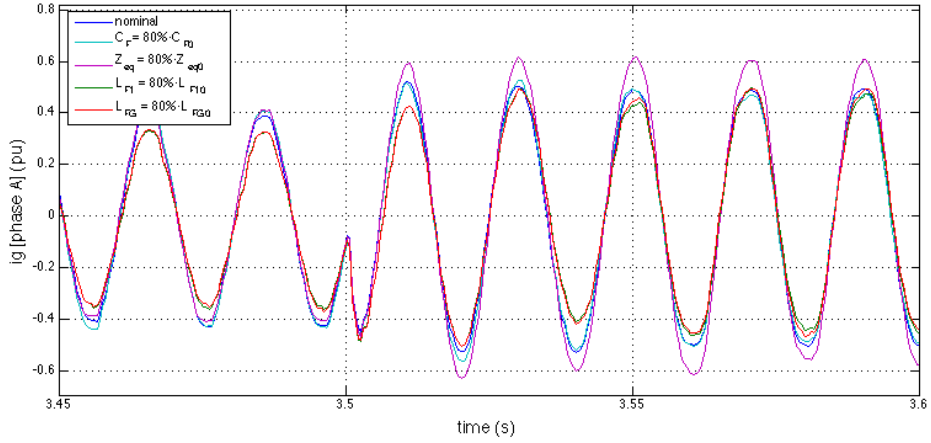


FIGURE 6.17: LVRT testing with different Model Parameter Errors of WT_{Grid2} (conditions: 1phG fault, $\lambda=0$, $\alpha=0$, $Z_{eq0}=0.1$)

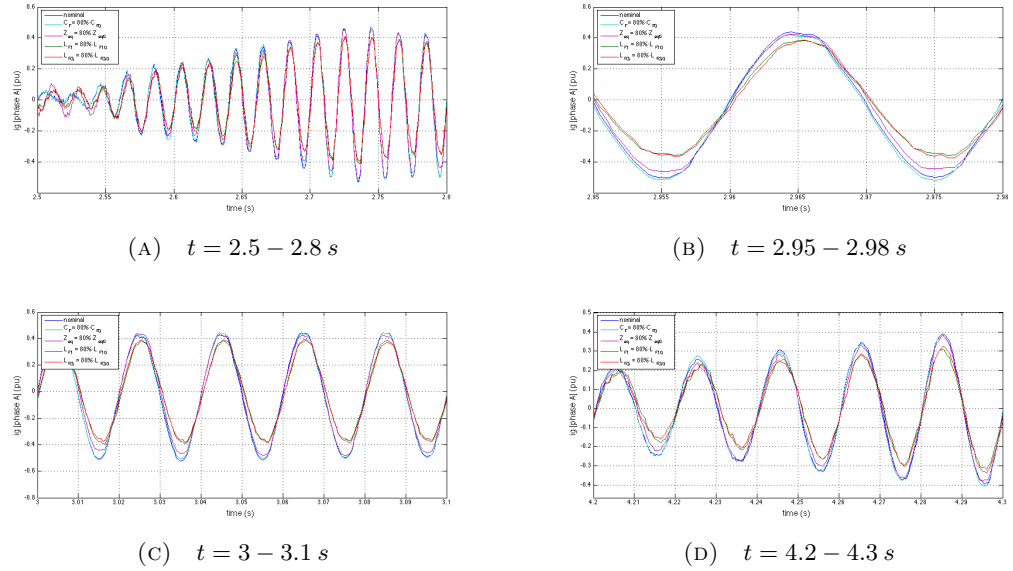


FIGURE 6.18: Detailed overview of Phase A of I_G for WT_{Grid2} .

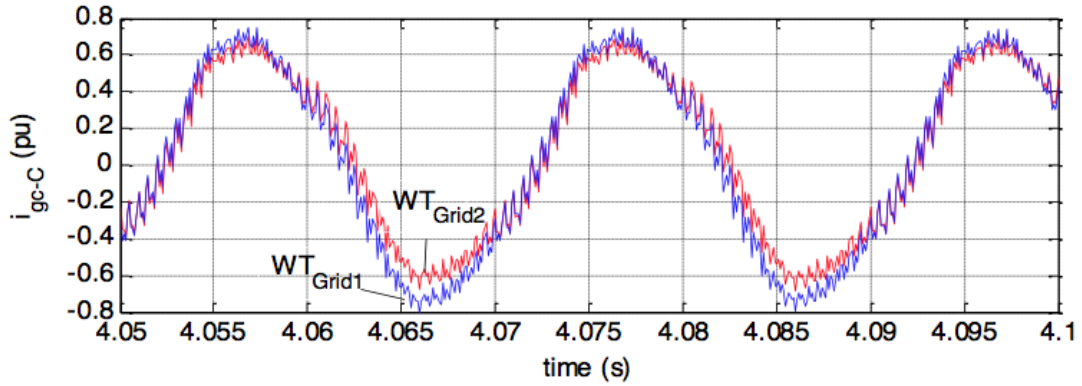


FIGURE 6.19: Current unbalance in the parallel grid WTs (same conditions as Fig. 17 but $L_{F1} = 60\%L_{F10}$ in the controller of WTGrid2)

TABLE 6.2: Relative error due to model parameters error of WT_{Grid2}

$L_{F1}=60\%\cdot L_{F10}$	$L_{FG}=60\%\cdot L_{FG0}$	$C_F=60\%\cdot C_{F0}$
dI %	7.1%	7.8%

6.7 WT Speed Regulation and Limitation

Speed regulation plays an important role in the LVRT test. Figure 6.20 shows the evolution of the WT_{Test} speed during the mechanical start up. Once ω_r reaches 1 pu. at second $t_{trigger}$ the pitch control is activated. ω_r will increase for a small period of time but then will start decreasing until it reaches 1 pu again when the electrical process will begin. The whole mechanical start-up has a duration in the order of magnitude of minutes compared to the electrical part which takes seconds.

Figure 6.21 displays the evolution of the speed of the three WTs during the electrical part, including the LVRT test and its recovery.

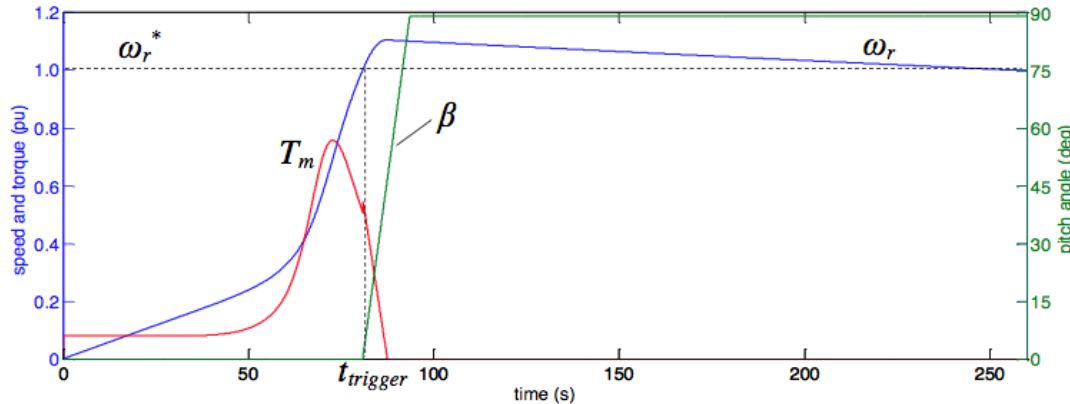


FIGURE 6.20: WT speed regulation during start-up by pitch control (wind speed $v_w = 10 \text{ m/s}$)

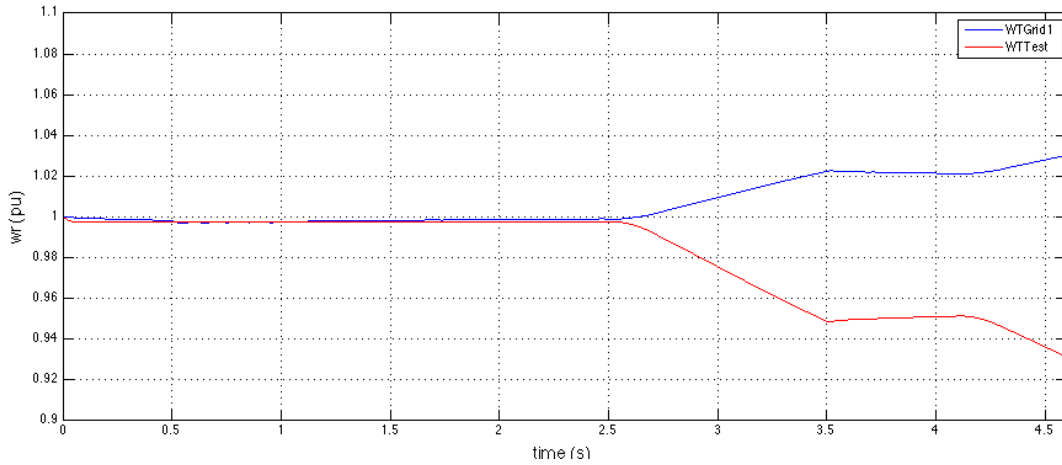


FIGURE 6.21: Grid WT speed rise during LVRT for WT_{Grid1} , WT_{Grid2} and WT_{Test} (conditions: 1phG fault, $\alpha=0$, $\lambda=0$, $Z_{eq} = 0.2$)

Chapter 7

Conclusions

To fulfil the requirement for flexible WT LVRT test, an on-site method is presented and studied systematically in this thesis. The basic idea is testing a WT by an emulated grid consisting of one or more WTs in the wind farm. A completed technical solution is achieved in the end with the help of the theoretic analysis and computer simulation and some conclusions can be drawn as follows:

- With proper control, the WT can be tested under any given LVRT conditions. The configurable test conditions include the fault type (1-3ph grounding faults and phase-phase fault), the fault severity, the impedance of wind farm network and the WT default power and speed.
- WTs operating in parallel can mitigate the mechanical and electrical impact imposed on the grid WT during the test. A voltage synchronized autonomous control strategy is proposed and simulation results show that, without direct high-speed communication, the unbalanced currents between the parallel WTs can be limited within 10% in the presence of 20% parameter errors.
- An open-loop pitch control is devised to regulate the speed of WTs. Theoretic calculation and simulation results show that the speed of grid WT must be kept within the safe operation range considering the over current and over speed constraints.

An academic article based on this thesis and written by the authors is, at the time of the publishing of this thesis, under peer-review for IEEE Transactions on Industrial

Electronics. It is hoped that the studied LVRT testing method could provide a simple and cost-effective technical option for wind power industry in the future.

Chapter 8

Future Work

There are multiples ways in which this novel on-site LVRT testing method could be further developed. The first and most important of which is to build a test rig. Simulations are an economical way to test new ideas. However building a test rig would result in more accurate results and empirical evidence of the validity of the method.

Alternatively, the research could be further developed into DFIG WT. Both a simulation and a test rig could be made for the DFIG.

Another possible line of research would be to upgrade the converters from 2-level to 3-level. In this way, the control of the converters would be further improved , but the complexity and speed of the simulations would also be affected.

Finally, if all these are carried out, a synthesis research paper on all the differences between WT types and converter level could be developed.

Appendix A

Wind Turbine PMSG Parameters

TABLE A.1: Wind Turbine PMSG (nonsalient poles) parameters [1]

Generator Type	PMSG, 2.0 MW, 690 V, 9.75 Hz	
Rated Mechanical Power	2.0 MW	1.0 pu
Rated Apparent Power	2.2419 MVA	1.0 pu
Rated Line-to-line Voltage	690 V (rms)	
Rated Phase Voltage	398.4 V (rms)	1.0 pu
Rated Stator Current	1867.76 A (rms)	1.0 pu
Rated Stator Frequency	9.75 Hz	1.0 pu
Rated Power Factor	0.8921	
Rated Rotor Speed	22.5 rpm	1.0 pu
Number of Pole Pairs	26	
Inertia	$6.25 \cdot 10^6 \text{ kg}\cdot\text{m}^2$	
Viscous Damping	0 N·m·s	
Static Friction	0 N·m	
Rated Mechanical Torque	848.826 kN·m	1.0 pu
Rated Rotor Flux Linkage	5.8264 Wb (rms)	0.896 pu
Stator Winding Resistance, R_s	0.821 mΩ	0.00387 pu
d-axis Synchronous Inductance, L_d	1.5731 mH	0.4538 pu
q-axis Synchronous Inductance, L_q	1.5731 mH	0.4538 pu
Base Flux Linkage, Λ_B	6.5029 Wb	1.0 pu
Base Impedance, Z_B	0.2124 Ω	1.0 pu
Base Inductance, L_B	3.4666 mH	1.0 pu
Base Capacitance, C_B	76865.87 μF	1.0 pu

Appendix B

LCL Filter Parameters

TABLE B.1: LCL Filter Parameters for grid-emulating WTs [2]

Parameter name	Value
L_g	$7.265 \cdot 10^{-2}$ mH
L_1	$8.19667 \cdot 10^{-4}$ mH
R_y	$6.19667 \cdot 10^{-2}$ Ω
C_y	$1.11426 \cdot 10^{-3}$ F

Appendix C

Park Transformation

The quantities in the $\alpha\beta0$ are useful in a number of applications but have the same oscillating nature as the quantities in the abc frame. For the controller design it is useful to have constant quantities. This can be achieved by using the Park transformation [43] and the so-called synchronous reference frame.

The Park transformation is given by

$$[x_{qd0}] = [T_{qd0}] \cdot [x_{abc}] \quad (\text{C.1})$$

and its inverse

$$[x_{abc}] = [T_{qd0}]^{-1} \cdot [x_{qd0}] \quad (\text{C.2})$$

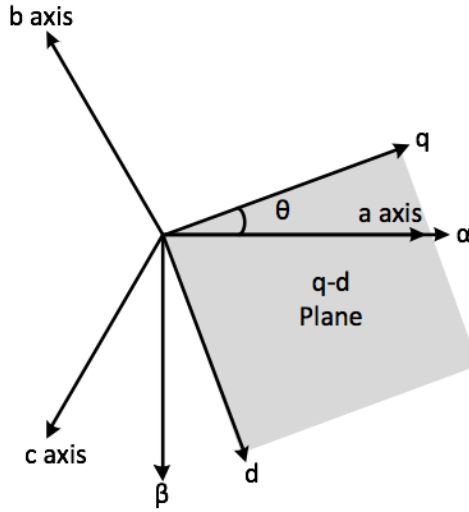
where x_{abc} is a vector with the three phase quantities in the abc frame and x_{qd0} is a vector with the transformed quantities in the $qd0$ frame.

The transformation matrix $T(\theta)$ can be written as

$$T(\theta) = \frac{2}{3} \cdot \begin{bmatrix} \cos(\theta) & \cos(\theta - \frac{2\pi}{3}) & \cos(\theta + \frac{2\pi}{3}) \\ \sin(\theta) & \sin(\theta - \frac{2\pi}{3}) & \sin(\theta + \frac{2\pi}{3}) \\ \frac{1}{2} & \frac{1}{2} & \frac{1}{2} \end{bmatrix} \quad (\text{C.3})$$

and its inverse

$$T^{-1}(\theta) = \begin{bmatrix} \cos(\theta) & \sin(\theta) & 1 \\ \cos(\theta - \frac{2\pi}{3}) & \sin(\theta - \frac{2\pi}{3}) & 1 \\ \cos(\theta + \frac{2\pi}{3}) & \sin(\theta + \frac{2\pi}{3}) & 1 \end{bmatrix} \quad (\text{C.4})$$

FIGURE C.1: qd plane representation

The Park transformation can be also seen as a geometric transformation which combines the Clarke transformation and a rotation as illustrated in Fig. C.1 [38] .

Figure C.2 [38] shows an example of three-phase voltages in the abc and $qd0$ frames. Note that by choosing the right θ angle, constant values are obtained.

C.1 Instantaneous power theory in the synchronous reference frame

As mentioned earlier, to obtain constant steady state quantities, the angle θ employed in the Park transformation corresponds to the electrical voltage angle [44]. Replacing θ for the electrical angle $\theta = \omega \cdot t + \varphi_0$, and transforming

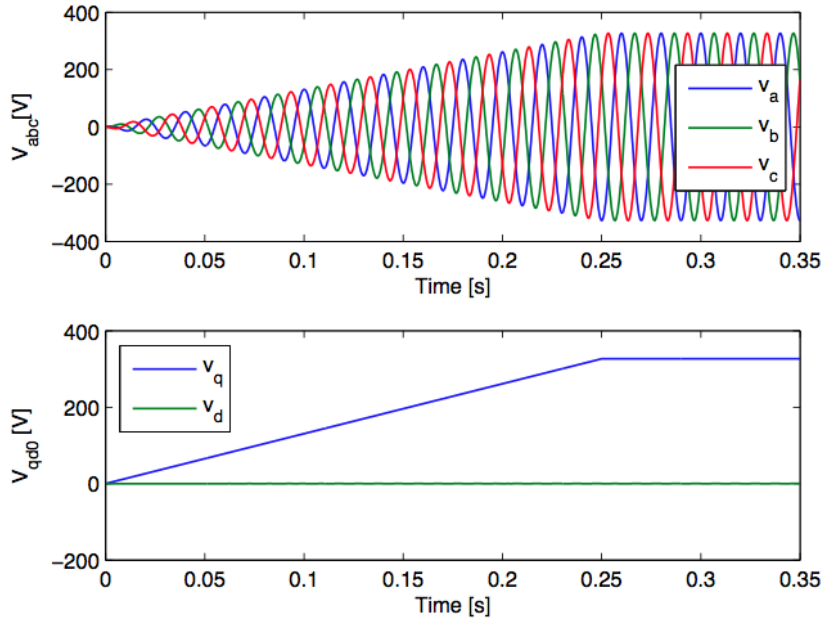


FIGURE C.2: Example of three-phase voltages in the abc and $qd0$ frames

abc voltages and currents to the $qd0$ frame the following voltage and current phasors can be defined, similarly to the Clarke transformation case, as

$$\underline{V}^{qd} = \frac{v_q - jv_d}{\sqrt{2}} [T_{qd0}]^{-1} \cdot [x_{qd0}] \quad (\text{C.5})$$

$$\underline{I}^{qd} = \frac{i_q - ji_d}{\sqrt{2}} [T_{qd0}]^{-1} \cdot [x_{qd0}] \quad (\text{C.6})$$

The power of a three-phase system yields

$$\underline{S} = P + jQ = 3 \cdot \underline{V}^{qd} \cdot \underline{I}^{qd*} = 3 \cdot \frac{v_q - jv_d}{\sqrt{2}} \cdot \frac{i_q - ji_d}{\sqrt{2}} \quad (\text{C.7})$$

Reordering expression (C.7), active and reactive power can be expressed as

$$P = \frac{3}{2} \cdot (v_q \cdot i_q + v_d \cdot i_d) \quad (\text{C.8})$$

$$Q = \frac{3}{2} \cdot (v_q \cdot i_d + v_d \cdot i_q) \quad (\text{C.9})$$

obtaining the expression of active and reactive power as functions of voltages and currents in the $qd0$ frame [44].

Appendix D

Commonly used control blocks

D.1 Current Loop Control

By assuming $v_{zd} = 0$ (this is done by the PLL as described in Section D.2), the voltage equations can be written as [38]:

$$\begin{bmatrix} v_{zd} \\ 0 \end{bmatrix} - \begin{bmatrix} v_{lq} \\ v_{ld} \end{bmatrix} = \begin{bmatrix} r_l & -l_l \cdot \omega_e \\ l_l \cdot \omega_e & r_l \end{bmatrix} \cdot \begin{bmatrix} i_q \\ i_d \end{bmatrix} + \begin{bmatrix} l_l & 0 \\ 0 & l_l \end{bmatrix} \cdot \frac{d}{dt} \begin{bmatrix} i_q \\ i_d \end{bmatrix} \quad (\text{D.1})$$

where it is clear that there exist a coupling between the q and d components of voltages and currents. In order to control the i_q and i_d there are mainly two different control approaches:

- Multi-variable control, controlling the q and d components with a single two dimension controller.
- Decoupling and independently controlling q and d components.

The present chapter uses the second approach of decoupling and controlling i_q and i_d separately. The q and d components can be decoupled using [38]:

$$\begin{bmatrix} v_{lq} \\ v_{ld} \end{bmatrix} = \begin{bmatrix} -\hat{v}_{lq} + v_{zq} - l_l \cdot \omega_e \cdot i_{ld} \\ -\hat{v}_{ld} + l_l \cdot \omega_e \cdot i_{lq} \end{bmatrix} \quad (\text{D.2})$$

where \hat{v}_{lq} and \hat{v}_{ld} are the outputs of the current controllers and v_{lq} and v_{ld} are the voltages to be applied by the converter. Substituting in the voltage equations:

$$\begin{bmatrix} \hat{v}_{lq} \\ \hat{v}_{ld} \end{bmatrix} = \begin{bmatrix} r_l & 0 \\ 0 & r_l \end{bmatrix} \cdot \begin{bmatrix} i_q \\ i_d \end{bmatrix} + \begin{bmatrix} l_l & 0 \\ 0 & l_l \end{bmatrix} \cdot \frac{d}{dt} \begin{bmatrix} i_q \\ i_d \end{bmatrix} \quad (\text{D.3})$$

Applying the *Laplace* transformation, the transfer function between the controller voltages and converter currents can be derived as:

$$\frac{\hat{v}_{lq}(s)}{i_q(s)} = \frac{1}{l_l \cdot s + r_l} \quad (\text{D.4})$$

$$\frac{\hat{v}_{ld}(s)}{i_d(s)} = \frac{1}{l_l \cdot s + r_l} \quad (\text{D.5})$$

The controller can be designed using the *Internal Model Control* technique, resulting the following controller [38]:

$$G_{ciq}(s) = G_{cid}(s) = \frac{K_p \cdot s + K_i}{s} \quad (\text{D.6})$$

where the constants can be calculated as:

$$K_p = \frac{l_l}{\tau} \quad (\text{D.7})$$

$$K_i = \frac{r_l}{\tau} \quad (\text{D.8})$$

where τ is the closed loop time constant of the electrical system. This constant must be chosen considering the converter physical restrictions. It is usual to define it a number of times (i.e 10 times) faster than the converter switching frequency.

The implementation of the overall current controller is sketched in Figure D.1 [44]:

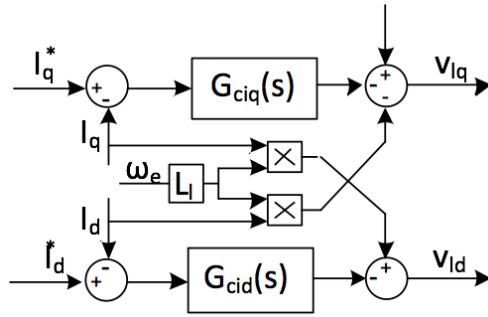


FIGURE D.1: Current loop controller implementation

D.2 Phase-Locked Loop (PLL)

A phase-locked loop (PLL) is used to determine the angle and the angular velocity of the electrical network. A three-phase PLL consists in a feedback of the d -axis voltage component filtered by a PI controller. The output of the controller corresponds to the angular velocity ω_e of the electrical grid and the integration of this signal corresponds to the grid angle θ_e . A typical PLL scheme is illustrated in Figure D.2 [44].

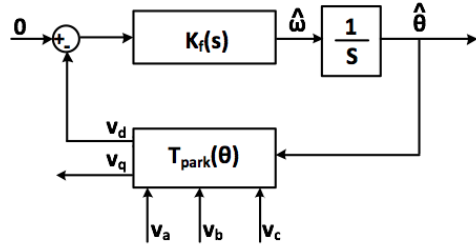


FIGURE D.2: Phase-locked loop control scheme

To study the design of the PLL controller, the system can be linearized by assuming the angle error to be small. The following second order system is obtained [38] [45]:

$$\frac{\hat{\theta}(s)}{\theta(s)} = \frac{2\xi\omega_n s + w_n^2}{s^2 + 2\xi\omega_n + w_n^2} \quad (\text{D.9})$$

where $\hat{\theta}(s)$ is the estimated grid angle and $\theta(s)$ is the real grid angle. The PLL controller can be defined as:

$$K_f(s) = K_p \cdot \left(\frac{\frac{1}{\tau_{PLL}} + s}{s} \right) \quad (\text{D.10})$$

where τ_{PLL} is the PLL time constant.

The controller parameters K_p and τ_{PLL} can be computed using expressions [38] [45]:

$$\omega_n = \sqrt{\frac{K_p \cdot E_m}{\tau_{PLL}}} \quad (\text{D.11})$$

$$\xi = \frac{\sqrt{\tau_{PLL} \cdot K_p \cdot E_m}}{2} \quad (\text{D.12})$$

where E_m is the admitted peak voltage value, ξ is the damping ratio, ω_n is the natural frequency. An example of the initial transient of a PLL is illustrated in Figure D.3 [44]:

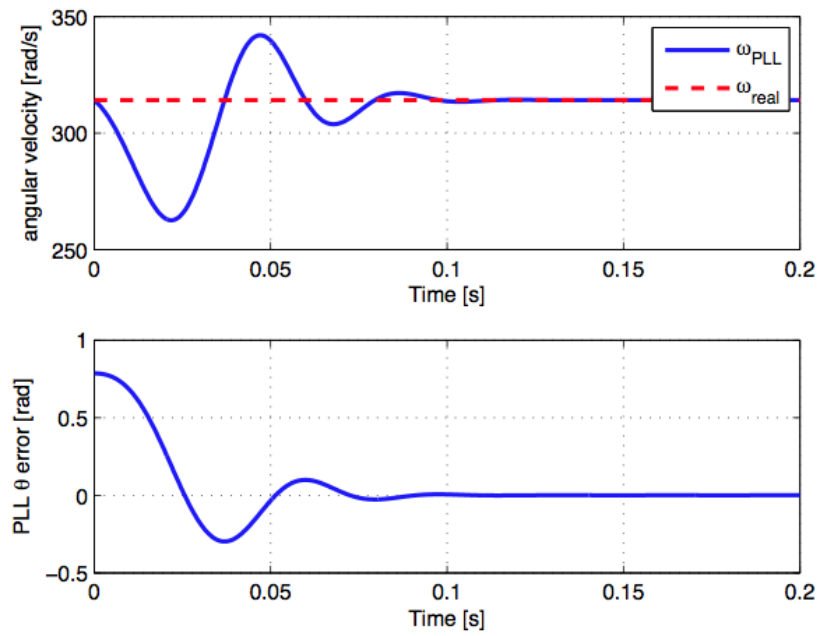


FIGURE D.3: An example of phase-locked loop initial transient

Appendix E

MATLAB Simulink Schematics

The aim of this appendix is to show the main architecture of the MATLAB Simulation developed. The appendix is divided in two parts: grid emulating WTs (WT_{Grid1} and WT_{Grid2}) and under-test WT (WT_{Test}). After showing the architecture of each WT, the schematics of grid-side and machine-side converters are displayed. Those converters are different not only in between the architecture of the WT (grid emulating or under-test) but also also in their mode of operation (normal operation or grid-emulating (WT_{Grid1} and WT_{Grid2}) / LVRT (WT_{Test}) operation).

E.1 Grid emulating WTs: WT_{Grid1} and WT_{Grid2}

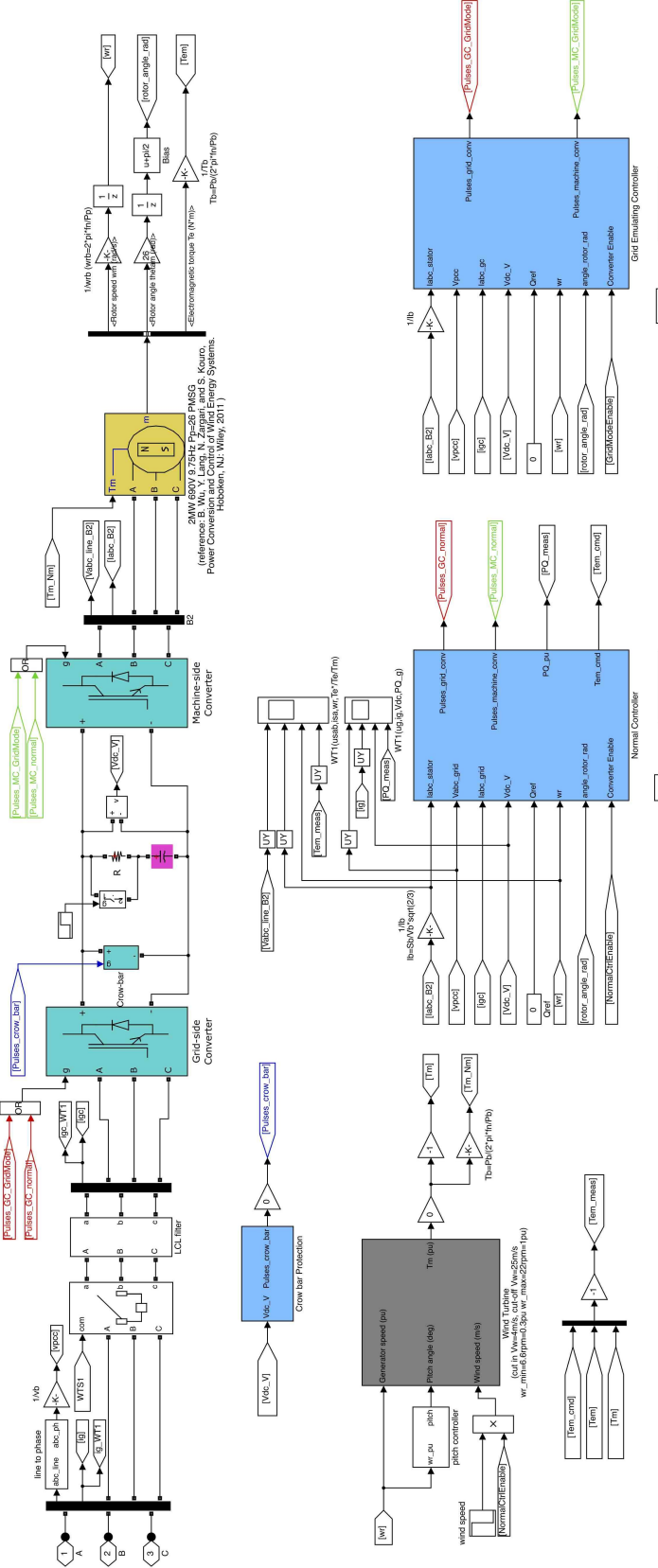
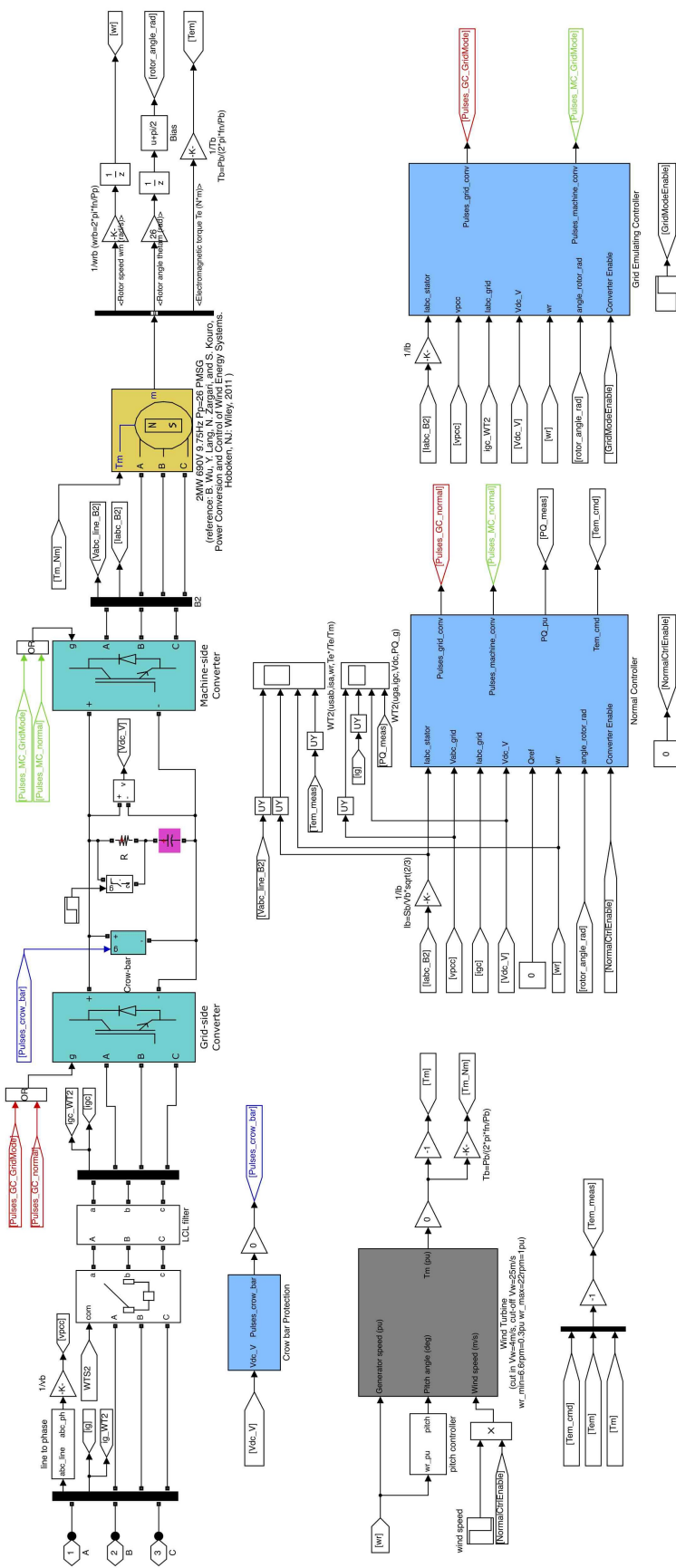


FIGURE E.1: MATLAB Simulink Schematics of WT_{Grid1}

FIGURE E.2: MATLAB Simulink Schematics of WT_{Grid}

Wind Turbine controls - Grid-side converter control system

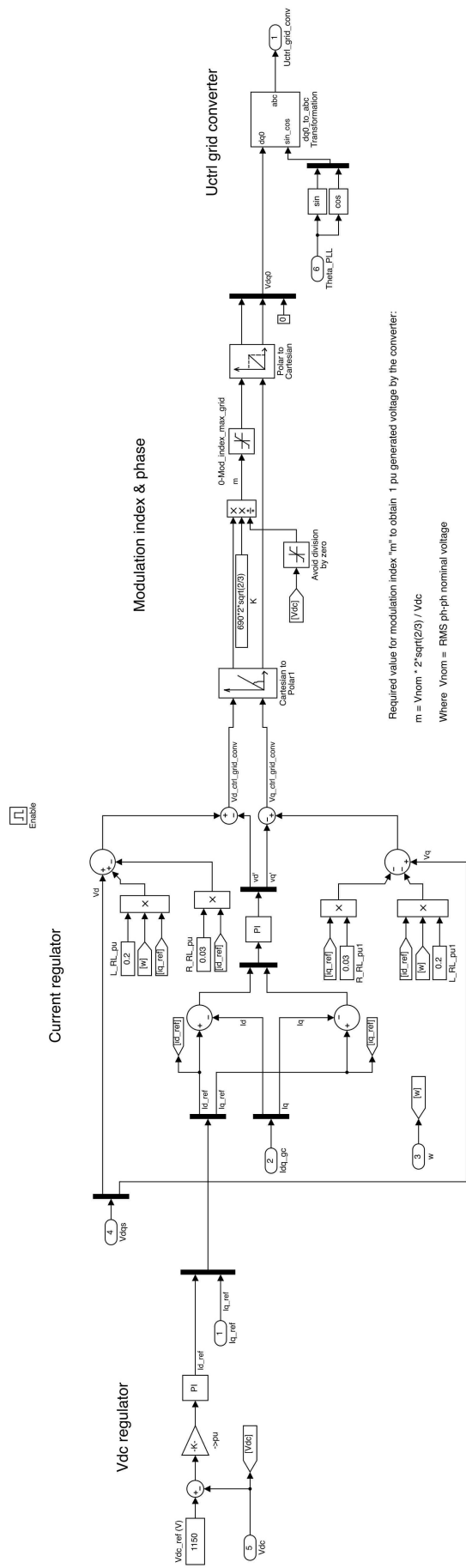


FIGURE E.3: MATLAB Simulink Schematics of WT_{Grid1} and WT_{Grid2} Grid-Side Controller for Normal Operation

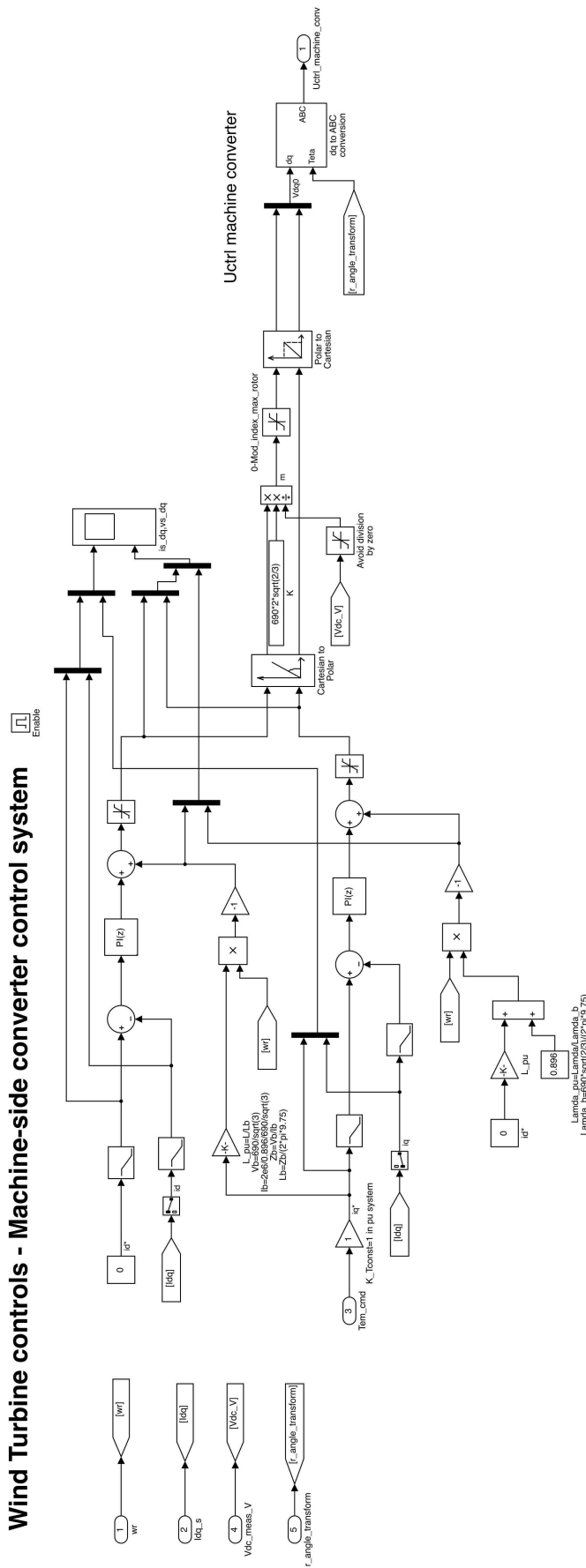
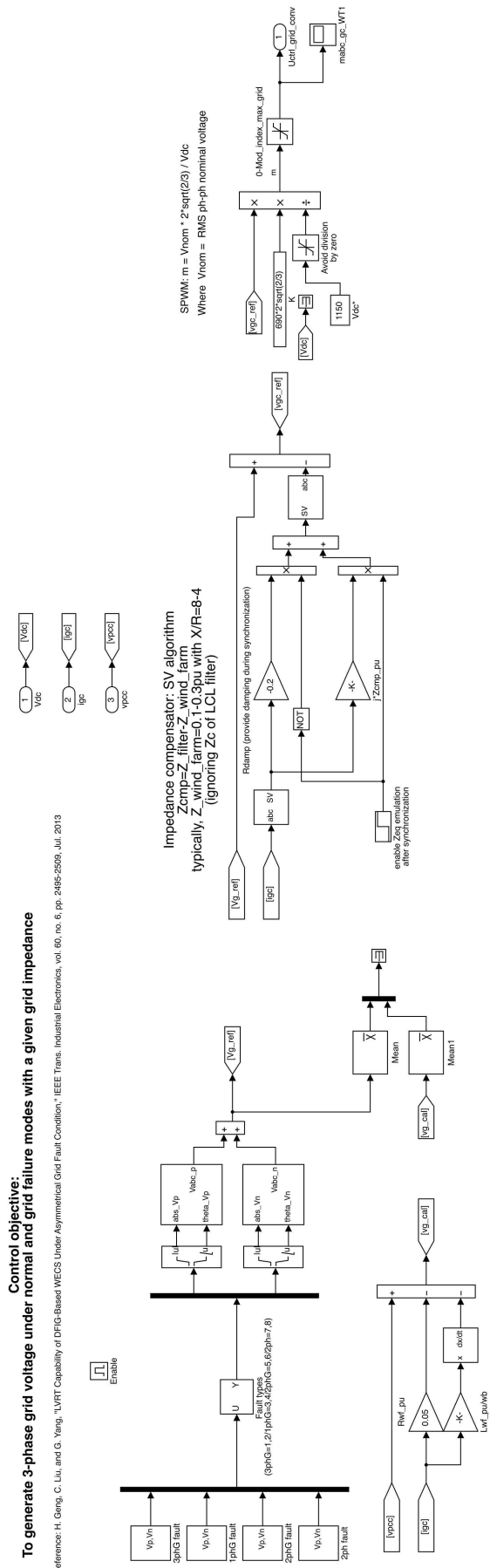
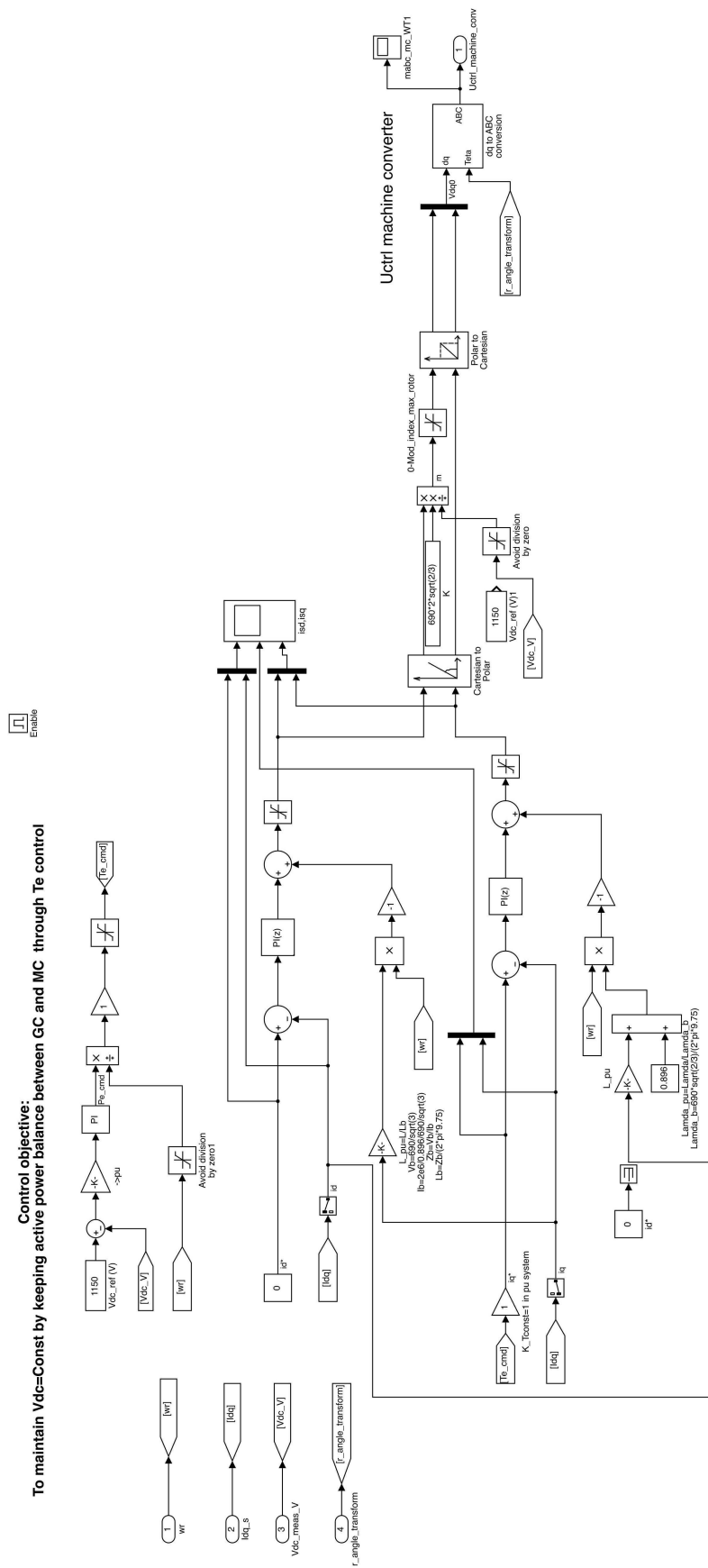
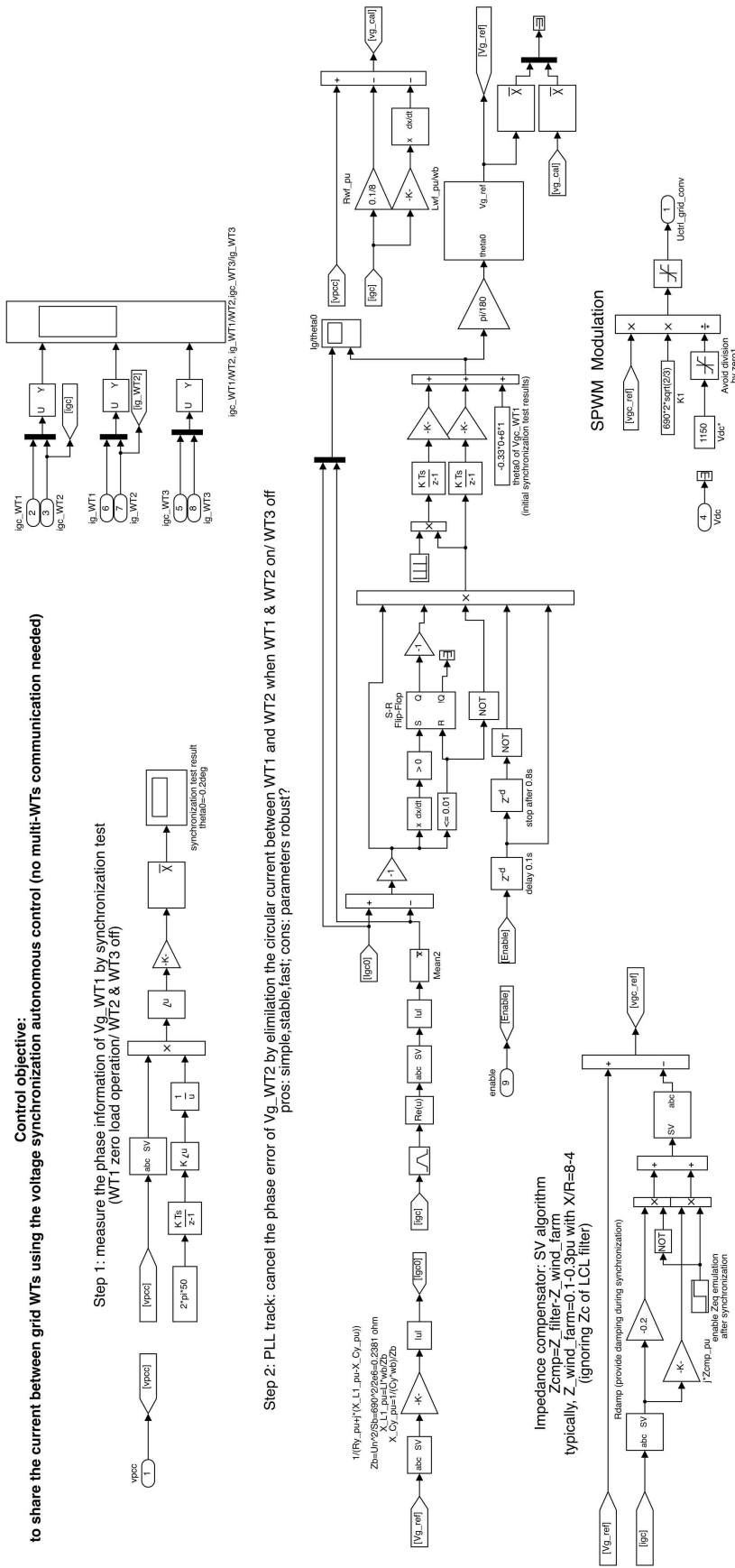
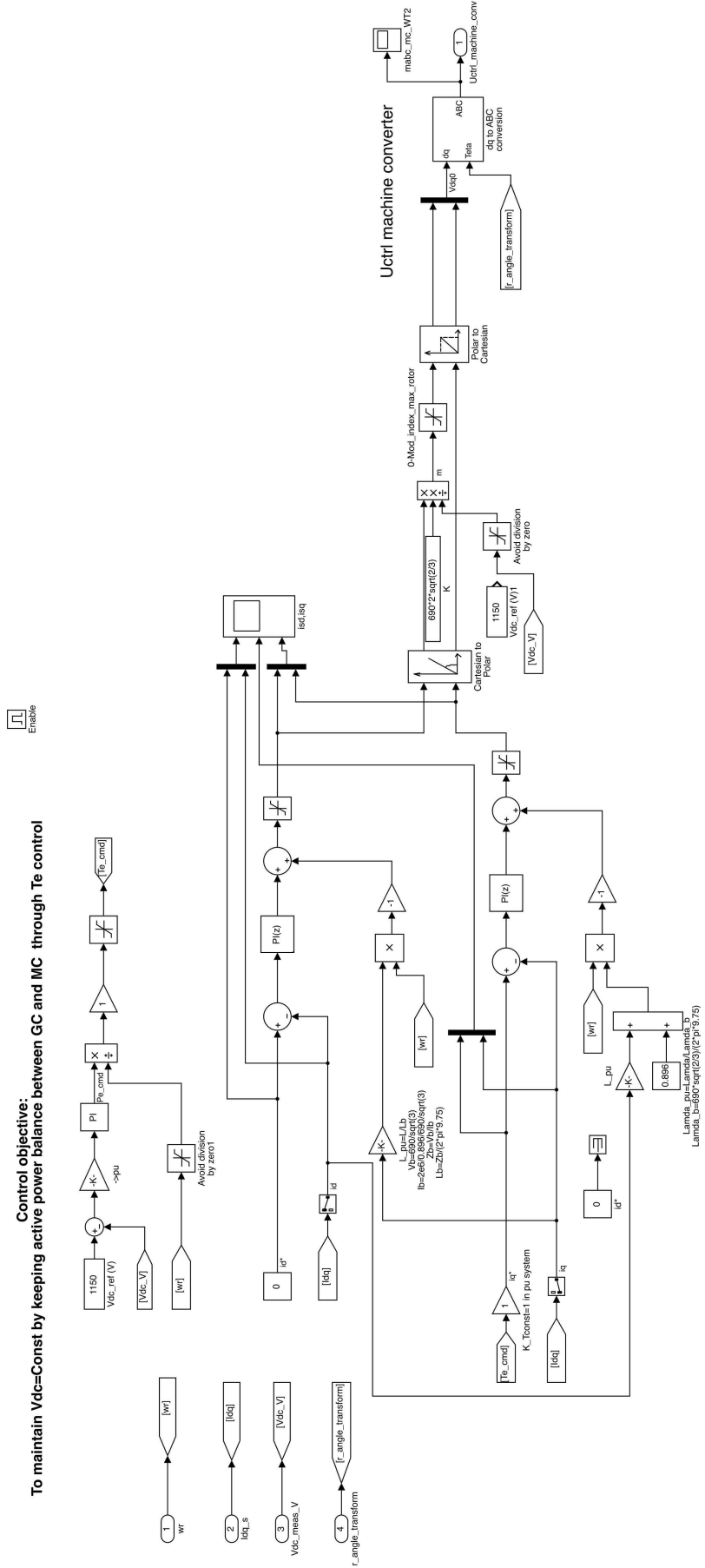


FIGURE E.4: MATLAB Simulink Schematics of WT_{Grid1} and WT_{Grid2} Machine-Side Controller for Normal Operation

FIGURE E.5: MATLAB Simulink Schematics of WT_{Grid1} Grid-Side Controller for Grid-Emulating Operation

FIGURE E.6: MATLAB Simulink Schematics of WT_{Grid1} Machine-Side Controller for Grid-Emulating Operation

FIGURE E.7: MATLAB Simulink Schematics of WT_{Grid2} Grid-Side Controller for Grid-Emulating Operation

FIGURE E.8: MATLAB Simulink Schematics of WT_{Grid2} Machine-Side Controller for Grid-Emulating Operation

E.2 Under-test WT: WT_{Test}

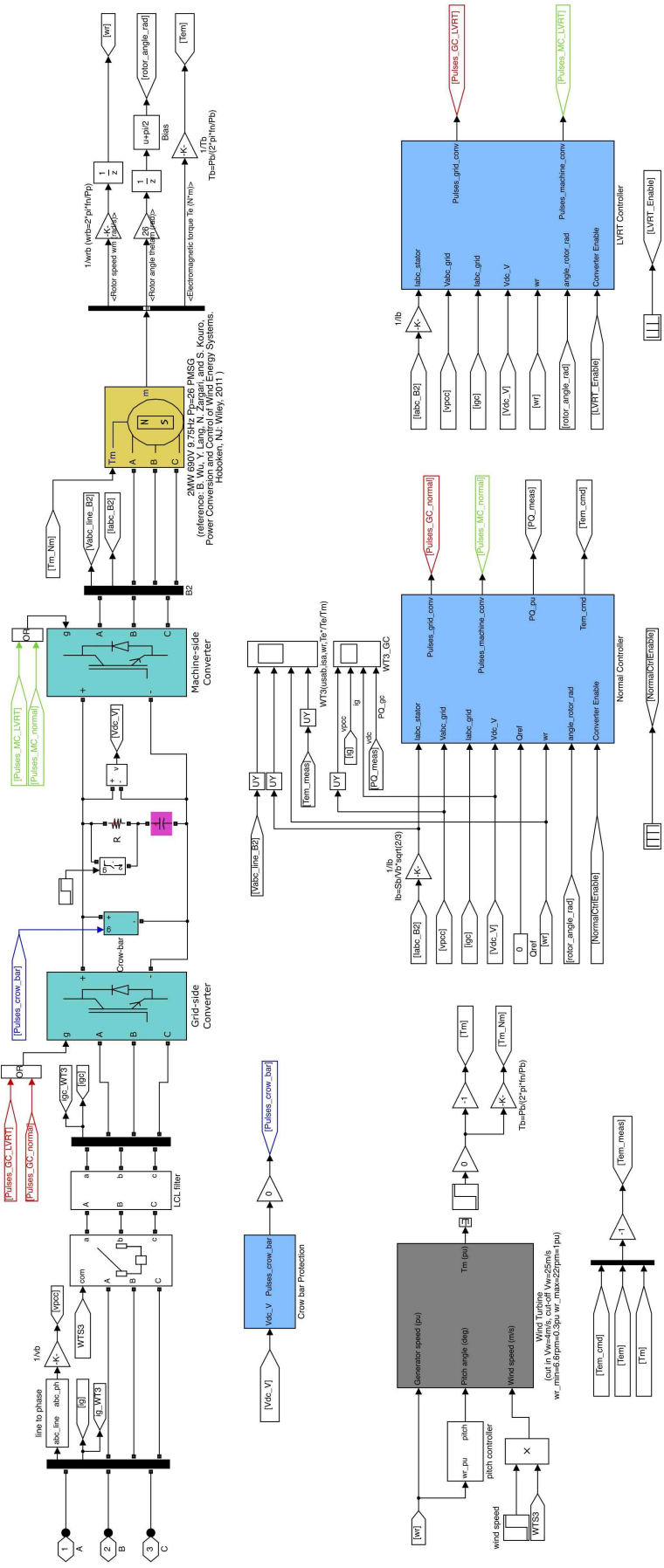


FIGURE E.9: MATLAB Simulink Schematics of WT_{Test}

Wind Turbine controls - Grid-side converter control system

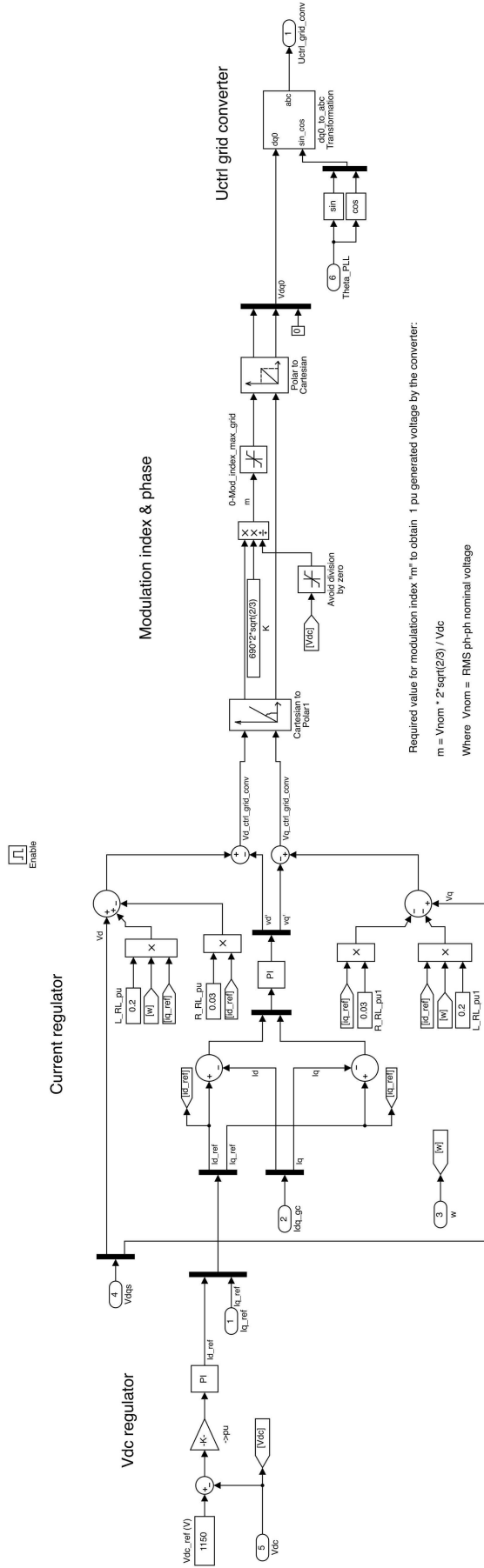


FIGURE E.10: MATLAB Simulink Schematics of WT_{Test} Grid-Side Controller for Normal Operation

Wind Turbine controls - Machine-side converter control system

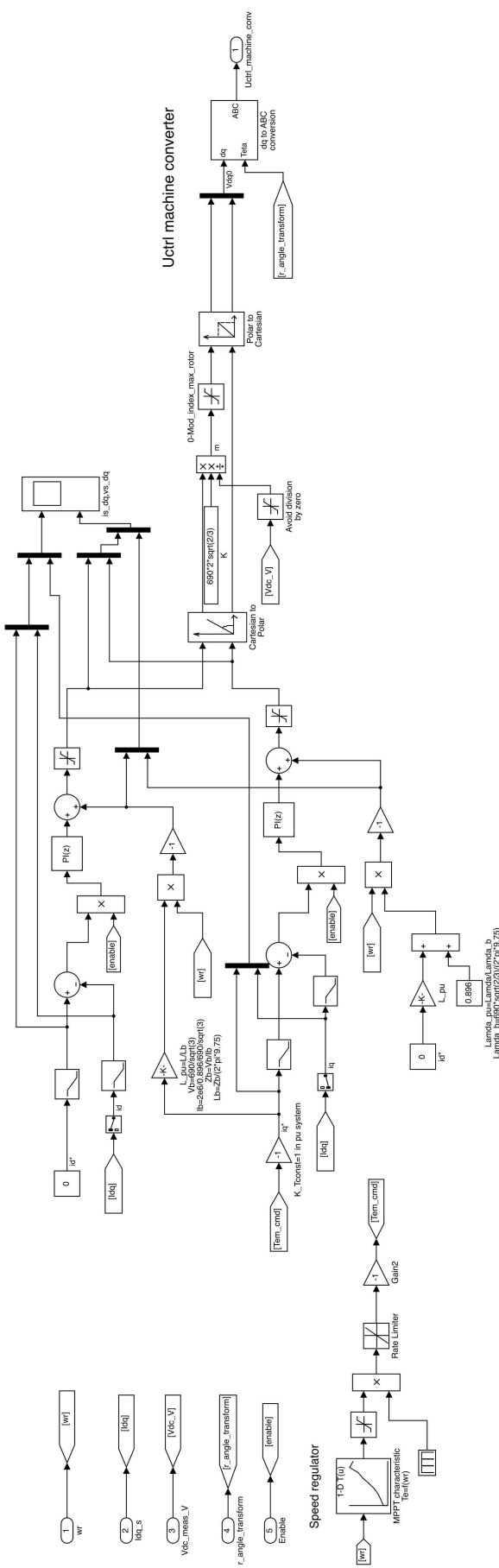
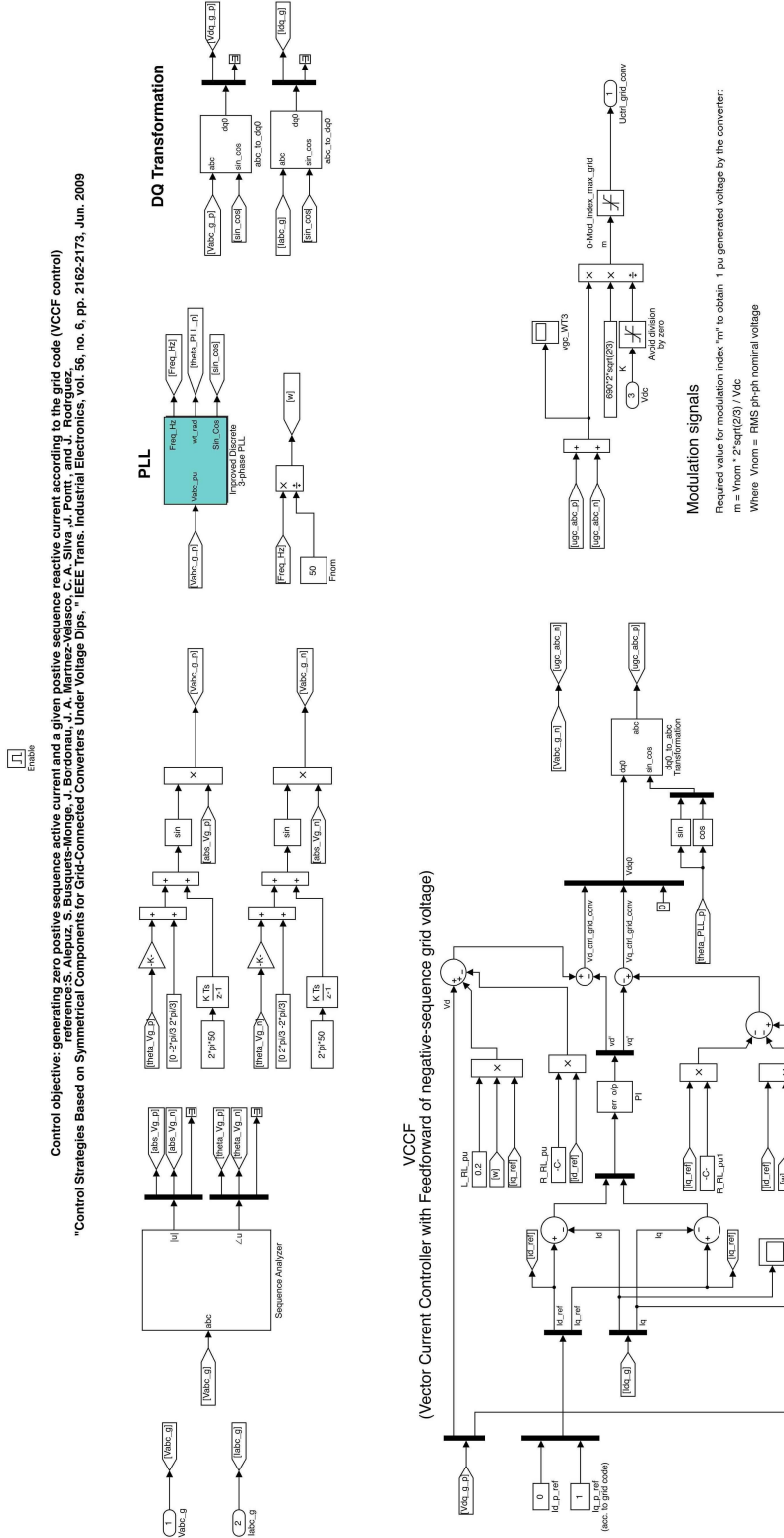
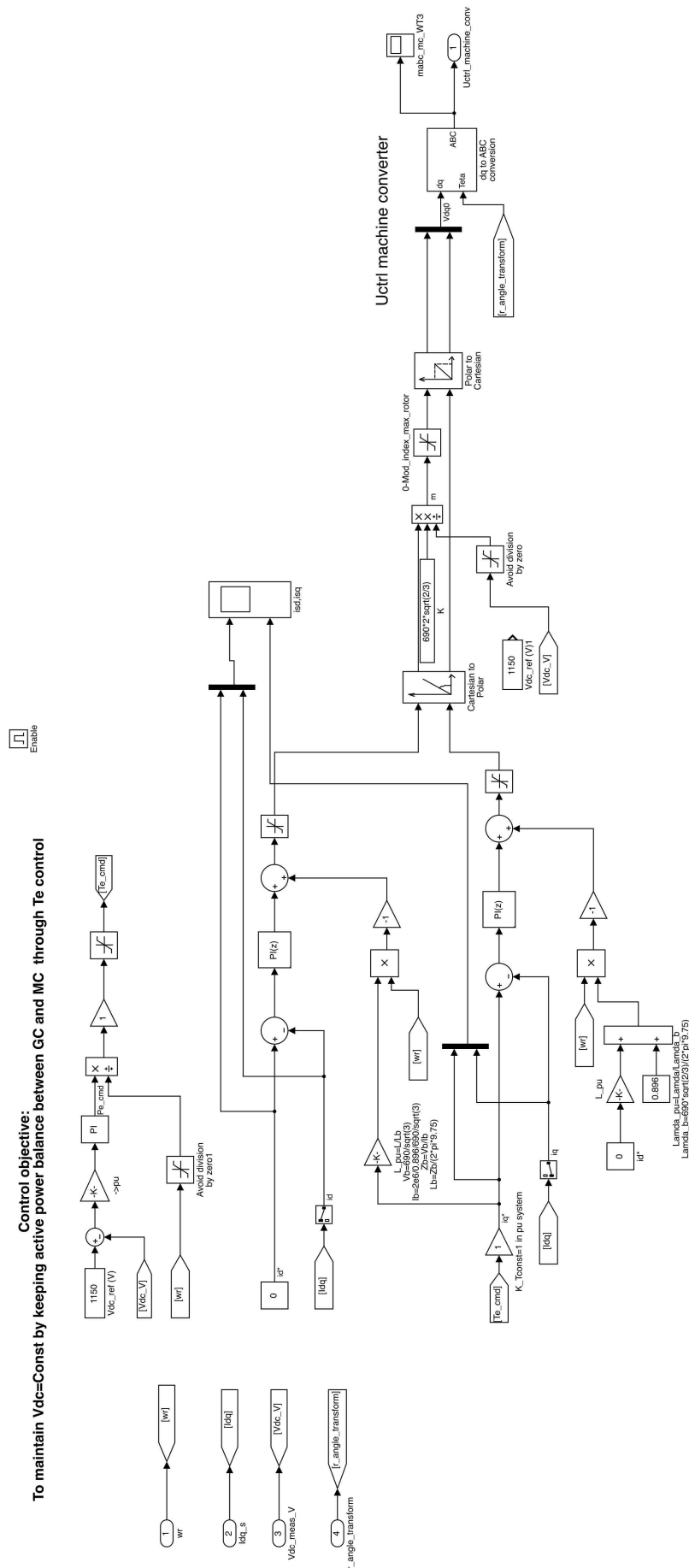


FIGURE E.11: MATLAB Simulink Schematics of WT_{Test} Machine-Side Controller for Normal Operation

FIGURE E.12: MATLAB Simulink Schematics of WT_{T_{est}} Grid-Side Controller for LVRT Operation

FIGURE E.13: MATLAB Simulink Schematics of WT_{Test} Machine-Side Controller for LVRT Operation

Bibliography

- [1] B. Wu, Y. Lang, N. Zargari, and S. Kouro. *Power Conversion and Control of Wind Energy Systems*. Wiley-IEEE Press, July 2011.
- [2] D.K. Yoon, H.G. Jeong, and K.B. Lee. *The Design of an LCL-Filter for the Three-Parallel Operation of a Power Converter in a Wind Turbine*. IEEE Trans. Energy Convers., pp. 1537-1544, September 2010.
- [3] F. Blaabjerg, M. Liserre, and K. Ma. *Power Electronics Converters for Wind Turbine Systems*, volume 48. IEEE Trans. Industry Applications, pp. 708-718, March 2012.
- [4] N. Espinoza, M. Bongiorno, and O. Carlson. *Grid code testing of full power converter based wind turbine using back-to-back voltage source converter system*. EWEA 2013 Annual Event Conference Proceedings, February 2013.
- [5] D. Xiang, L. Ran, P.J. Tavner, and S. Yang. *Control of a doubly fed induction generator in a wind turbine during grid fault ride-through*, volume 21. IEEE Trans. Energy Convers., pp. 652-662, September 2006.
- [6] S. Xiao, G. Yang, H. Zhou, and H. Geng. *An LVRT Control Strategy Based on Flux Linkage Tracking for DFIG-Based WECS*, volume 60. IEEE Trans. Industrial Electronics, pp. 2820-2832, July 2013.
- [7] C. Wessels, R. Lohde, and F.W. Fuchs. *Transformer Based Voltage Sag Generator to perform LVRT and HVRT Tests in the Laboratory*. 14th International Power Electronics and Motion Control Conference, 2010.
- [8] H. Geng, C. Liu, and G. Yang. *LVRT Capability of DFIG-Based WECS Under Asymmetrical Grid Fault Condition*, volume 60. IEEE Trans. Industrial Electronics, pp. 2495-2509, July 2013.
- [9] IEC61400-21. *Wind turbines - Part 21: Measurement and assessment of power quality characteristics of grid connected wind turbines*. Germany: International Electrotechnical Commission, 2008.

- [10] N. Espinoza, M.Bongiorno, and O. Carlson. *Novel LVRT Testing Method for Wind Turbines Using Flexible VSC Technology*. IEEE Transactions on Sustainable Energy, January 2014.
- [11] Henk Polinder, Deok-Je Bang, H. Li, and Z. Chen. *Integrated Wind Turbine Design*. UpWind, December 2007.
- [12] M. Tsili and S. Papathanassiou. *A review of grid code technical requirements for wind farms*, volume 3. IET Renew. Power Gener., pp. 308-332, September 2009.
- [13] F. D. Bianchi, H. D. Battista, and R. J. Mantz. *Wind Turbine Control System*. Springer, 2007.
- [14] M. Valentini. *Fault Current Contribution from VSC-based Wind Turbines to the Grid*. Master Thesis, Aalborg University, 2008.
- [15] V. Akhmatov. *Analysis of Dynamic Behaviour of Electric Power Systems with Large Amount of Wind Power*. PhD thesis, Technical University of Denmark, pp. 9-13, 2003.
- [16] The Switch publication. PMG vs. dFIG - the big generator technology debate, 2014. URL http://www.theswitch.com/wp/wp-content/uploads/2014/03/Technology_Point_-PMG_DFIG_06032014.pdf.
- [17] Rain Byars. Power system architecture: Finding the best solution for a 5mw turbine. Technical report, Nextwind, Inc., November 2011.
- [18] H. Akagi, E.H. Watanabe, and M. Aredes. *Instantaneous power theory and applications to power conditioning*. IEEE Press Series of Power Engineering, 2007.
- [19] Deblock Consulting Ltd. Chinese wind farm power grid disconnection accident, April 2011. URL <http://deblockconsulting.com/blog/china-news/chinese-wind-farm-power-grid-disconnection-accident/>.
- [20] *Grid Code*. E.ON, 2006.
- [21] *The Grid Code, Issue 5, Revision 9*. National Grid, 2014.
- [22] *IEC 61400-1*. IEC, 2005.
- [23] G. O. Suvire. *Wind Farm - Technical Regulations, Potential Estimation and Siting Assessment*. InTech, pp. 16-24, 2011.
- [24] IEC 61400-21 ed2.0. *Wind turbines - Part 21: Measurement and assessment of power quality characteristics of grid connected wind turbines*. Germany: International Electrotechnical Commission, 2008.

- [25] Energy to Quality. Testing wind turbines generators with ulysses. URL http://www.nrel.gov/electricity/transmission/pdfs/turbine_sim_05_inductive_fault_simulator_field_testing.pdf.
- [26] Ruan Jiayang. Detailed modelling of a 1.5mw wind turbine based on direct-driven pmsg, May 2013. URL <http://www.mathworks.com/>.
- [27] Ali M. Eltamaly. *Modeling of Wind Turbine Driving Permanent Magnet Generator with Maximum Power Point Tracking System*, volume 19. Journal of King Saud University, pp. 223-228, 2007.
- [28] J. F. Conroy and R. Watson. *Low-voltage ride-through of a full converter wind turbine with permanent magnet generator*, volume 1. IET Renew. Power Gener., pp. 182–189, September 2007.
- [29] Ali M. Eltamaly and Ammar Anwar Khan. *Investigation of DC link Capacitor Failures in DFIG based Wind Energy Conversion System*, volume 1. Trends in Electrical Engineering, pp. 12-21, May 2011.
- [30] Siegfried Heier. *Grid Integration of Wind Energy Conversion Systems*. John Wiley and Sons Ltd, 2006.
- [31] P. K. Chaturvedi, S. Jain, P. Agrawal, R. K. Nema, and K. K. Sao. *Switching losses and harmonic investigation in multilevel inverters*, volume 54. IETE Journal of research, pp. 297-307, 2008.
- [32] Rosyadi Marwan. *Stability Augmentation of Grid Connected Wind Farm by Variable speed Permanent Magnet Wind Generator*. PhD thesis, Kitami Institute of Technology, 2013.
- [33] J. Rodríguez, J. S. Lai, and Fang Zheng Peng. *Multilevel inverters: A survey of topologies, controls and applications*, volume 49. IEEE Trans. Ind. Electron., pp. 724-738, 2002.
- [34] J. Morren and S.W. Haan. *Ride through of wind turbines with doubly-fed induction generator during a voltage dip*, volume 20. IEEE Trans. Energy Convers., pp. 435-441, June 2005.
- [35] I. Erlich, J. Kretschmann, J. Fortmann, S. Mueller-Engelhardt, and H. Wrede. *Modeling of wind turbines based on doubly-fed induction generators for power system stability studies*, volume 22. IEEE Trans. Power Syst., pp. 909-919, August 2007.
- [36] J. Morren and S. W. Haan. *Short circuit current of wind turbines with doubly fed induction generator*, volume 22. IEEE Trans. Energy Convers., pp. 174-180, March 2007.

- [37] Bing Liu. *Temporary Rotor Inertial Control of Wind Turbine to Support the Grid Frequency Regulation*. Norwegian Research Centre for Offshore Wind Technology, 2012.
- [38] Agustí Egea-Alvarez, Adrià Junyent-Ferré, and Oriol Gomis-Bellmunt. *Active and reactive power control of grid connected distributed generation systems*. Modeling and Control of Sustainable Power Systems, Green Energy and Technology, pp. 47-81, 2012.
- [39] Salvador Alepuz, Sergio Busquets-Monge, Josep Bordonsau, Juan A. Martínez-Velasco, César A. Silva, Jorge Pontt, and José Rodríguez. *Control Strategies Based on Symmetrical Components for Grid-Connected Converters Under Voltage Dips*, volume 56. IEEE Transactions on Industrial Electronics, pp. 2162-2173, June 2009.
- [40] R. Portillo, M. M. Prats, J. I. Leon, J. A. Sanchez, J. M. Carrasco, E. Galvan, and L. G. Franquelo. *Modeling strategy for back-to-back three-level converters applied to high-power wind turbines*, volume 53. IEEE Trans. Ind. Electron., pp. 1483-1491, October 2006.
- [41] M. Fatu, C. Lascu, G. D. Andreeescu, R. Teodorescu, F. Blaabjerg, and I. Boldea. *Voltage sags ride-through of motion sensorless controlled PMSG for wind turbines*, volume 1. Conf. Rec. IEEE IAS Annu. Meeting, pp. 171–178, September 2007.
- [42] J. Niiranen, S. Seman, J.P. Matsinen, R. Virtanen, and A. Vilhunen. *Technical paper: Low voltage ride-through testing of wind turbine converters at ABB helps wind turbines meet the requirements of IEC 61400-21 more quickly*. ABB, 2009.
- [43] R. H. Park. *Two-reaction theory of synchronous machines*, volume 48. AIEE Transactions, pp. 716-730, 1929.
- [44] Lingfeng Wang. *Modeling and Control of Sustainable Power Systems: Towards Smarter and Greener Electric Grids*. Springer, 2012.
- [45] Se-Kyo Chung. *A phase tracking system for three phase utility interface inverters*, volume 15. IEEE Transactions on Power Electronics, pp. 431-438, 2000.